UNIVERSITY OF CALIFORNIA

Santa Barbara

The importance of sub-watershed variability for predicting ecohydrologic responses to inter-annual climate variability and climate warming in California's Sierra Nevada watersheds

A dissertation submitted in partial satisfaction of the
requirements for the degree Doctor of Philosophy
in Environmental Science and Management

by

Kyongho Son

Committee in charge:

Professor Christina (Naomi) Tague, Chair

Professor Arturo Keller

Professor Jeff Dozier

September 2015

The dissertation of Kyongho Son is approved.

_____

Arturo A. Keller

_____

Jeff Dozier

_____

Christina (Naomi) Tague, Committee Chair

August 2015

The importance of sub-watershed variability for predicting ecohydrologic responses to inter-annual climate variability and climate warming in California's Sierra Nevada watersheds

ACKNOWLEDGEMENTS

I would like to express my thanks to many people who have helped me in various ways during my PhD program. In particular, I appreciate Professor Naomi Tague, my committee chair. She is always available and she supports me all along with great passion and new ideas. Her creativity and patience helps me to finally reach this stage of submitting my dissertation. I also thank to my committees, Professor Arturo Keller and Professor Jeff Dozier for providing feedback on my research. I also thank the members of Southern Critical Zone Observatory's group for their corroboration and supports. My field experiments would not have been completed successfully without their helps, especially for Matt and Peter. I also thank the members of ecohydrology group in Bren school. Through lab meeting as well as daily interaction with them, I can be exposed to various research ideas. In particular, I am very grateful that I have worked and developed the friendship with Annelen, Aubrey, Elizabeth, Erin, Jun, Maki and Oliver. Finally, I would like to acknowledge financial support from The National Science Foundation funded CZO grant, and the Kearney Foundation of Soil Science grant and UCSB Dean Fellowship.

VITA OF KYONGHO SON
September 2015

EDUCATION
Bachelor of Environmental Engineering, Pusan National University, 1996
Masters of Environmental System Engineering, The University of Western Australia, 2006
Masters of Geography, The State University of New York at Buffalo, 2008
Doctor of Philosophy in Environmental Science, University of California Santa Barbara, 2015

PROFESSIONAL EMPLOYMENT
January 2015-Feburary 2015: Staff Engineer, Geosyntec Consultants
January 2015-March 2015: Teaching Assistant, Bren School of Environmental Science & Management, University of California Santa Barbara
2008-2013: Research Assistant, ICESS, University of California Santa Barbara
2008: Research Assistant, Department of Geography, The State University of New York at Buffalo.
2005-2007: Researcher, Korea Institute of Water and Environment

PUBLICATIONS

J.Kim, J. Noh, K.Son, I.Kim. Impacts of GIS data quality on determination of runoff and suspended sediments in the Imha watershed in Korea, *Geosciences Journa*l, Vol. 16, No. 2. (1 June 2012), pp. 181-192, doi:10.1007/s12303-012-0013-8.

K.Son, and Kim, J., Application of Proxy-basin Differential Split-Sampling and Blind-Validation Tests for Evaluating Hydrological Impact of Climate change Using SWAT, *Journal of KWRA*, Vol. 41, No. 10, 969-982, 2008. 10.

J. Kim, K.Son, J. Noh and S. Lee. Estimation of Suspended Sediment Load in Imha-Andong Watershed using SWAT Model, *J. of KSEE* / Vol. 30, No. 12, 2008.

K.Son and M. Sivapalan. Improving model structure and reducing parameter uncertainty in conceptual water balance models through the use of auxiliary data, *Water Resources Research*, VOL. 43, W01415, doi: 10.1029/2006WR005032, 2007.

J. Kim, K.Son, J. Noh, C. Jang and I. Ko. Multi-variable and multi-site calibration and validation of SWAT for the Gap river catchment, *Korea Water Resources Association*, 2006.

J. Kim, K.Son, J. Noh C. Jang and I. Ko. Evaluation of Urbanization effect and analysis of hydrological characteristics in the Gap river catchment using SWAT, *Korea Water Resources Association*, 2006.

AWARDS
Dean Fellowship, UC-Santa Barbara Graduate Division (2012-2013)

FIELDS OF STUDY
Major Field: Ecohydrology, Hydrologic modeling and uncertainty analysis

ABSTRACT

The importance of sub-watershed variability for predicting ecohydrologic responses to inter-annual climate variability and climate warming in California's Sierra Nevada watersheds

by

Kyongho Son

This dissertation improves the understanding of how accounting for fine-scale variability of topography and soil is important for modeling ecohydrologic responses to climate change and variability in California's Sierra Nevada watersheds. In the first chapter, I apply the Regional Hydrologic-Ecologic Simulation System (RHESSys) to eight small watersheds and investigate how the spatial resolution of digital elevation model (DEM) resolution affects the accuracy of modeling streamflow and model estimates of ecohydrologic responses to inter-annual climate variability. Modeled streamflow estimates become worse with DEM resolution coarser than 10m, the explanation lying in the corresponding reduction in the spatial variance of the wetness index ($\ln(a/\tan\beta)$). In the second chapter, I use Generalized Likelihood Uncertainty Estimation (GLUE) to investigate the effect of soil parameter uncertainty in modeling ecohydrologic estimates in the two small watersheds with different snow regimes. The predictive uncertainty of annual evapotranspiration and net primary production estimates for a transient snow watershed are larger than those for a snow-dominated watershed, but the predictive uncertainty in model estimates for daily streamflow is larger for the snow-dominated watershed. The effect of soil parameter uncertainty varies seasonally, between wet and dry years, and its effect on ecohydrologic estimates is often large relative to the effect of climate warming. In the third chapter, I investigate the different hydrologic responses to climate warming between a snow-dominated watershed and a

transient snow watershed. The modeling results show that the snow-dominated watershed has greater sensitivity to climate warming than the transient snow watershed. In the both watersheds, leaf area index and wetness index are primary factors controlling spatial patterns of seasonal evapotranspiration under both of historical climate conditions and climate warming scenarios. Climate warming results in increased spatial variability in monthly evapotranspiration, especially in the summer period. In the last chapter, I develop a strategic sampling design for collecting soil moisture and sapflux data to capture watershed ecohydrologic responses to inter-annual climate variability in a transient snow watershed. The comparison of model-based calculated hydrological similarity indicators with measured values shows that spatial patterns of field-sampled soil moisture data are similar to those of model-based estimates. However, the model fails to capture the soil moisture and sapflux dynamics in the riparian zone site, and in a site where lateral subsurface flow may not follow surface topography. Future research will reduce these errors by the use of finer-scale representations of microclimate, topography, vegetation, and soil properties in the model.

TABLE OF CONTENTS

Introduction and Overview 1

1. Effects of model spatial resolution on ecohydrologic predictions and their sensitivity to inter-annual climate variability in California's Sierra Nevada watersheds 6

Abstract 6

1. 1 Introduction 7

1.2 Research Site 10

1.2.1 Providence Watersheds 10

1.2.2 Bull Watersheds 11

1.3 Methodology 12

1.3.1 Effect of DEM resolution on topographic parameters 12

1.3.2 Model Description 14

1.3.3 Model calibration 17

1.3.4 Effect of DEM resolution on model accuracy and long-term ecohydrologic responses to climate 20

1.4 Results 22

1.4.1 Effect of DEM resolution on snow predictions 22

1.4.2 Effect of DEM resolution on streamflow prediction accuracy 22

1.4.3 Sensitivity of estimated ecohydrologic variables to DEM resolution 24

1.5 Discussion and summary 25

Figures 30

Tables 39

2. Interaction between soil parameter uncertainty and climate forcing in estimating ecohydrologic fluxes for California's Sierra watersheds 44

Abstract....44
2.1 Introduction....45
2.2 Study sites and methodology....48
2.2.1 Study sites....48
2.2.2 Ecohydrologic-modeling framework....49
2.2.3 Model parameterization and uncertainty analysis....51
2.3 Results....59
2.3.1 Comparison of model accuracy and predictive uncertainty between the transient snow watershed (TSW) and the snow-dominated watershed (SDW)....59
2.3.2 The Impact of soil parameter uncertainty on long-term ecohydrologic predictions....61
2.3.3 Comparison between climate-warming and soil parameter uncertainty effects on ecohydrologic predictions....63
2.4 Summary and discussion....64
Figures....71
Tables....79
3. Hydrologic responses to climate warming for a snow-dominated watershed and a transient snow watershed in the California Sierra....85
Abstract....85
3.1 Introduction....86
3.2 Study sites and model calibration....89
3.2.1 Study sites....89
3.2.2 RHESSys model parameterization and calibration....90

3.2.3 Impact of climate warming on hydrologic fluxes of TSW and SDW 98
3.3 Results.....100
3.3.1 Climate warming's effects on inter-annual hydrologic responses in TSW and SDW 100
3.3.2 Climate warming's effects on seasonal hydrologic responses in TSW and SDW.....102
3.3.3 Climate warming's effects on spatial structure of seasonal ET and its relationship with physiographic parameters 103
3.4 Summary and Discussion 106
Figures 112
Tables.....121
4. A top-down soil moisture and sap flux sampling design to capture the effect of inter-annual climate variation on ecohydrologic response of a transient snow watershed 128
Abstract.....128
4.1 Introduction.....129
4.2 Methodology.....132
4.2.1 Top-down approach sampling design for soil moisture and vegetation water use 132
4.2.2 Watershed descriptions.....133
4.2.2 Model calibration.....134
4.2.3 Clustering analysis.....137
4.3 Results.....140
4.3.1 Clustering analysis.....140

4.3.2 Spatial and temporal variability of measured soil moisture and sapflux 142

4.3.3 Validation of suggested sampling design 144

4.4 Discussion and summary 145

Figures 150

Tables.....161

References.....164

Introduction and Overview

Hydrologic models are the primary tools used to predict the plausible impact of climate variability and change for mountain ecohydrology. Because mountain watersheds have high spatial heterogeneity in atmospheric forcing, topography, soil and vegetation, a key challenge in modeling for climate change assessment of mountain watersheds is how to account for their variables in mountain watersheds. This dissertation investigates the importance of sub-watershed variability in modeling ecohydrologic responses to climate change in small watersheds in California's Sierra Nevada. The first chapter uses a process-based model, the Regional Hydrologic-Ecologic Simulation System (RHESSys) to test the importance of fine-scale topographic variability in estimating streamflow and ecohydrologic responses to inter-annual climate variation. The second chapter explores the importance of soil parameter uncertainty in assessing the effect of climate warming on ecohydrologic estimates in two watersheds with different snow regimes. The third chapter investigates the difference of hydrologic responses to climate warming in a snow-dominated watershed and a transient snow watershed. The fourth chapter presents the top-down approach for collecting soil moisture and sapflux data in order to capture watershed echydrologic responses to inter-annual climate variability.

The first chapter addresses the effect of Digital Elevation Model (DEM) resolution on ecohydrologic estimates in the context of climate change effect analysis. Three hypotheses are developed to test the DEM sensitivity between watersheds and between the variables of interest. The first hypothesis is that model estimates for transient snow watersheds (TSWs) will have higher sensitivity to DEM resolution than the model estimates for snow-dominated watersheds (SDWs). The second hypothesis is that spatial variation of wetness index (

$\ln(a/\tan\beta)$) can explain the watershed sensitivity to DEM resolution. The third hypothesis is that flow estimates may be more sensitive to DEM resolution than are estimates of evapotranspiration and net primary production. I explore the effect of DEM resolution on topographic parameters (elevation, slope, aspect and wetness index[*Beven and Kirkby*, 1979]) in eight watersheds. For all watersheds and for all DEM resolutions (10m, 30m, 90m and 150m), the watershed mean values of slope and wetness index are significantly different (p-value<0.01) from those computed using the 5m resolution. The effect of DEM resolution on watershed snow water equivalent is minor. Modeling results show that the TSWs tend to have larger reduction of streamflow than SDWs. However, the reduction of streamflow accuracy with coarsening DEM resolution is due to the reduction in spatial variance of the wetness index rather than change in snow prediction. Coarsening DEM also causes the largest change in summer flow and increases the coefficient of variance (COV) in annual evapotranspiration and net primary production. In this chapter, I demonstrate that accounting for fine-scale topographic variability in hydrologic modeling may be necessary for predicting accurate streamflow and climate driven inter-annual ET and NPP variability in the small Sierra Nevada watersheds.

The second chapter investigates the impact of soil parameter uncertainty on the estimation of four ecohydrologic variables to inter-annual climate variation and climate warming in the two small watersheds: a transient snow watershed (TSW) and a snow-dominated watershed (SDW). Four ecohydrologic variables include annual streamflow, summer flow, annual evapotranspiration and annual net primary productivity. Two small watersheds (P301 and B203) within the Upper Kings River basin in the California Sierra are used as case study examples of TSW and SDW. RHESSys is used to test the impact of soil parameter uncertainty on model estimates in the two watersheds with Generalized

Likelihood Uncertainty Estimation (GLUE) [*Beven and Freer*, 2001]. I hypothesize that the sensitivity of model estimates will vary with the variable of interest (e.g. streamflow, ET, NPP) and between TSW and SDW. TSW and SDW have different timing and magnitudes of snow accumulation and melt, and ET [*Bales et al*., 2012; *Goulden et al*., 2012; *Hunsaker et al*., 2012]. I test whether or not the hydrologic differences between the two watersheds lead to different predictive uncertainty of model estimates across soil parameter uncertainty. The modeling results show that the predictive uncertainty of annual evapotranspiration and net primary production estimate for TSW is larger than those for SDW but the predictive uncertainty in model estimates for daily streamflow is larger for SDW. I propose that ET and NPP estimates is sensitive to soil parameters that influence storage. Because TSW experiences generally more water limited conditions than SDW, TSW tends to have higher predictive uncertainty of annual ET and NPP compared to SDW. I also propose that shallower groundwater level of SDW contributes to higher predictive uncertainty of daily streamflow due to the nonlinearity of soil drainage parameters and groundwater level. I also show that the sensitivity of annual streamflow estimates to soil parameter uncertainty for the both watersheds is the highest in the dry years, and the sensitivity of annual ET and NPP estimates to soil parameter uncertainty is the highest in the intermediate wet years. The effect of soil parameter uncertainty on estimated inter-annual variation in seasonal ecohydrologic model estimates is equally important in summer period compared with the effect of inter-annual climate variability. In both TSW and SDW, soil parameter uncertainty tends to have a larger influence on estimated annual ecohydrologic estimates than the two warming scenarios (2 $^{\circ}$ C and 4 $^{\circ}$ C). In this chapter, I develop a simple conceptual model for explaining the difference in the effect of soil parameter uncertainty between TSW and SDW, and demonstrate that proper soil parameterization in hydrologic model is important

for capturing the ecohdrologic response to climate, particularly in dry years and during summer.

The third chapter uses a process-based model approach to predict the effects of climate warming on two small Sierra Nevada watersheds: a snow-dominated watershed (SDW) and a transient snow watershed (TSW). Specifically, I investigate the effect of climate warming (2° C and 4° C) on seasonal and inter-annual variation of hydrologic fluxes as well as the spatial structure of seasonal ET and its relationship with physiographic parameters in TSW and SDW. I find that climate warming results in reducing snow accumulation and accelerating the snowmelt, increasing annual ET, and decreasing annual streamflow and summer flow in both watersheds. The change in the magnitude of these hydrologic fluxes under climate warming is larger for SDW than for TSW. I also find that in the both watersheds, leaf area index (LAI) and wetness index have high correlation with seasonal ET under both of historical climate conditions and climate warming scenarios. Climate warming increases the spatial variability in monthly ET, especially in the summer period. Empirical approaches have difficulty in assessing the effect of climate warming on individual watersheds due to the confounding effect of other hydrologic properties [*Peel and Bloschl*, 2011]. To demonstrate these compounding effects, I examine whether the differences of air temperature between TSW and SDW can explain the different hydrologic responses to climate warming. I show that SDW under 2° C warming scenarios has similar magnitude and the timing of monthly SWE as well as average air temperature compared to TSW under historical climate conditions. However, SDW under 2° C warming scenarios generates higher annual streamflow (including summer flow) due to shallower groundwater storage, and experiences less water-limitation due to lower ET (lower LAI), compared to TSW under historical climate conditions. In this chapter, I present the similarity and dissimilarity

between TSW and SDW in terms of the climate warming's effect on hydrologic cycles and suggest that vegetation structure and subsurface properties may be as important as the difference of air temperature in explaining hydrologic response to warming in the two Sierra Nevada watersheds

The fourth chapter presents a strategic sampling design for collecting soil moisture and sapflux data in order to capture the watershed scale responses to inter-annual climate variation. The sampling design is based on RHESSys predictions. Initial model implement for running RHESSys has several simplified assumptions: 1) spatial uniform soil properties, 2) spatial uniform rooting depths, 3) spatial interpolation of air temperature with simple lapse rate approach, 4) spatial uniform precipitation and 5) 30m resolution topographic map and LAI map. RHESSys is calibrated with measured snow depth and streamflow data. Calibrated RHESSys is used to estimate five hydrologic similarity indices that represents seasonal pattern of snow, soil moisture and transpiration. Through clustering analysis and field survey, the number of sampling site, and the location of sampling sites for instrumentation are identified. Soil moisture and sapflux data are collected at the six sites. To validate the suggested sampling design, model-based calculated hydrological similarity indicators are compared with measured values. The comparison shows that spatial patterns of field-sampled soil moisture data are similar to those of model-based estimates. However, the model failed to capture the soil moisture and sapflux dynamics in the riparian zone site (C6), and in a site (C4) where lateral subsurface flow does not follow surface topography. I develop a framework for reducing these errors by using measured soil moisture and sapflux data. I propose that using local parameter values including microclimate, topography, soil and vegetation (rooting depths) will improve the prediction of soil moisture and sapflux data at the plot scale and the catchment scale. I will explore this strategy in future research.

1. Effects of model spatial resolution on ecohydrologic predictions and their sensitivity to inter-annual climate variability in California's Sierra Nevada watersheds

Abstract

The importance of accounting for fine-scale topographic patterns in model estimates of ecohydrologic responses to climate change in California's Sierra Nevada watersheds is not well understood. This study tested the effect of Digital Elevation Model (DEM) resolution on model accuracy and estimates of the sensitivity of annual flow, summer flow, annual evapotranspiration (ET) and annual net primary production (NPP) to inter-annual climate variability. The Regional Hydro-Ecologic Simulation System (RHESSys) was applied to eight small, high elevation watersheds located in the Sierra National Forest. Each watershed was calibrated with measured snow depth (or snow water equivalent), and daily streamflow. The accuracy of modeled streamflow estimates is sensitive with coarsening DEM resolution, even with resolution-specific calibration of soil drainage parameters. For model resolutions coarser than 10m, the accuracy of streamflow estimates largely decreased. Reduced model accuracy is related to the reduction in spatial variance of wetness index ($\ln(a/\tan\beta)$) with coarser DEM resolutions rather than the change in snow water equivalent. This study also found that among the long-term average ecohydrologic estimates, summer flow estimates are the most sensitive to DEM resolution, and coarser resolution models overestimate the climatic sensitivity for ET and NPP. Therefore, accounting for fine-scale topographic variability in hydrologic modeling may be necessary for assessing reliable climate change effects on small Sierra Nevada watersheds.

1. 1 Introduction

In recent decades, warmer temperatures in the western United States have led to a reduction of snow accumulation as well as earlier melt and streamflow [*Knowles and Cayan*, 2002; *Maurer and Duffy*, 2005;*Mote et al*., 2005]. Changing snowmelt input has also altered the timing and magnitude of soil moisture, vegetation water use and productivity [Goulden and Bales, 2014]. Many hydrological models are used to assess the effect of climate change on ecohydrologic response at the watershed scale or larger scales [*Knowles and Cayan*, 2002; *Miller et al.*, 2003; *Null et al.*, 2010]. However, spatial units in these models tend to be defined at relatively coarse spatial resolutions (>100m) and thus ignore the fine-scale variation of topography. Particularly in mountain environments, substantial variation in topographic properties over relatively short spatial scales is observed, and the topographic properties are related to the distribution of atmospheric forcing variables (radiation, temperature and precipitation), and local and lateral moisture distribution. Therefore, ignoring the fine-scale variation of topography of mountain watersheds may result in poor predictions of ecohydrologic responses to climate change.

Previous studies have emphasized the importance of detailed topographic information in characterizing the hydrologic and geomorphic properties of watersheds and obtaining accurate hydrologic and ecologic predictions [*Zhang and Montgomery*, 1994; *Laussuer et al*., 2006; *Cline et al*., 1998]. *Cline et al*. [1998] show that the mean snow water equivalent (SWE) predictions using a 90m DEM are different from the predictions obtained using a 30m DEM in the Emerald Lake Watershed in California. *Zhang and Montgomery* [1994] show that TOPMODEL [*Beven and Kirkby*, 1979] which uses a DEM with 10m resolution, improved streamflow predictions compared to the model simulations using coarser DEM (30m and 90m) for two small catchments in the western United States. *Lassueur et al*.

[2006] demonstrate the usefulness of a fine-resolution DEM to estimate plant species richness in an alpine landscape.

However, the response of model performance to DEM resolution varied between watersheds. *Kuo et al*. [1999] shows that model estimates for slowly undulating landscapes tend to be less degraded with increasing grid size than those for landscapes with steep valleys. Their research also finds that runoff does not change with grid size in wet years, but does change in dry years. Model predictions for snow-dominated watersheds may be more sensitive to DEM resolution than those for rain-dominated watersheds because topographic parameters (elevation, aspect and slope) determine the energy input, thereby controlling the snow melt patterns [*Jost et al.*, 2007; *Musselman et al.*, 2008]. DEM resolution also affects the snow accumulation estimates because many snow models use a simple lapse rate based on air temperature and elevation to partition the total precipitation into snow and rain.

The effect of DEM resolution on model predictions also varies with the variable of interest[*Chaubey et al.*, 2005]. Using SWAT modeling, coarsened DEM resolution reduces the accuracy of both streamflow and NO3-N load prediction, but does not reduce the accuracy of total P load predictions [*Chaubey et al.*, 2005]. A distributed hydrologic model used to predict average soil moisture and streamflow at the hillslope scale shows that using a coarser DEM does not reduce model accuracy, but the spatial pattern of soil moisture is distorted[*Mahmood and Vivoni*, 2011]. Grid-size effect on NPP estimate using a distributed ecohydrologic model for a large Loess Plateau basin, China.is more significant than on ET estimates [*MO et al.*, 2009].

These previous studies have focused on the effect of DEM resolution on model predictions in general. However, the importance of fine-scale topographic variation in hydrologic modeling specifically for climate change effect studies is not well understood.

The declines in accuracy with coarsening resolution noted above may or may not be critical for using models to make inferences about climate change effects. Vegetation water and productivity are important variables for assessing the effect of climate change on ecosystem productivity, but previous hydrologic studies do not integrate the effect of DEM resolution on changes in water availability and the related impacts on modeled ET and NPP.

This study aims to test the effect of DEM resolution on the accuracy of modeled streamflow, specifically for rain-snow transition watersheds to snow-dominated watersheds that are expected to be particularly sensitive to climate change. This study also explicitly tests the sensitivity of modeled ecohydrologic responses (annual streamflow, summer flow, annual ET and annual NPP) to inter-annual climate variability. The Regional Hydrologic-Ecologic Simulation System (RHESSys) [*Tague and Band*, 2004] is applied to eight small Sierra Nevada watersheds. The watersheds have different dominant precipitation phases (snow vs rain), topographic properties (elevation, slope and aspect), and vegetation properties (leaf area index, rooting depths). This study answers three questions: (1) does the total precipitation phase (snow vs rain) control the sensitivity of model estimates to DEM resolution, (2) which topographic parameters determine the sensitivity of model estimates to DEM resolution, and (3) which variable of interest among model estimates is the most sensitive to DEM resolution? To answer these questions, this study follows the framework outlined in Figure 1.1. First, this study investigates the effect of DEM resolution on topographic parameters (elevation, slope, aspect and wetness index) in the eight watersheds. Second, this study identifies the watershed sensitivity based on difference in estimates of snow water equivalent (SWE), and accuracy of modeled daily streamflow between various resolution models. Finally, this study estimates the sensitivity of the model estimates of the four ecohydrologic variables (annual streamflow, summer streamflow, annual ET and

annual NPP) to DEM resolution. These tests provide a guideline for determining the appropriate DEM resolution in hydrologic modeling for climate effect assessment on the Sierra Nevada watersheds.

1.2 Research Site

This study uses research sites that are monitored as part of the Southern Sierra Critical Zone Observatory (SSCZO), located in King River Experiment Watersheds (KREW) in California (Figure 1.2). RHESSys is implemented for gauged sub-watersheds within the large Providence watershed (P301, P303, P304 and D102) and Bull watershed (B201, B203, B204 and T003). Detailed descriptions of each watershed are provided below.

1.2.1 Providence Watersheds

The Providence Creek watersheds include P301 (0.99km^2), P303 (1.32km^2), P304 (0.49km^2) and D102 (1.2km^2). The major soil types are Shaver soil and Gerle-Cagwin soil [Hunsaker et al., 2012]. The dominant forest type is Sierran mixed-conifer forest with some mixed chaparral and barren land cover. Sierran mixed-conifer vegetation in this location consists largely of white fir (Abies concolor), ponderosa pine (Pinus ponderosa), Jeffrey pine (Pinus Jeffrey), black oak (Quercus kelloggii), sugar pine (Pinus lambertiana) and incense cedar (Calocedrus decurrens). Average annual precipitation (from year 2002 to year 2006) is 1350 mm. The elevation ranges from 1485m to 2115m. Precipitation occurs primarily in the winter period as mixture of snow and rain, and with little contribution of storm rainfall during the summer. In Providence watersheds, 20 to 50% of the annual precipitation falls as snow[*Hunsaker et al*., 2012]. Following the snow regime classification developed by Jefferson [2011], P301, P303, P304 and D102 are transient snow watersheds

(TSWs). Two climate stations are located near or in the P303 watershed. A station is located near the outlet of the P303 watershed, while the other station is at the top of the P303 watershed. At the two stations, hourly precipitation, minimum and maximum air temperature, relative humidity, solar radiation, wind speed and direction and snow depth have been measured since 2002. The snow depth data is collected using acoustic snow-depth sensors (Judd Communications ^{TM} LLC). At the upper climate station, SWE is measured with snow pillows (Mendenhall Manufacturing, McClellan, CA). Each sub-watershed has two flumes at the outlet of watershed to measure low and high flow.

1.2.2 Bull Watersheds

Bull watersheds include B201 (0.53km^2), B203 (1.4km^2), B204 (1.7km^2) and T003 (2.3km^2). Average annual precipitation (from year 2003 to year 2007) is 1300 mm. The elevation ranges from 2050m to 2490m. Bull watersheds are more snow-dominated watersheds (75% to 95% fall as snow) than Providence watersheds. B201, B203, B204 and T003 are classified as snow-dominated watersheds (SDWs). The major soil types are Cagwin soil [*Hunsaker et al*., 2012]. Similar to the Providence watersheds, the dominant forest types in the Bull watershed are Sierra mixed conifers, however, red fir is more dominant than white fir. Two climate stations are located near or in the B204 watersheds. The lower climate station is located near the outlet of the B204 watershed, while the upper station is located at the top of the B204 watershed. The station measures the same meteorological variables as at the Providence meteorological stations, and the meteorological data has been collected since year 2003. Each sub-watershed has two flumes at the outlet of the watershed to measure high and low flow, and streamflow has been

measured since 2003. A detailed description of measurements and instruments is provided by *Hunsaker et al*. [2012].

1.3 Methodology

1.3.1 Effect of DEM resolution on topographic parameters

This study tested the effect of DEM resolution on topographic parameters including elevation, aspect, slope and topographic wetness index for the eight Sierra Nevada watersheds. The topographic wetness index [*Beven and Kirkby*, 1979] is defined as $\ln(a/\tan\beta)$, where a is the local upslope contributing area per unit contour length and β is the slope angle of the ground surface. Each DEM product was derived from a 1m LIDAR DEM (available at https://eng.ucmerced.edu/snsjho/files/MHWG/LiDAR) with a bilinear interpolation algorithm. Providence and Bull watersheds boundaries were derived based on 5m LIDAR DEM in order to minimize the effect of DEM resolution on deriving watershed area. However, due to the irregular edges, the error in estimating watershed area is unavoidable. Other topographic parameters including elevation, slope, aspect and wetness index were derived with 5 different resolutions (5m, 10m, 30m, 90m and 150m).

The Wilcox rank-sum test was used to quantify the difference of the topographic parameters between the finest DEM (5m) and other coarser DEM resolutions (10m, 30m, 90m and 150m) (Table 1.1). Values for topographic parameters are taken from each grid cell within the watershed boundaries. For all watersheds and for all DEM resolutions, the watershed mean values of slope and wetness index are significantly different (p-value<0.01) from those computed using the 5m resolution. However, coarsening the DEM generally does not influence the mean values of elevation and aspect except in few cases. For example, for

two of Providence's transient snow watersheds (D102 and P304), the mean values of elevation using 10m are significantly different (p-value<0.05) than those computed using 5m. Among the snow-dominated watersheds, B204's mean aspect values using 90m and 150m are significantly different (p-value<0.1) from those computed using 5m. T003 also has significantly different (p-value<0.1, p-value<0.01) mean values of aspect using 5m compared with those computed using 10m, and the resolution greater than 10m respectively.

Density plots were used to qualitatively compare the overall distributions of the topographic parameters. Here the density plots for only slope and wetness index parameters are presented in Figure 1.3 and Figure 1.4 because these two parameters have the most significant change with coarsening DEM. In general, coarsening DEM decreases the mean of slope and its variation for all watersheds. Across all watersheds in Bull and Providence, the largest difference in distribution of slope occurs between 5m and 90m, and between 5m and 150m; there is a similar distribution of slope between 5m and 10m, and 30m.

Coarsening the DEM increases the mean of wetness index, but inconsistently changes the variance of the wetness index (Figure 1.4). The changes in wetness index distribution with resolution are not linear and different resolutions often have different shapes of the wetness index distribution. TSWs and SDWs have substantial change in the distribution of the wetness index at resolutions coarser than 10m, and 30m respectively. These results suggest that DEM resolution may have a larger effect on local moisture estimates and lateral flow drainage patterns.

This study also estimated the watershed-scale mean and standard deviation of slope and wetness index computed using the different DEM resolutions (Figure 1.5). At 5m, D102 and T003 have the largest mean slope as 19.2 and 15.7 for TSWs and SDWs respectively. Among TSWs, P304 has the largest change in mean slope (5.3, 38%), and among SDWs,

T003 has the largest change in mean slope (6.0, 38%) with different DEM resolutions. TSWs tend to have larger spatial variance of slope at 5m than SDWs, but the change in spatial variance of slope with coarsening DEM is similar between TSWs and SDWs. SDWs tend to have larger mean wetness index at 5m than TSWs, but TSWs tend to have larger spatial variance of wetness index at 5m than SDWs. Increasing DEM resolution generally decreases the mean and standard deviation of slope, and increases mean wetness index for all watersheds. The changes in standard deviation of wetness index with coarsening the DEM have more complex patterns than other parameters. Among TSWs, the spatial variances of wetness index for P303 and D102 tend to decrease with coarsening DEM. Their variances for P301 and P304 increase with coarsening resolution up to at 30m, and their variances decrease at 90m and 150m respectively. Among SDWs, the spatial variances of wetness index for B203 and B204 increase for resolutions up to at 30m, and then decreases. Its variance for B201 slightly decreases with coarsening DEM. However, its variance for T003 increases with coarsening DEM.

1.3.2 Model Description

The RHESSys [*Tague and Band*, 2004] was used to investigate the effect of DEM resolution on model estimates of ecohydrologic fluxes of the eight small Sierra Nevada watersheds in California. RHESSys is a physically- based, distributed ecohydrologic model. RHESSys is under continuous development. In this study, version 5.15.r326 was used. A detailed description of the model is provided in [*Tague and Band*, 2004].

The RHESSys has a hierarchic spatial structure to partition the landscape: basins, hillslope, zones, patches and canopy strata. Patch and canopy strata are the smallest spatial units, and it can be derived using various layers: landcover, soil and elevation maps. In this

study, a patch is defined as grids with same elevation. Hydrological variables including snow, soil moisture and evapotranspiration are computed at the patch level. Within a patch, multiple horizontal and vertical canopy layers can be potentially used, but in this study we use a simple, single vertical layer canopy strata with the same horizontal (spatial) resolution as the patch. In addition to a canopy layer, patches also contain a litter layer. Zones are used to characterize the spatial and temporal distribution of climate inputs including precipitation, air temperature and solar radiation. To account for the fine-scale variability of climate within a watershed, we define zones using the same spatial data (elevation grids) that are used to define the patches. In RHESSys, basins are the largest spatial unit, and it is generally defined as a hydrologically closed drainage area. In this study, the basins are created based on the stream gauging station, using r.water.outlet (Grass GIS, (http://grass.osgeo.org/)). Hillslope maps are created using r.watershed, and multiple flow direction algorithm[*Holmgren*, 1994] is used to create the flow direction maps, and a hillslope drains a single stream reach. Lateral flow is organized within a hillslope, and computed at the patch level.

The minimum climate data required for model simulation include daily precipitation, and daily maximum and minimum air temperature data. Other climate data including solar radiation, saturation vapor pressure, relative humidity, etc. are computed using a climate interpolation model (MT-CLIM, [*Running et al*., 1987]). Mountain watersheds have frequently experienced a lack of available climate data usable for hydrologic modeling, largely due to high climate variability along steep topographic gradients. MT-CLIM has been tested and improved using field data, and has successfully reproduced the field measured climate data[*Hungerford et al.*, 1989; *Glassy and Running*, 1994; *Coughlan and Running*, 1997; *Thornton et al.*, 1997]. Energy, wind and water are attenuated through the

aboveground canopy, using standard approaches such as Beer's Law for radiation extinction as a function of vegetation leaf area index. Snowmelt is estimated using a combination of an energy budget approach for radiation-driven melt and advective-driven melt (rain on snow) with a temperature-index based approach for sensible and latent heat exchange. The partitioning of total precipitation into snow versus rain is calculated based on linear temperature threshold values. Transpiration from the canopy and evaporation of intercepted water and soil are computed using the Penman-Monteith [*Monteith*, 1965] approach, where stomatal conductance for vegetation is computed using a Jarvis multiplicative model of radiation, vapor pressure deficit, rooting zone soil moisture and temperature controls [*Jarvis*, 1976]. Net primary productivity is estimated as the difference between gross photosynthesis and respiration. Gross photosynthesis is estimated using the Farquhar model [*Farquhar et al.*, 1980]. Respiration is computed separately for different plant components (leaves, live/dead wood and roots) as a function of biomass, nitrogen content and air temperature[*Ryan*, 1991]. Infiltration and vertical drainage between unsaturated and saturated stores is a function of soil hydraulic parameters. A lateral shallow groundwater flux is calculated based on hydraulic gradients (determined by surface topography) and soil hydraulic conductivity, and is explicitly routing between patches. The explicit routing scheme is based on topographic slope and soil transmissivity. The model also includes a bypass flow mechanism to simulate direct drainage through macropores from surface to deep groundwater storage. The flow from deep groundwater storage is calculated based on a linear storage equation.

This study compared RHESSys estimates from model implementations using 5 different resolutions (5m, 10m, 30m, 90m and 150m). For RHESSys, DEM is used to derive topographic parameters (elevation, aspect, slope and flow drainage parameter (e.g. wetness

index)) that determine the distribution of microclimate (radiation, temperature, etc.), and local and lateral moisture distribution. Changing the DEM resolution is therefore expected to affect the RHESSy model estimates, including SWE, ET, NPP and streamflow. Each resolution model has same vegetation definition map. The vegetation type for all watersheds is assigned as mixed conifer. Associated vegetation type parameters are taken from RHESSys parameter libraries (http://fiesta,bren.ucsb.edu/~rhessys/index.html). Leaf Area Index (LAI) was derived from LIDAR point cloud using a deterministic approach [*Richardson et al.*, 2009] and was used to initialize vegetation carbon and nutrient stores. To minimize the effect of LAI resolution on model estimates, 30m LAI was used for all resolution models. Each implementation was calibrated separately and the best model was selected based on the streamflow prediction.

1.3.3 Model calibration

Snow-related parameters were estimated by comparing model SWE predictions with measured snow depths (or measured SWE) at the climate stations. Table 1.2 shows estimated air temperature and snow-related parameters for Providence and Bull watersheds. The two climate stations are located in the top and bottom of the watersheds respectively. Thus, air temperature lapse rates for the Providence and Bull watersheds were estimated using the difference of elevations and the difference of measured air temperatures at the two climate stations respectively. Positive lapse rates for maximum daily temperature and negative lapse rates for minimum daily temperature are obtained for the both watersheds. Since the climate stations (Lower Providence and Lower Bull) at lower elevations are located in valley or potential cold pool drainage area, the measured air temperature data at the station may reflect the temperature inversion in nighttime. The two snow-related

parameters, temperature melt coefficient and temperature threshold value for the partitioning of precipitation into rain and snow, are estimated by adjusting the parameter values until model prediction is similar to measured snow depth or SWE. The Providence and Bull watersheds have similar temperature lapse rates and same temperature melt coefficients and temperature threshold values. To compare the model estimate of SWE and measured snow depths, the day of complete snowmelt in the four climate stations are calculated (Table 1.2). Model estimates are compared to measurements taken by acoustic snow-depth sensors. The model reproduces the timing of observed snowmelt at the four climate stations. The comparison of the model estimates with measured values results in R^2 values of 0.92, 0.86 in Providence stations and Bull stations. The comparison of the modeled SWE with measured SWE at the Upper Providence and the Upper Bull stations results in R^2 of is 0.91 and 0.83. In general, the model accuracy for SWE estimate is slightly better at the Providence station (transient snow watersheds) than at the Bull station (snow-dominated watersheds).

After snow-related parameters were estimated, soil parameters were calibrated by comparing daily estimates of model streamflow to measured streamflow. The calibrated soil parameters are anisotropic saturated hydraulic conductivity (Ksat_h, Ksat_v), decay coefficient of saturated hydraulic conductivity with depth (m), proportion coefficient of macro-pore drainage into deep groundwater storage (gw1), air entry pressure (ae) and pore size index (psi). The linear coefficient of deep groundwater storage (gw2) is fixed as zero to reflect deep groundwater losses that are not captured by the stream gauge [*Son and Tague*, 2014]. In addition, to account for observed difference of rooting depth across watersheds, Providence watersheds are assigned a 2-m rooting depth, and Bull watersheds are assigned a 1-m rooting depth [*Hunsaker et al*., 2012].

To evaluate the model streamflow accuracy, this study adopts a multi-objective approach. Many hydrologic modeling studies show that using a single accuracy measure can bias the evaluation of model performance [*Dunn*, 1999]. This study's accuracy measures are listed in equations 1-4. Each measure focuses on an aspect of flow variation. The Nash-Sutcliffe efficiency (NSE) [*Nash and Sutcliffe*, 1970] focuses on peak streamflow. LNSE is the log value of the Nash-Sutcliff efficiency and focuses on low flow. PerErr is percent volume error and focuses on flow bias The three accuracy measures are combined to evaluate the model streamflow accuracy robustly (Equation 4). This accuracy measure ranges from 0 to 1.

$$\mathrm{NSE} = 1 - \frac{\sum_i \left(Q_{obs,i} - Q_{sim,i}\right)^2}{\sum_i \left(\overline{Q_{obs}} - Q_{sim,i}\right)^2} \tag{1}$$

$$\mathrm{LNSE} = 1 - \frac{\sum_i \left(\log(Q_{obs,i}) - \log(Q_{sim,i})\right)^2}{\sum_i \left(\log(\overline{Q_{obs,}}) - \log(Q_{sim,i})\right)^2} \tag{2}$$

$$\mathrm{PerErr} = \frac{\left(\overline{Q_{obs}} - \overline{Q_{sim}}\right)}{\overline{Q_{obs}}} \tag{3}$$

$$\text{Total accuracy} = \mathrm{NSE} \times \mathrm{LNSE} \times \left|1 - \mathrm{PerErr}\right| \tag{4}$$

Where $Q_{obs,i}$ is the observed streamflow and $Q_{sim,i}$ is the simulated flow at daily time step (i), and $\overline{Q_{obs}}$ and $\overline{Q_{sim}}$ are the long-term average of observed daily streamflow and simulated streamflow, respectively.

Mean annual values for each flux (flow, ET and NPP) were computed to quantify the long-term average ecohydrologic responses to climate. The coefficient of variation (COV) was also calculated to quantify the inter-annual variation of each flux for climate sensitivity. The sensitivity of the mean and COV for each flux to DEM resolution was calculated. Here

a long-term historical climate data (>50 years) is required to investigate the sensitivity of model estimates to inter-annual climate variability. However, in the Providence and Bull watersheds, the streamflow and basic climate data are relatively short, 5 years. Therefore, this study used the long-term climate data of the Grant Grove station where the station is located at 20km away from the Bull watersheds. The Grant Grove station has a similar temporal precipitation and temperature patterns to the Providence and the Bull climate stations. The long-term climate data for the Providence and the Bull climate stations were estimated by fitting the local climate station data to Grove Grant station data. Mean annual precipitation of the Bull and Providence stations for the period of 2003 to 2007, and 2002 to 2006 respectively was divided by mean annual precipitation of Grant Grove station in order to estimate precipitation scaling factors for each station. To generate long-term daily precipitation data for the Providence and the Bull stations, the respective precipitation scaling factor (1.22 and 1.21) was applied to Grant Grove station's daily precipitation data. To generate long-term daily maximum and minimum air temperature data for the two watersheds, linear regression models were estimated by fitting the local temperature data from the Providence and Bull climate stations to the Grant Grove station's climate ($0.73<R^2<0.89$).

1.3.4 Effect of DEM resolution on model accuracy and long-term ecohydrologic responses to climate

This study tested the effect of DEM resolution on the accuracy of modeled streamflow (Equation 1-4), and on the sensitivity of estimated ecohydrologic response to inter-annual climate variability. Three hypotheses were developed with respect to differences in the sensitivity of the model estimates to DEM resolution for transient snow watersheds (TSWs)

and snow-dominated watersheds (SDWs). The first hypothesis is that the flow estimates for TSWs are more sensitive to DEM resolution than the flow estimates for SDWs. The underlying assumption for this hypothesis is that TSWs may have a larger change in precipitation phase (snow vs rain) with changing spatial resolution of DEM because TSWs more frequently experience air temperature close to 0 °C (threshold temperature, Table 1.2) than SDWs. The change in precipitation phase affects snow accumulation, which influences melt rates and streamflow estimates. Flow estimates in TSWs therefore will be more sensitive to DEM resolution than flow estimates in SDWs. The second hypothesis is that the change in spatial variance of wetness index is the dominant topographic parameter that determines the flow sensitivity to DEM resolution. When DEM resolution is coarser, a larger change in the spatial variance of wetness index for the eight watersheds is observed (Figure 1.5d). Even though RHESSys does not use wetness index directly for calculating the flow, change in spatial variance of wetness index with a coarsening DEM may reflect the influence of DEM resolution on the flow network in RHESSys and ultimately the accuracy of flow estimates [*Kenward et al.*, 2000].

This study also compared the sensitivity of four key ecohydrologic estimates to DEM resolution - annual streamflow, summer streamflow (August flow), annual ET and annual NPP. The third hypothesis is that the sensitivity of annual and summer streamflow estimates are more sensitive to DEM resolution than annual ET and NPP estimates. Here it is assumed that flows are controlled by topographic variation; the dominant controls of ET and NPP are climate and vegetation properties.

1.4 Results

1.4.1 Effect of DEM resolution on snow predictions

To evaluate the effect of DEM resolution on SWE estimates, we calculated the watershed scale peak SWE at the five different resolutions and the mean absolute difference in the watershed averaged daily SWE estimates between the 5m resolution and other coarser resolutions (Figure 1.6). Peak SWE across the watershed ranges from 303mm to 607mm for the 5m resolution model. The change in peak SWE estimate between the different resolutions is always less than 3% (Figure 1.6a). The mean absolute difference in watershed averaged SWE between 5m and other coarser resolutions varies between watersheds (Figure 1.6b). The differences range from 0.3mm to 4.5mm. For most watersheds, coarsening the DEM increases the absolute difference in SWE estimate between the 5m resolution and each of the coarser resolutions. For most watersheds, the largest change in SWE estimate occurs for estimates using the 90m and 150m resolutions. Among TSWs, P301 has the largest SWE change at 90m and 150m as 2.4mm and 4.3 mm, compared with the 5m resolution. Among SDWs, T003 has the largest SWE change at 90m as 2.4mm, and B203 has the largest SWE change at 150m as 4.5mm. The difference in SWE change with coarsening DEM is minor between the eight watersheds.

1.4.2 Effect of DEM resolution on streamflow prediction accuracy

To quantify the effect of DEM resolution on streamflow predictions, we calculated the change in the four different streamflow accuracy measures with coarsening DEM and compared the change in the streamflow accuracies between the eight watersheds. Figure 1.7 shows that the model accuracies declined with coarsening DEM resolutions for all watersheds. In general, there is a threshold resolution (10m) above which coarser resolutions

have a larger effect on streamflow prediction accuracy. Among TSWs, P304 and D102 equally have the largest reduction in streamflow total accuracy (eq.4) from 0.30 to 0.09(71%) between 10m and 30m, and from 0.30 to 0.09(71%) between 5m and 90m respectively. P301 has the smallest reduction in streamflow accuracy (Eq.4) from 0.48 to 0.36(25%) between 5m and 90m. Among SDWs, B203 has the largest reduction in streamflow accuracy from 0.64 to 0.29 (55%) between 5m and 150m. T003 has the smallest reduction in streamflow accuracy (eq.4) from 0.55 to 0.47(15%) between 10m and 90m. In general, streamflow estimates for the SDWs are more accurate and less sensitive to coarsening DEM resolution than were the TSWs.

Among the accuracy measures, PerErr changes most with coarsening DEM compared to the other individual measures (Figure 1.7b, 1.7c and 1.7d). High sensitivity of PerErr may reflect the model error due to different watershed boundaries and the impact of resolution on evapotranspiration estimates. LNSE values for most watersheds are least sensitive to DEM resolution (Figure 1.7c). NSE values for the TSWs are more sensitive to changes in DEM resolution than NSE values for the SDWs (Figure 1.7b). Among TSWs, NSE and LNSE values for P301 are the least sensitive to DEM resolution. The streamflow estimates for P304 are also the least accurate by all measures compared to the other TSWs. Most watersheds have the highest streamflow accuracy at 5m, however in P304, the 5m resolution model failed to reproduce observed streamflow at an acceptable level (Eq.4>0). In RHESSys, surface topography is assumed to reflect the subsurface topography, but this assumption may not be valid in this watershed. Among TSWs, P304 with poor model performance has the highest summer flow rate [*Hunsaker et al*., 2012], and shows different sediment load variability, sources and erosion rates than other TSWs [*Hunsaker and Neary*, 2012].

The 150m resolution models for transient snow watersheds, P301, P304 and D102 have higher accuracy than the 90m resolution models. Similar results are observed for some SDWs where the 5m resolution model has lower streamflow accuracy than the 10m resolution model. Among SDWs, the streamflow accuracy for B201 is similar to those for TSWs, especially regarding LNSE measure and NSE and LNSE for B201 are more sensitive to DEM resolution compared to the other watersheds. According to the study of [*Liu et al.*, 2012], B201 has lower subsurface flow component, compared with other seven watersheds, and the authors hypothesize that the bedrock geomorphology at B201 may be different from the other watersheds. These results suggest that the model accuracy of streamflow depends on how well surface topography at different resolution may reflect the subsurface topography for individual watersheds.

1.4.3 Sensitivity of estimated ecohydrologic variables to DEM resolution

This study investigated how DEM resolution affects the long-term average ecohydrologic responses (annual flow, summer flow, annual ET, and annual NPP) to climate (Figure 1.8). Mean annual streamflow generally increases with coarser DEMs, especially for resolutions that are coarser than 30m resolution. P304 and B203 are exceptions. T003 has the largest increase (44%) in mean annual flow, and B204 has the smallest increase (8%) in mean annual flow. Of the eco-hydrologic variables that we examined, mean summer flow is the most sensitive to DEM resolution, especially for SDWs and generally increases with coarser DEMs. Among SDWs, T003 has the largest increase (150%) in mean summer flow with coarsening DEM. Among TSWs, P303 has the smallest decrease (21%) in mean summer flow. Mean annual ET for SDWs are more sensitive to DEM resolution than TSWs. Coarsening DEM reduces mean annual ET. B201 has largest change (33% decreases) in

mean annual ET, and P301 has the smallest change (16% decreases) in mean annual ET. For most watersheds, coarsening the DEM decreases the mean annual NPP. Compared with TSWs, mean annual NPP for SDWs is more sensitive to DEM resolution. T003 has the largest (50%) decreases in mean annual NPP, and P303 has least (14%) decreases in mean annual NPP.

We investigated the effect of DEM resolution on the sensitivity of each flux to inter-annual climate variation by calculating the COV at each resolution (Figure 1.9). TSWs tend to have higher COV than SDWs for estimated annual streamflow, summer flow, annual ET, and annual NPP at 5m. Coarsening the DEM has varied effects on the COV between watersheds, and the variables of interest. Between watersheds, SDWs have higher changes in COV with coarsening DEM resolution than TSWs. SDWs have larger increase in COV for annual NPP, and have larger decrease in COV for summer flow. There is not a large difference in change of COV values for annual flow and annual ET between TSWs and SDWs. The COV values of annual NPP have the largest change with coarsening DEM, and the COV values of annual flow have the smallest change.

1.5 Discussion and summary

This study aimed to improve our understanding of how DEM resolution affects the ecohydrologic estimates in the context of climate change effect analysis in mountain watersheds. Three hypotheses were developed to test the DEM sensitivity between watersheds and between the variables of interest: 1) model estimates for transient snow watersheds (TSWs) will have higher sensitivity to DEM resolution than the model estimates for snow-dominated watersheds (SDWs); 2) changes in spatial variation of wetness index

will explain the watershed sensitivity to DEM resolution; and 3) flow estimates will be more sensitive to DEM resolution than ET and NPP estimates.

This study showed that there is a clear threshold resolution (10m) above which coarser resolutions have large effects on streamflow prediction accuracy (Figure 1.7). Among the eight watersheds, TSWs tend to have both lower streamflow accuracy and larger reduction of streamflow accuracy with coarsening DEM resolution (Table 1.3). Among TSWs, streamflow accuracy for P304 and D102 are most sensitive to DEM resolution, but P301 is the second least sensitive watershed to DEM resolution between the eight watersheds. The first hypothesis that implied that sensitivity to DEM resolution is closely linked snow accumulation and melt characteristics is, therefore, not supported. The change in peak SWE with coarsening DEM is very minor for all eight watersheds, and P301, with lowest sensitivity to DEM resolution, has the largest change in watershed absolute difference in SWE between 5m and 150m (Figure 1.5). Thus, the difference in dominant precipitation phase between TSWs and SDWs do not lead to consistent differences in the sensitivity of flow estimates to changes in the model resolution.

Among topographic parameters, we hypothesized that the change in spatial variation of the wetness index can explain the watershed sensitivity to DEM resolution. Changing the spatial variance of wetness index has a complex relationship with coarsening DEM, and varies between watersheds. However, the lowering in spatial variance of wetness index with coarsening DEM corresponds with a reduction of streamflow accuracy (Table 1.3). For example when the 5m resolution model was compared with coarser resolution models, P301 and D102 have the smallest reduction (-9%) and the largest reduction (-26%) of spatial variance of wetness index, respectively, which corresponds with the smallest and largest reductions of streamflow accuracy for the two watersheds (-25% and -71%, respectively).

Among the eight watersheds, T003 has smallest reduction (-15%) of streamflow accuracy and the watershed shows an increase (11%) of spatial variance of wetness index. RHESSys does not use the wetness index directly to calculate lateral flow. However, the wetness index includes the component of topographic slope and flow accumulating area. RHESSys actually uses these components to determine the lateral flow paths. Previous studies of using TOPMODEL [*Beven and Kirkby*, 1979] also showed that decreasing resolution reduces the spatial variance of topographic index [*Pradhan et al*., 2008; *Zhang and Montgomery*, 1994]. *Pradhan et al*. [2006] showed that when a coarser DEM resolution (1000m) reproduces the cumulative distribution of topographic index at the fine resolution (50m), the model streamflow estimates using the coarser 1000m DEM resolution matches the simulated streamflow in the 50m DEM resolution TOPMODEL without recalibration. Results in this study suggest that the change in wetness index distribution will also be a good indicator of whether coarsening the DEM will lead to reduced accuracy for an explicit routing model. Kenward et al. [2000] tested the impact of DEM resolution on streamflow accuracy and spatial pattern of predicted saturated area using DHSVM[*Wigmosta et al.*, 1994] that has similar routing scheme to RHESSys. Their study also showed that the spatial distribution of wetness index correspond to the depth to saturation and runoff production for a rain-dominated system in the WF-38 experimental watershed at the Mathantango Creak, PA. Our study confirms that the impact of DEM resolution on flowpaths is also likely to be important for snow and rain-snow transition watersheds and that the impact of model resolution of the lateral redistribution of water may be more important than its impact on snow accumulation and melt for models of low order, headwater watersheds.

Our modeling results found that among the four ecohydrologic estimates of interest, DEM resolution has the largest effects on mean summer flow and COV of annual ET and

NPP (Figure 1.7 and 1.8). One of the eight watersheds, T003 has the least reduction in streamflow accuracy with coarsening DEM. but changes of mean summer flow (150%), COV of annual ET (65%), and COV of annual NPP (60%) are observed. These results therefore emphasize that accurate streamflow prediction does not guarantee model ability to capture long-term ecohydrologic responses to climate change. Our study also suggests that using a fine-resolution DEM in hydrologic modeling is essential to capture the long-term observed summer flow. Since summer flow is an important water resource and has important ecological effects (e.g., salmon habitat) in California, fine-scale hydrologic modeling for assessing the effect of climate change in the Sierra Nevada watershed is necessary[*Tague and Dugger*, 2010].

Our modeling study clearly showed that coarsening DEM resolution results in increase in COV of both ET and NPP. This result implies that coarser resolution models overestimate the sensitivity of theses processes to climate variation. This result is important for studies on climate change's effect on ecosystem health. The reduced sensitivity of ET and NPP of the finer resolution models may illustrate the role of micro-refuge created by substantial variation in topographic properties in mountain environments[*Dobrowski*, 2011]. *Dobrowski* [2011] showed case studies that terrain allows for local climate condition to be decoupled from regional climate, and the sites decoupling with regional climate can be good candiation for micro-refuges.

In summary, this study demonstrated that using fine-scale topographic variation in hydrologic modeling is required to reproduce the measured streamflow as well as capture climate driven inter-annual ET and NPP variability; coarser resolution models tend to have lower streamflow accuracy and overestimate climate sensitivity for ET and NPP. This study demonstrated that due to the non-linear resolution between model accuracy/sensitivity and

DEM resolution, substantial improvement are made by increasing resolution from 30m to 10m, and further increasing the resolution to 5m results in smaller gains in performance, compared to the computation cost.

Figures

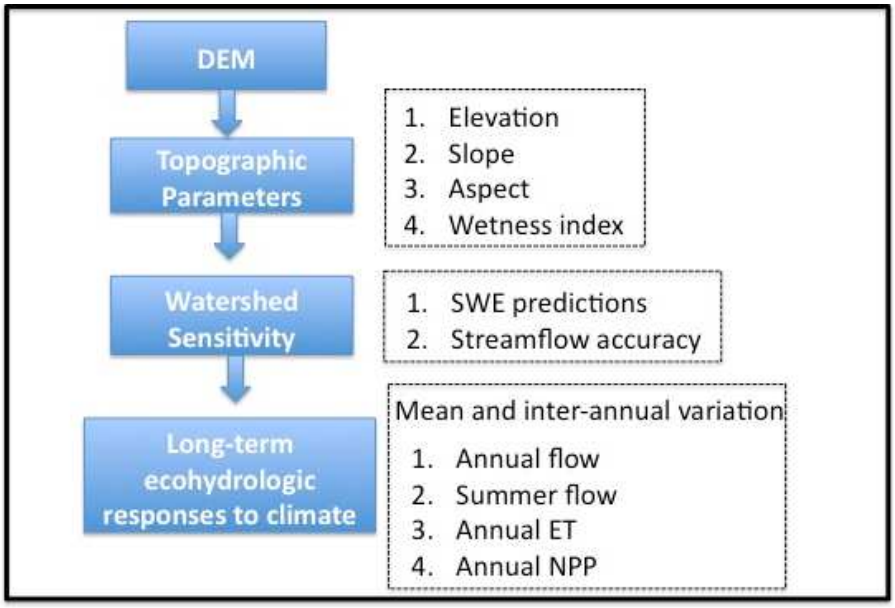

Figure 1.1. Framework for studying the effect of DEM resolution on the topographic parameters, the watershed sensitivity and the long-term ecohydrologic responses to climate in the eight Sierra Nevada watersheds.

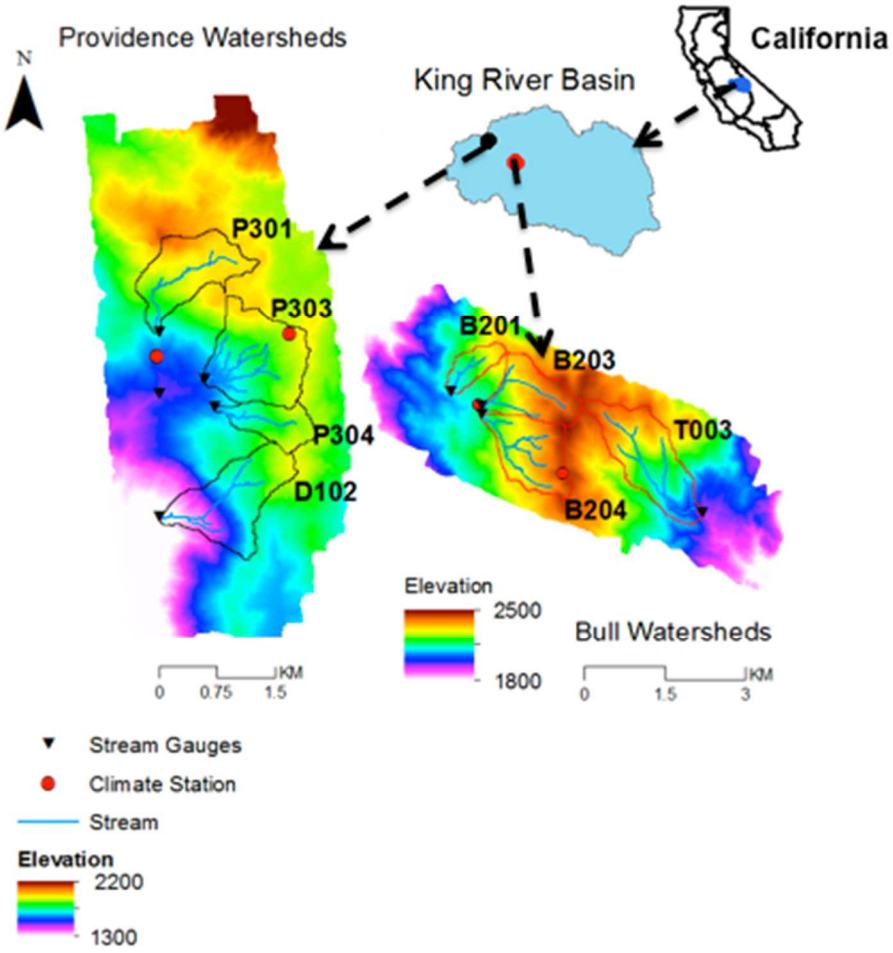

Figure 1.2. The location of climate stations, streamflow gauges stations and elevation gradients of study sites: (left) Providence watersheds and (right) Bull watersheds.

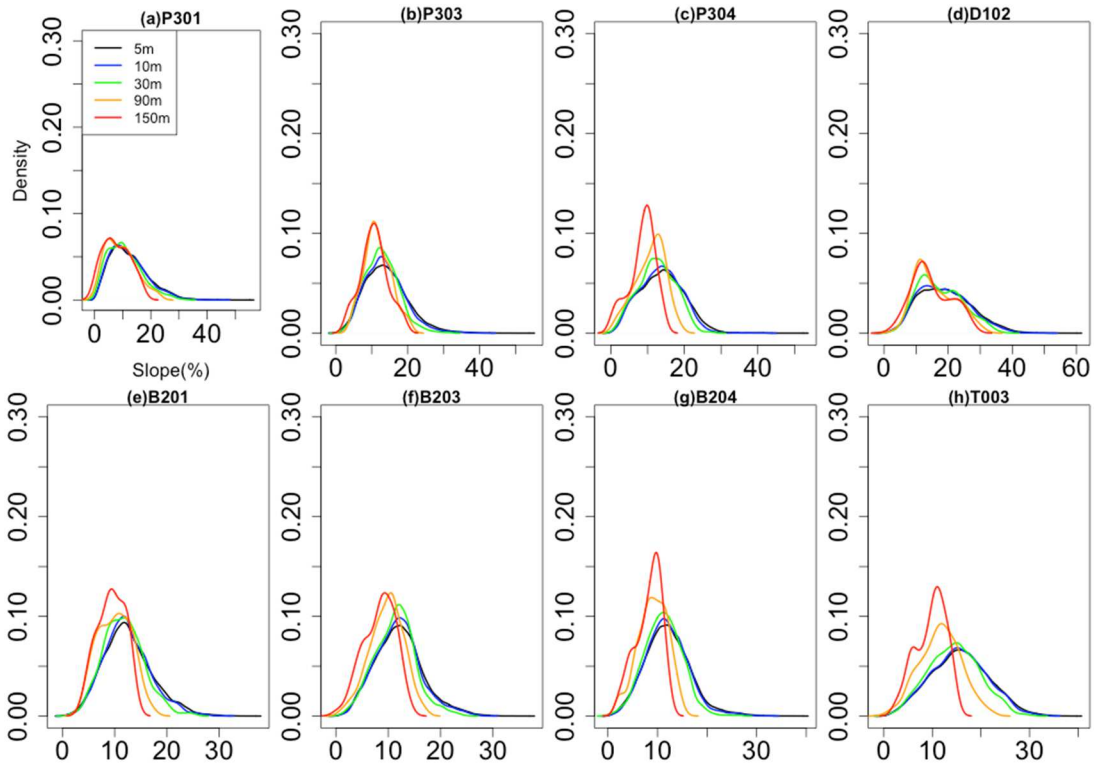

Figure 1.3. Distribution of slope computed using different DEM resolutions: (a) P301, (b) P303, (c) P304, (d) D102, (e) B201, (f) B203, (g) B204 and (h) T003. The first column displays the TSWs, and the second column displays the SDWs.

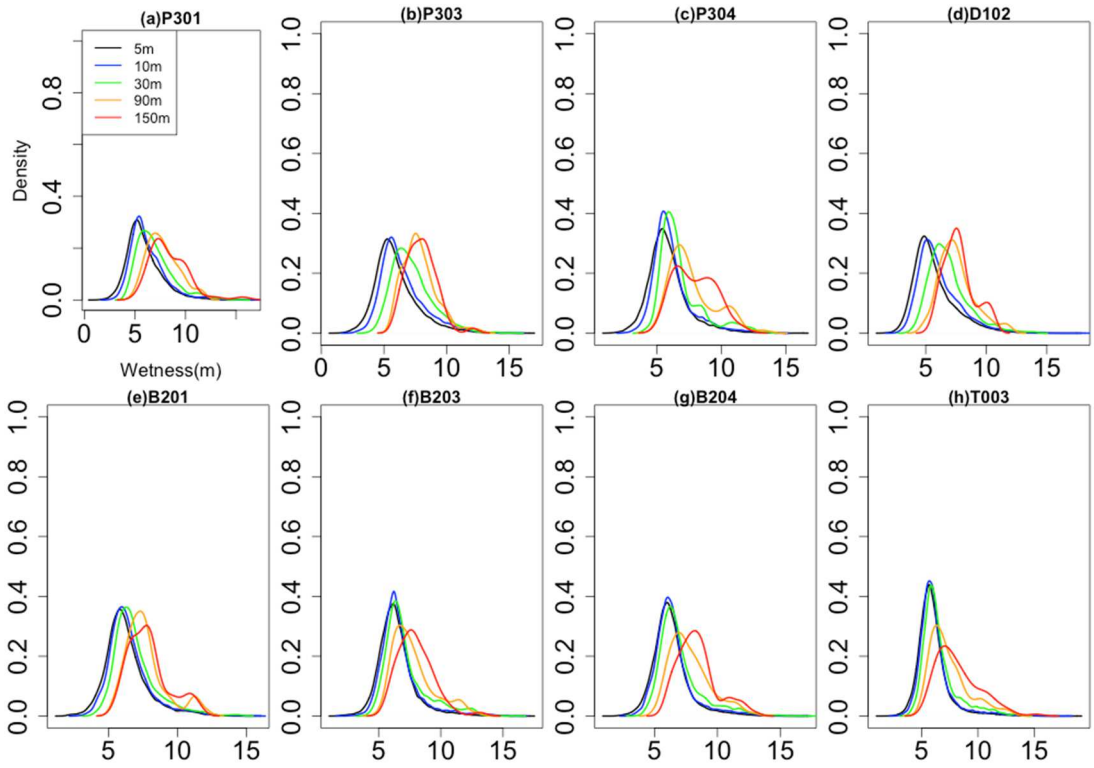

Figure 1.4. Distribution of topographic wetness index computed using different DEM resolutions: (a) P301, (b) P303, (c) P304, (d) D102, (e) B201, (f) B203, (g) B204 and (h) T003. The first column displays the TSWs, and the second column displays the SDWs.

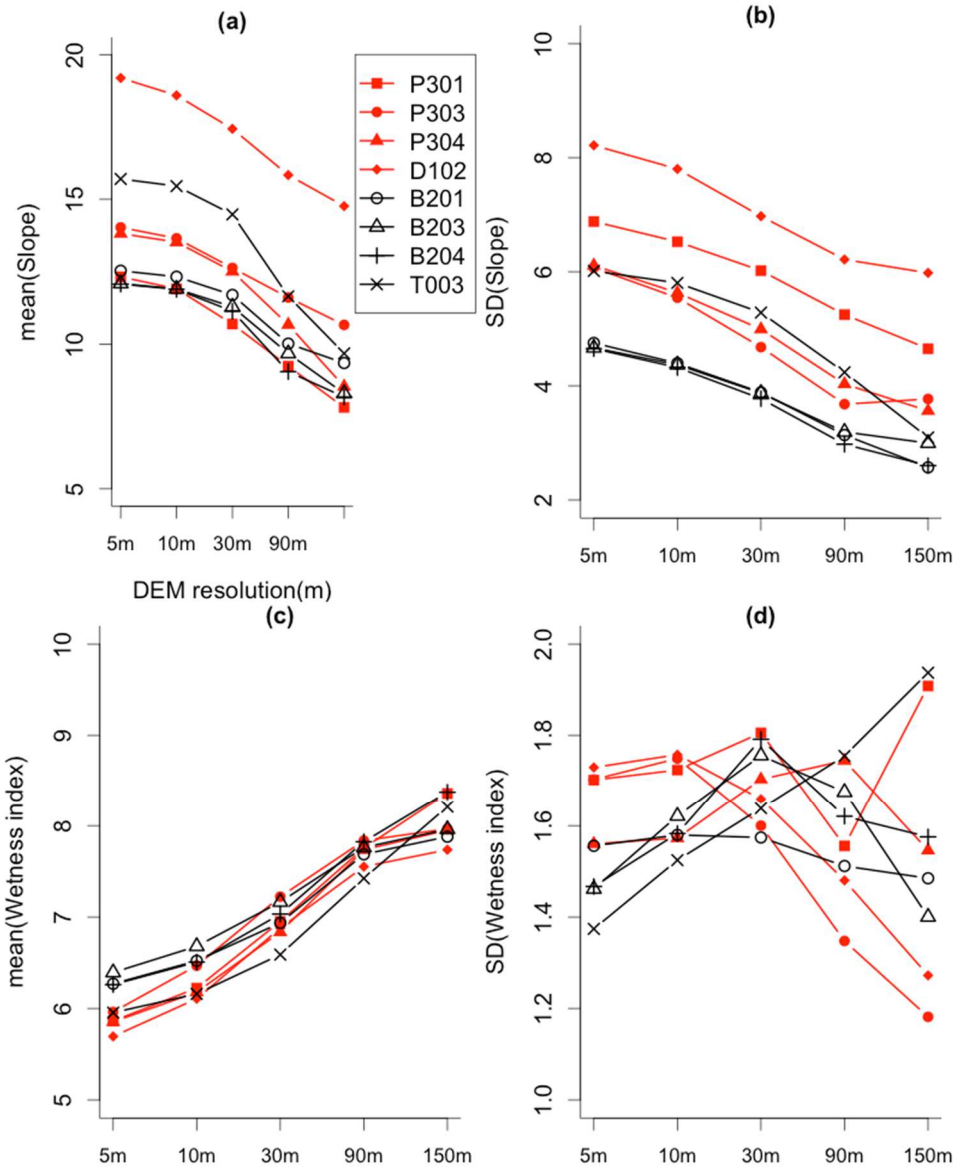

Figure 1.5. Watershed-scale statistical properties (mean and stand deviation) for slope and wetness index in the eight Sierra Nevada watersheds computed with increasingly coarse DEM resolution: (a) watershed mean values of slope, (b) watershed standard deviation values of slope, (c) watershed mean values of wetness index, and (d) watershed standard deviation values of wetness index. Red color refers to TSWs; black color refers to SDWs.

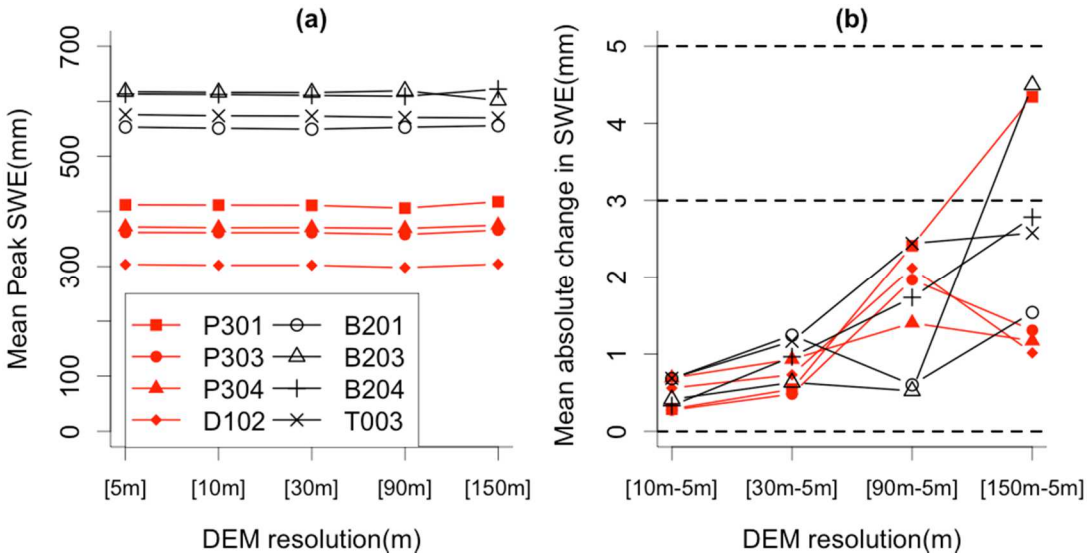

Figure 1.6. Watershed peak SWE estimate between various resolution and absolute difference in watershed mean SWE estimate between the 5m resolution and the coarser resolutions (10m, 30m, 90m, and 150m) in the eight Sierra Nevada watersheds: (a) peak SWE, and (b) the difference in mean absolute watershed SWE between 5m and coarser resolutions.

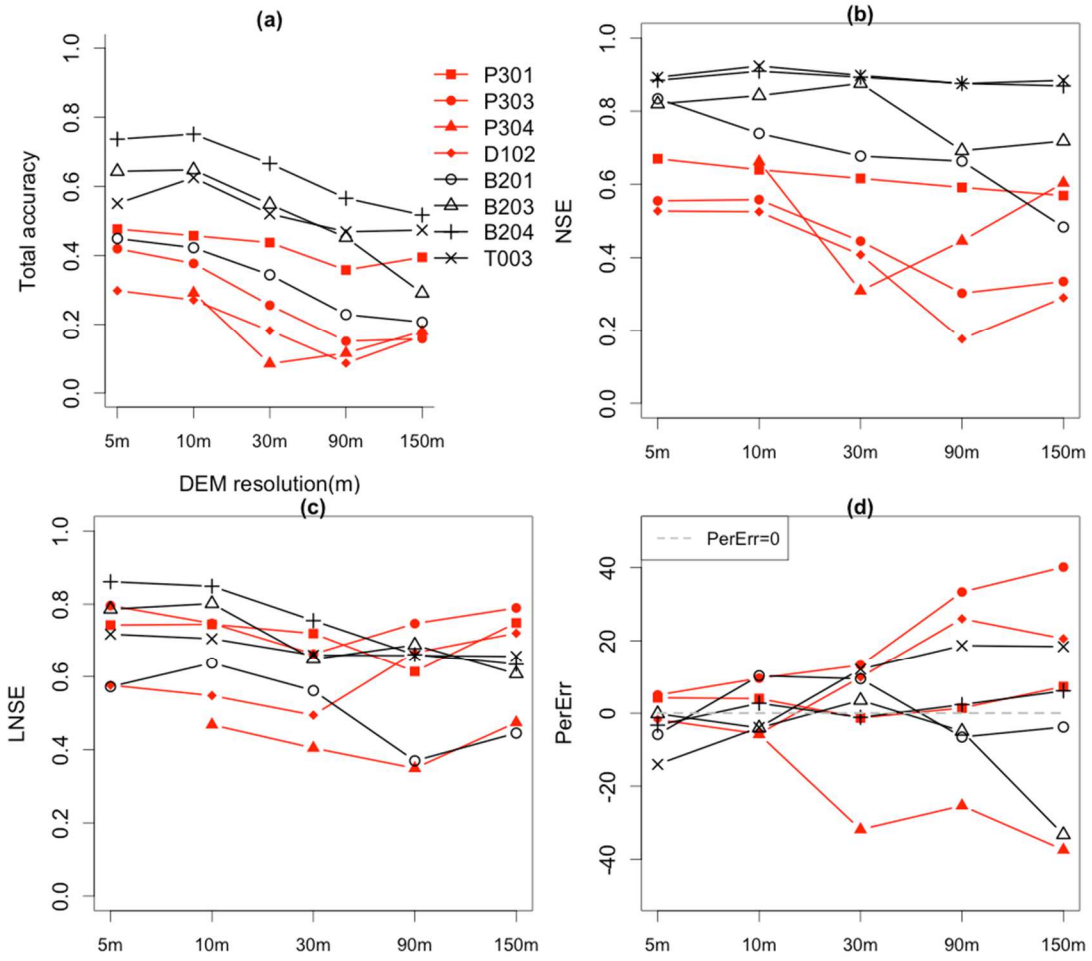

Figure 1.7. The model performance of streamflow prediction with different DEM resolutions: (a) Total accuracy measure combing NSE, LNSE and PerErr, (b) NSE, (c) LNSE, and (d) PerErr (Percent Error).

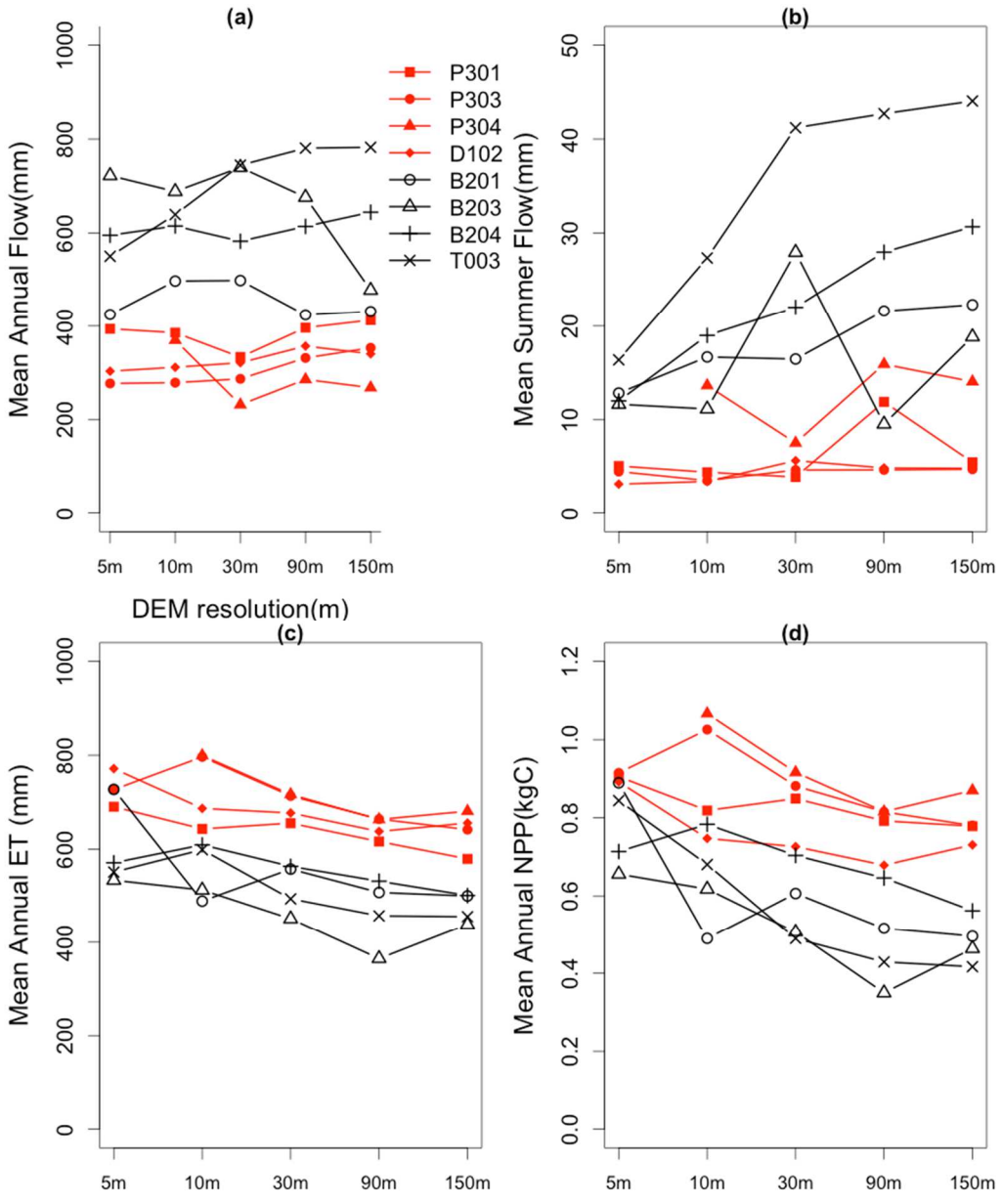

Figure 1.8. Annual mean of estimated ecohydrologic responses to climate with different DEM resolution (a) mean annual flow, (b) mean summer (August) flow, (c) mean annual ET, and (d) mean annual NPP

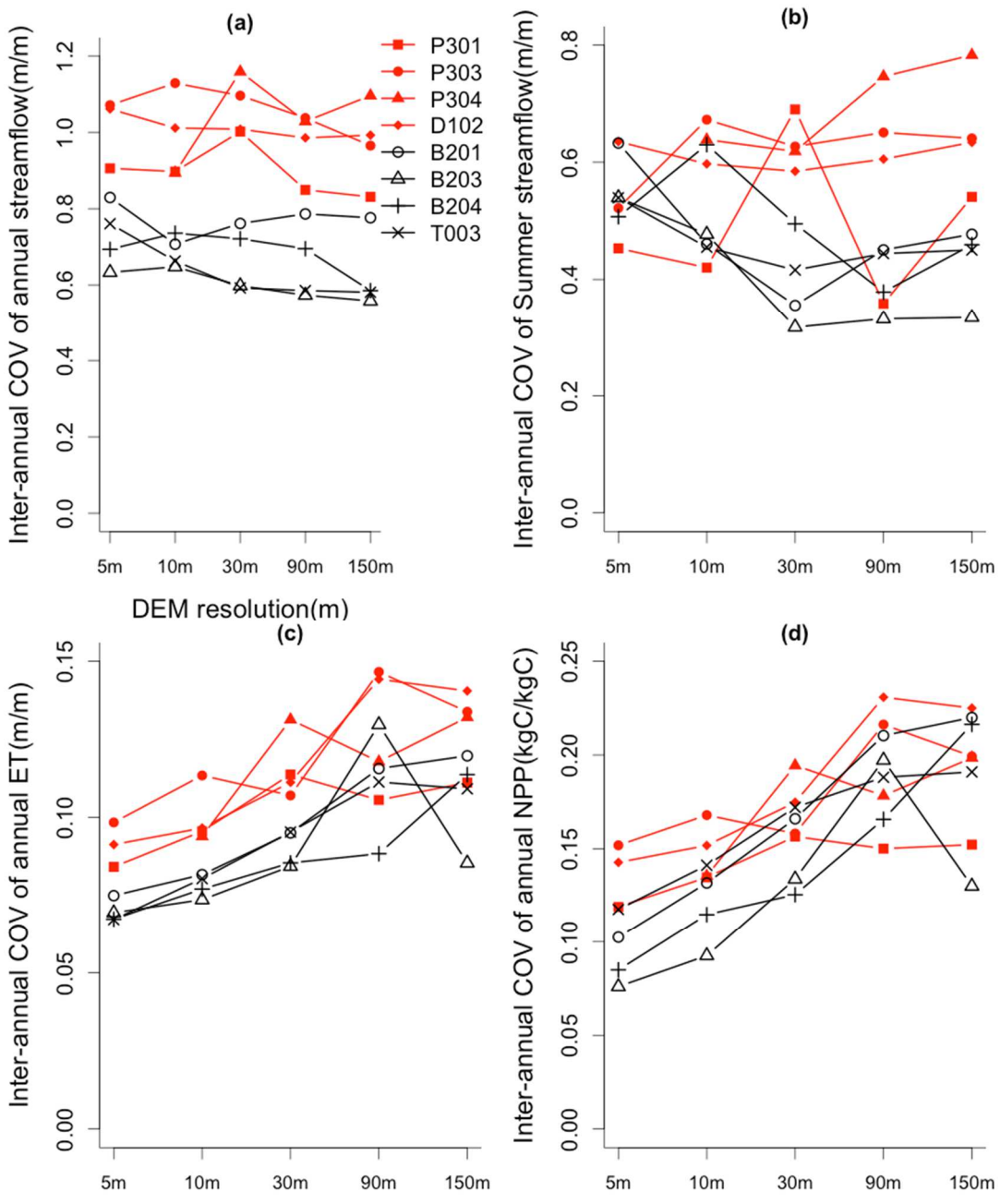

Figure 1.9. Inter-annual variability (coefficient of variance (COV)) of estimated ecohydrologic responses to climate with different DEM resolution (the variability was measured by coefficient of variance (COV)): (a) inter-annual streamflow variability, (b) inter-annual August streamflow variability, (c) inter-annual ET variability and (d) inter-annual NPP variability.

Tables

Table 1.1. The watershed mean values of topographic parameters with various DEM resolution (5m, 10m, 30m, 90m and 150m) for the Providence watersheds and the Bull watersheds.

Watershed	Watershed mean value of topographic parameters[1]					
	Parameter	DEM Resolution				
		5m	10m	30m	90m	150m
P301	Elevation (m)	1975.9	1976.6	1976.7	1975.5	1982.1
	Slope (°)	12.3	11.9 ***	10.7***	9.2***	7.8***
	Aspect[2] (°)	258.8	259.0	256.5	256.3	266.6
	Wetness (m)	5.9	6.2***	7.0***	7.8***	8.4***
P303	Elevation (m)	1894.8	1894.5	1895.4	1890.9	1901.7
	Slope (°)	14.0	13.7***	12.6***	11.6 ***	10.7***
	Aspect[2] (°)	214.4	214.9	214.4	212.4	218.2
	Wetness (m)	6.0	6.5***	7.2***	7.8***	8.0***
P304	Elevation (m)	1898.1	1896.8*	1898.1	1894.3	1905.5
	Slope (°)	13.8	13.5***	12.5***	10.7***	8.5***
	Aspect[2] (°)	165.8	166.5	167.1	162.5	169.7
	Wetness (m)	5.9	6.2***	6.8***	7.7***	8.0***
D102	Elevation (m)	1772.0	1774.8**	1772.8	1767.4	1785.4

	Slope (°)	19.2	18.6***	17.4	15.8***	14.8***
	Aspect^2 (°)	200.8	200.9	200.8	199.6	203.4
	Wetness (m)	5.7	6.1***	6.9***	7.6***	7.7***
B201	Elevation (m)	2253.8	2253.7	2254.4	2251.9	2248.4
	Slope (°)	12.5	12.3***	11.7 ***	10.0***	9.3***
	Aspect^2 (°)	217.2	217.2	215.8	215.4	214.8
	Wetness (m)	6.3	6.5***	6.9***	7.7***	7.9***
B203	Elevation (m)	2371.9	2371.6	2372.4	2372.7	2369.6
	Slope (°)	12.1	11.9***	11.3***	9.7***	8.3***
	Aspect^2 (°)	189.4	189.5	188.9	184.9	184.0
	Wetness (m)	6.4	6.7 ***	7.2***	7.8***	8.0***
B204	Elevation (m)	2360.3	2360.0	2360.7	2361.0	2357.3
	Slope (°)	12.1	11.9***	11.1***	9.0***	8.2***
	Aspect^2 (°)	178.2	177.8	176.7	173.2*	172.6*
	Wetness (m)	6.3	6.5***	7.0***	7.8***	8.4***
T003	Elevation (m)	2286.5	2287.0	2285.8	2283.2	2292.8
	Slope (°)	15.7	15.5***	14.5***	11.7***	9.7 ***
	Aspect^2 (°)	304.0	304.1*	305.1***	309.3***	308.8***

Wetness (m)	6.0	6.2***	6.6***	7.4***	8.2***

1: Watershed-scale parameter values, 2: Aspect is calculated with Grass GIS program (r.slope.aspect): 90° is North, 180° is West, 270° is South, and 360° is East. The aspect having zero is used to indicate undefined aspect in flat areas with slope having zero. p-value of Wilcox rank-sum test; Asterisks indicate a significant difference in mean values between the topographic parameters computed using the 5m DEM and those using the coarser DEM (*p<0.1; **p<0.05;***p<0.01),

Table 1.2. Calibrated snow-related parameters and the model accuracy of snow predictions for the Providence and Bull watersheds.

	Snow-related parameters			Model accuracy of snow predictions	
Watershed	Temperature laps rates[1] (tmax /tmin) (°C/m)	Temperature threshold for rain vs snow[2] (°C)	Temperature melt coefficient[3] (m/°C)	Day of snow melt[4]	SWE[5]
Providence	0.0063/-0.0064	-3-3	0.005	0.92	0.91
Bull	0.0068/-0.0060	-3-3	0.005	0.83	0.83

1: Since fine-spatial scale air temperature is not available in the two watersheds, air temperature within a watershed is spatially interpolated with the given elevation and the calculated temperature laps rates.

2: To partition total precipitation into snow and rain, we use the air temperature as a proxy variable, and the proportion of snow and rain in the total precipitation is linearly interpolated based on the minimum and maximum temperature values.

3: Temperature melt coefficient accounts for snow melt due to latent heat and sensible heat.

4: The day of snowmelt is estimated using observed snow depths and modeled SWE value, and the correlation coefficient is measured.

5: The measured SWE data are available in the upper Providence and upper Bull station.

Table 1.3. Watershed sensitivity to DEM resolution.

Watershed group	Watershed	Change in spatial variance of wetness index (%)	Change in streamflow accuracy (Eq.4) (%)	Model-based Rank[5]
	P301	-9[1](3)[2]	-25[3](-14)[4]	7
TSWs	P303	-31(-14)	-64(-44)	3
	P304	-1(5)	-71(-42)	1
	D102	-26(-11)	-71(-41)	2
SDWs	B201	-5(-1)	-54(-33)	5
	B203	-4(11)	-55(-25)	4
	B204	7(12)	-30(-15)	6
	T003	11(25)	-15(-5)	8

1: the largest change in spatial variance of wetness index between the five resolution models

2: the mean change in spatial variance of wetness index between the five resolution models

3: the largest change in streamflow accuracy between the five resolution models (Eq.4)

4: the mean change in streamflow accuracy between the five resolution models (Eq.4)

5: Ranked from highest to lowest sensitivity to DEM resolution, based on change in modeled streamflow accuracy

2. Interaction between soil parameter uncertainty and climate forcing in estimating ecohydrologic fluxes for California's Sierra watersheds

Abstract

This paper investigates the impact of soil parameter uncertainty on the estimation of ecohydrologic responses (streamflow, evapotranspiration (ET) and net primary productivity (NPP)) to inter-annual climate variation and climate warming in a transient snow watershed (TSW) and a snow-dominated watershed (SDW) located in Sierra National Forest, California. The Regional Hydro-Ecologic Simulation System (RHESSys) and Generalized Likelihood Uncertainty Estimation (GLUE) were used to quantify the predictive uncertainty of model estimates. Results showed that the model estimates for SDW had higher predictive uncertainty for daily streamflow than those for TSW, while the model estimates of annual ET and NPP for SDW had lower predictive uncertainty than those for TSW. At annual time scales, drier years have the highest sensitivity of annual streamflow estimates to soil parameter uncertainty in both watersheds, and intermediately wet years have highest sensitivity of annual ET and NPP estimates to soil parameter uncertainty in both watersheds. At monthly time scales, the effect of inter-annual climate variability on estimated monthly streamflow, ET and NPP in spring and winter are more significant than the effect of soil parameter uncertainty. However, the effect of soil parameter uncertainty and climate drivers on estimated inter-annual variation in monthly streamflow, ET and NPP is equally important in summer period. The effect of soil parameter uncertainty on estimating annual ecohydrologic variables is often greater than climate warming effects, and the soil parameter uncertainty effect becomes greater in drier years. The results emphasized the importance of

accounting for soil parameter uncertainty when estimating ecohydrologic responses to climate.

2.1 Introduction

Hydrologic models are the primary tools used to predict how climate change will alter hydrologic and ecologic conditions in watersheds. In most applications, hydrologic models are calibrated with measured streamflow, and optimum parameter values are selected. However, selecting an optimum parameter value may be misleading because many different parameter values reproduce the observed streamflow with similar accuracy [*Beven and Freer*, 2001]. Among model parameters, soil parameters are a major source of uncertainty in hydrologic modeling [*Loosvelt et al*., 2011; *Shields and Tague*, 2012]. Soil parameters control vertical drainage and lateral soil moisture distribution along hillslopes, and influence the available water for plants and drainable water that affects the runoff generation [*Rodriguez-Iturbe*, 2000; *Loosvelt et al.*, 2011; *Shields and Tague*, 2012]. However, determining the appropriate soil parameter values at the large scales (hillslope and catchment) remains challenging [*Samaniego et al.*, 2010]. Field-based estimation of soil properties (depth, hydraulic conductivity and porosity, etc.) is labor intensive, and soil parameters estimated using soil core samples only represent matrix flow.

The sensitivity of model estimates to soil parameter uncertainty varies with study site and the variable of interest [*Kay et al.*, 2010; *Lundquist and Loheide*, 2011; *Jung et al.*, 2012; *Shields and Tague*, 2012]. *Shields and Tague* [2012] found seasonal differences in the sensitivity of evapotranspiration and streamflow estimates to soil parameter uncertainty for a semi-arid mountain environment. Streamflow estimates were sensitive to soil parameters in the winter (early season runoff), and evapotranspiration estimates were sensitive to soil

parameter uncertainty in the growing season (spring and summer). *Jung et al*. [2012] compared a rain-dominated watershed with a snow-dominated watershed in terms of the model parameter uncertainty and its effect on future streamflow projections. Their research found that the prediction of winter runoff is more sensitive to model parameter uncertainty in a snow-dominated watershed than in a rain-dominated watershed. However, their study does not separate snow-related parameter effects from total parameter uncertainty effects and the snow-related parameters contribute to the greater parameter uncertainty in the snow-dominated watershed compared with the rain-dominated watershed. Since snow regimes are expected to change under a warming climate, the results of *Jung et al*. [2012] highlight the need for reduced uncertainty in snow parameters or improvements in snow models. Soil parameters differ from snow parameters because they may be expected to remain relatively stable at decadal time scales. Nonetheless uncertainty in these parameters may influence model estimates. In this study we focus specifically on soil parameter uncertainty and its relative influence on estimating ecohydrologic responses to climate for a snow-dominated watershed (SDW) and a transient snow watershed (TSW).

In recent decades, mountain regions in the western United States have experienced reductions in snow accumulation and earlier melt and streamflow peaks [*Stewart et al.*, 2004, 2005]. We also expect that changing snow accumulation and melt will alter soil moisture and vegetation water use and productivity [*Tague and Grant*, 2009; *van Mantgem et al*., 2009; *Goulden and Bales*, 2014], and this condition will be exacerbated in coming decades [*Maurer and Duffy*, 2005; *Cayan et al.*, 2008]. These changes can lead to water supply problems for downstream users [*Null et al.*, 2010], and may increase tree mortality [*van Mantgem et al.*, 2009] and fire frequency [*Westerling et al.*, 2006]. Many climate change impact studies in Sierra watersheds focus on large basin scales (>100km^2) that are

relevant for regional water management. However, because forest management practices and stream restoration projects are frequently applied within low-order *(<5th)* catchments, there is a need for climate impact studies at this scale. Studies of low-order catchments also contribute to a mechanistic understanding of climate change sensitivity.

In Sierra Nevada watersheds, a number of modeling studies have investigated the impact of climate change (warming and change in precipitation) on streamflow, evapotranspiration and vegetation productivity *[Knowles and Cayan, 2002; Maurer and Duffy, 2005; Tague and Grant*, 2009; *Goulden and Bales*, 2014]. Several of these studies have examined the sensitivity of model predictions to the uncertainty in climate change scenarios but to our knowledge, none have explicitly examined the impact of soil parameter uncertainty on estimates of future change. On the other hand, a number of studies [*Steinschneider et al*., 2012; *Wilby*, 2005] have developed uncertainty frameworks for explicitly incorporating parameter uncertainty in climate change impact analysis. However, their studies mainly focused on estimating streamflow and its predictive uncertainty under different climate scenarios and did not explicitly address the sensitivity of vegetation water use and productivity change to soil parameter uncertainty. Vegetation water use and productivity is strongly linked to available water in soil, and precipitation patterns and changes in vegetation water use will alter streamflow generation processes.

This study has two objectives: (1) we compare model accuracy of streamflow, and predictive uncertainty of ecohydrologic estimates (streamflow, evapotranspiration (ET) and net primary productivity (NPP)) due to soil parameter uncertainty for a TSW, and a SDW in the California Sierra, (2) we compare the variation of ecohydrologic fluxes to soil parameter uncertainty with the variation of these ecohydrologic fluxes due to climate warming. We expect that the sensitivity of model estimates will vary with the variable of interest (e.g

streamflow, ET, NPP) and between TSW and SDW. We use two small watersheds within the Upper Kings River basin in the California Sierra as case study examples of TSW and SDW. Previous field-based studies show that these two case study watersheds, TSW and SDW are expected to have different timing and magnitudes of snow accumulation and melt, and ET [*Bales et al*., 2011; *Goulden et al*., 2012; *Hunsaker et al*., 2012] due to elevation-based differences in air temperature. We test whether or not the hydrologic differences between the two watersheds lead to different predictive uncertainty of model estimates across soil parameter uncertainty. We use the Regional Hydrologic-Ecologic Simulation System (RHESSys) [*Tague and Band*, 2004] to test the impact of soil parameter uncertainty on model estimates. Uncertainty analysis is conducted with Generalized Likelihood Uncertainty Estimation (GLUE) [*Beven and Freer*, 2001].

2.2 Study sites and methodology

2.2.1 Study sites

We apply RHESSys to two small watersheds in California's Sierra Nevada, the Providence sub-watershed (P301, 1.32km^2) and the Bull sub-watershed (B203, 1.4km^2) located in the Kings River Basin (Figure 2.1), and part of Kings River Experimental Watersheds and Southern Sierra Critical Zone Observatory (SSCZO). In P301, 20 to 50% of the annual precipitation falls as snow. In B203, 75 to 95% falls as snow [*Hunsaker et al*., 2012]. Precipitation falls mostly between October and April, and the difference of mean annual precipitation between the two watersheds is less than 1%. Following the snow regime classification by *Jefferson* [2011], P301 is a transient snow watershed (TSW), and B203 is a snow-dominated watershed (SDW). Each watershed has two climate stations (Upper and

Lower Providence climate stations for TSW, Upper and Lower Bull climate stations for SDW). In both watersheds, one of the stations is located near the highest elevation of the watershed and the other station is located near the lowest elevation of watershed. The climate stations measure 15-min precipitation, air temperature, relative humidity, solar radiation, wind speed and direction, snow depth. The Upper climate stations in Providence and Bull also measure snow water equivalent (SWE) using snow pillow [Hunsaker et al., 2012]. In addition, each watershed has two stream flow gauge stations to measure low and high flows, and the two gauging stations are located at the outlet of each watershed. The elevation of TSW ranges from 1794 to 2102m and the elevation of SDW ranges from 2182 to 2490m (Figure.2.1). SDW has steeper slopes than TSW. SDW has a slightly higher wetness index [Beven and Kirkby, 1979] than TSW (Table 2.1). Both watersheds include Sierran mixed conifer forest with some mixed chaparral and barren land cover. The Sierran mixed conifer class is composed of white fir (Abies concolor), Red fir (Abies magnifica), ponderosa pine (Pinus ponderosa), Jeffrey pine (Pinus Jeffrey), black oak (Quercus kelloggii), suger pine (Pinus lambertiana) and Incense cedar (Calocedrus decurrens). The dominant forest type of TSW is white fir and the dominant forest type of SDW is red fir. We estimated the Leaf Area Index (LAI) based on Light Detection and Ranging (LIDAR) vegetation product (Table 2.1). TSW has denser tree cover (higher LAI) than SDW. The dominant soil type of TSW is Shaver (66%) and of SDW is Cagwin (80%). Both soil types are highly permeable and have high percentages of sand.

2.2.2 Ecohydrologic-modeling framework

We use the RHESSys model that was developed to simulate climate and land use change impacts on hydrology, carbon and nutrient cycling. The model includes a climate

interpolation model (MT-CLIM)[*Running et al.*, 1987] that predicts basic climate variables (solar radiation, saturation vapor pressure and relative humidity, etc.) and spatially interpolates those variables across landscapes. For example, atmospheric solar radiation is estimated based on site latitude, zone slope, aspect and east-west horizon values, and the incoming radiation is adjusted based on atmospheric transmissivity. The model calculates snow accumulation based on air temperature, and uses a quasi-energy budget approach to calculate the snow melt. Snow melt is computed based on radiation, a combination of sensible and latent heat, and advective heat (rain on snow). RHESSys accounts for vertical and horizontal water fluxes: vegetation interception, soil evaporation, transpiration, infiltration, capillary rise, shallow and deep groundwater lateral fluxes. A lateral shallow groundwater flux is calculated based on topography and soil hydraulic conductivity. Drainage from deep groundwater storage to the stream uses a simple linear reservoir model. A fixed percentage of infiltrated water is assumed to bypass the soil zone to the deep groundwater storage to account for preferential flow through soil macropores and bedrock fractures. RHESSys accounts for sunlit versus shaded leaves and canopy gaps in its radiative transfer routines. Evapotranspiration, including evaporation and sublimation of intercepted water, transpiration, soil and litter evaporation, is calculated using the Penman-Monteith equation. Stomatal conductance in the transpiration calculation is computed using the Jarvis model [*Jarvis*, 1976]. RHESSys has extended and adapted a carbon cycling model (BioME-BGC, [*Thornton et al*., 1998]), nutrient cycling model (Century model, [*Parton et al.*, 1998]) and vegetation regrowth model [*Landsberg and Waring*, 1997; *Dickinson and Shaikh*, 1998]. Net primary productivity is estimated as the difference between gross photosynthesis and respiration where gross photosynthesis is estimated using the Farquhar model [*Farquhar et al.*, 1980] and respiration is computed separately for different plant components (leaves,

live-dead wood and roots) as a function of biomass, nitrogen content and air temperature[*Ryan*, 1991]. RHESSys potentially has these capabilities but for this study, nutrient cycling model (Century model, [*Parton et al.*, 1998]) and vegetation carbon allocation sub model [*Landsberg and Waring*, 1997; *Dickinson and Shaikh*, 1998] are not used to alter canopy structure or soil biogeochemical cycling. If the model runs in "dynamic mode" where vegetation changed, the time trajectory of vegetation growth may confound the relationship between soil parameter uncertainty and the climate inputs. Therefore, for this study, vegetation is assumed to be static. A detailed description of the model equations is provided in the [*Tague and Band*, 2004]. RHESSys is under continuous development, and in this study, we use version 5.15.r326.

2.2.3 Model parameterization and uncertainty analysis

RHESSys requires basic climate data (daily minimum and maximum temperature and precipitation), and topography, vegetation and soil type maps to estimate model parameters. We use the Providence and Bull climate station data (daily minimum and maximum temperature and precipitation) from year 2003 to year 2008 for model calibrations. However, to estimate the sensitivity of model estimate to inter-annual climate variability, we use a long-term climate data set from the Grant Grove station located 20km away from SDW. Grant Grove station had similar timing and magnitude of precipitation and temperature to the climate stations in TSW and SDW. Long-term climate input data for TSW and SDW watersheds are estimated by adjusting Grant Grove station data based as follows: Mean annual precipitation of the Bull and Providence stations for the period of 2003 to 2007, and 2002 to 2006 respectively is divided by mean annual precipitation of Grant Grove station in order to estimate precipitation scaling factors for each station. To

generate long-term daily precipitation data for TSW and SDW, we apply the respective precipitation scaling factors (1.22 and 1.21) to Grant Grove station's daily precipitation data. To generate long-term daily maximum and minimum air temperature data for the two watersheds, linear regression models are estimated by fitting the local temperature data from the Providence and Bull climate stations to the Grant Grove station's climate. The correlation between minimum daily temperature and maximum daily temperature of Providence and Grant Grove stations results in R^2 of 0.89 and 0.85. The correlation between minimum daily temperature and maximum daily temperature of Bull and Grant Grove stations results in R^2 of 0.82 and 0.73. When the model was applied to both watersheds with the generated climate record, the streamflow accuracy is degraded for the both watersheds, especially for R_{eff} [Nash and Sutcliffe, 1970](0.88 to 0.79 for TSW and 0.94 to 0. 67 for SDW) but the model captures the seasonality of observed streamflow and the key difference between the two watersheds.

RHESSys has a hierarchical model structure that considers patch, zone, hillslope and watershed. Patches are the finest spatial model units related to snow, soil and vegetation dynamics. We use 30m LIDAR Digital Elevation Model (DEM) to define the patch map. The DEM was generated from 1m LIDAR DEM with the bilinear interpolation algorithm. Zones are related to climate processes (snow, air temperature and solar radiation). We set the zone map to be the same as the patch map to capture the fine-scale climate variation within these watersheds. The hillslope map is constructed based on the flow direction map, flow accumulation and streamline computed using Grass GIS routines (GRASS6.4). The watershed boundary is constructed using multiple flow direction algorithms (GRASS6.4). The vegetation type for study sites is assigned as mixed conifer. Associated vegetation type parameters are taken from RHESSys parameter libraries

(https://github.com/RHESSys/ParamDB). We use 30m Leaf Area Index (LAI) derived from LIDAR point cloud using a deterministic approach [*Richardson et al.*, 2009] and a set of allometric equations to initialize vegetation carbon and nutrient stores[*White et al.*, 2000].

We estimate snow-related parameters by comparing modeled SWE with measured snow depths at the two climate stations within the respective study sites. Table 2.2 shows estimated snow-related parameters for the two watersheds. Air temperature lapse rates with elevation are estimated using the difference of elevations and measured air temperatures at the two climate stations respectively. Temperature melt coefficients and temperature threshold values for partitioning incoming precipitation as rain or snow are estimated by adjusting the parameter values until the temporal trends of modeled SWE were similar to those of measured snow depth. The comparison of model estimated SWE and measured snow depth mainly focuses on whether model estimates captured the timing of snow accumulation and melts. The two watersheds have similar temperature lapse rates, and the same snow melt coefficient and temperature threshold values (Table 2.2). Figure 2.2 shows the result of comparison of the model SWE predictions with measured snow depths (or SWE) at the climate stations. To compare the model estimate of SWE and measured snow depths, we calculate the day of complete snowmelt in the four climate stations. The model reproduced the timing of observed snow accumulation and melt at the four climate stations. In general, the model has better snow prediction at the Providence stations than at the Bull station. The comparison in the day of complete snowmelt between model and observation yields R^2 of 0.92, 0.86 in Providence stations and Bull stations (Figure 2.2a and 2.2c). The comparison of the modeled SWE estimates with measured SWE at the Upper Providence and the Upper Bull stations results in R^2 of is 0.91 and 0.73. At the Upper Providence, the model tended to underestimate SWE in the dry years, 2004 and 2007. At the Upper Bull

station, the model underestimated the SWE in year 2004, and 2005, and overestimated SWE in the year 2008. The lower model accuracy in the Upper Bull station (Figure 2.2d) may be related to measurement errors in SWE [*White et al.*, 2000]. For example, we found that the first day of snow accumulation in year 2007 and 2008 based on the measured SWE values at the Upper Bull station occurs later than those at the Upper Providence station. The snow accumulation rate in year 2008 at the Upper Bull station is also lower than those at the Upper Providence station. These results are inconsistent with data from other years.

In this study, we hypothesized that the impact of soil parameter uncertainty on the predictive uncertainty of modeled ecohydrologic estimates varies between TSW and SDW as well as the variable of interest. In order to test this hypothesis, we quantified the model accuracy and predictive uncertainty based on streamflow calibration, and compared the annual, monthly and daily mean and variation of estimated ecohydrologic variables (annual streamflow, summer streamflow (August flow), annual ET and annual NPP) across selected parameter ranges between TSW and SDW. GLUE [Freer, et al., 1996; Beven and Freer, 2001] was used to quantify the predictive uncertainty. All soil parameters values for the uncertainty analysis were sampled using uniform distribution across specified parameter ranges since we did not have prior information about the distribution of soil parameters. Table 2.3 shows parameters ranges used in this study. Six soil parameters were calibrated: anisotropic saturated hydraulic conductivity (Ksat_h, Ksat_v), decay of Ksat_h and Ksat_v with depth (m), the fraction of infiltrated soil water that directly drains to deep groundwater stores (gw1), air entry pressure (ae) and pore size index (psi). In this study, we fixed the linear coefficient of deep groundwater storage (gw2) as zero to reflect deep groundwater losses that are not captured by the stream gauge. Sustainable low flow in the summer that is a good signature of contribution of deep groundwater flow to streamflow [*Jothityangkoon et*

al., 2001; *Jefferson and Nolin*, 2008] was not observed in our site. Further, because the stream weir is located on deeply weathered bedrock, and slopes are steep, we assume that deep groundwater flow may bypass at the stream gauging stations.

In addition to soil parameters, rooting depth is an important parameter for determining transpiration and streamflow generation [*Hwang et al*., 2009]. However, we did not calibrate the rooting depth because this study focuses on the sensitivity of model estimates to soil parameter uncertainty. Instead, we set rooting depths for each watershed to represent realistic rooting depths: 2m for TSW and 1m for SDW. Rooting depth estimates were based on reported values from field measurements [*Hunsaker et al*., 2012]. *Hunsaker et al*. [2012] reports effective rooting depths range from 0.76 to 2m and 0.5 to 1m for TSW and SDW, respectively. We used the maximum root depth due to under-sampling of deep roots in field-based studies.

Effect of soil parameter uncertainty on model estimates was quantified by measuring the range in estimated model values using behavioral (or acceptable) soil parameter sets. The behavioral soil parameter sets were selected based on streamflow prediction accuracy. In previous GLUE applications [*Beven and Freer,* 2001; *Grueger et al*., 2010], a single, subjectively chosen threshold accuracy value for selecting behavioral parameter sets was used. This study focuses on comparing the sensitivity of different model estimates to soil parameter uncertainty between two watersheds without accounting for uncertainty due to differences in model structure and input data error between the two watersheds. If a single threshold value is used for both watersheds, a watershed with higher model accuracy will obtain more behavioral soil parameter sets, resulting in higher predictive uncertainty regardless of watershed characteristics. An alternative method is to select the same number of behavioral parameter sets for the two watersheds. This method assumes that differences

in model accuracy between the two watersheds can be attributed to the difference in model structure and input data error.

We compare results using both of these approaches to determine whether using different methods for selecting behavioral soil parameter sets will change the results of our uncertainty analysis. To obtain the same number of behavioral soil parameter sets for the two watersheds, the best 1% of parameter sets from the total simulations (5000) are selected for each watershed. We chose 5000 simulations because streamflow accuracy and selected soil parameter sets did not differ when the number of simulations increases from 4000 to 5000.

To select a single threshold value for determining behavioral soil parameters, we used the minimum accuracy value of the 1% best soil parameters sets across both watersheds. In our analysis, TSW has lower streamflow accuracy than SDW. Therefore, the minimum accuracy value of the 1% best simulations in TSW is used as a single threshold value for selecting behavioral soil parameters for the both watersheds.

For both parameter selection approaches, the acceptable behavioral parameters sets can vary as a function of which accuracy measure is used to define goodness of fit between observed and modeled flow [*Dunn*, 1999]. Commonly used measures used to define flow accuracy emphasize different aspects of flow. For example, the Nash-Sutcliffe coefficient (R_{eff}) [*Nash and Sutcliffe*, 1970] tends to emphasize peak flow (equation 1), the Nash-Sutcliffe coefficient using log values (R_{logeff}) emphasizes recession characteristics and low flows (equation 2), and percentage of error (PerErr), emphasizes the estimate of total flow volume (equation 3). We account for these different measures of accuracy using equation (4).

$$R_{\text{eff}} = 1 - \frac{\sum_{i}\left(Q_{obs,i} - Q_{sim,i}\right)^2}{\sum_{i}\left(Q_{sim,i} - \overline{Q_{obs}}\right)^2} \quad (1)$$

$$R_{\text{logeff}} = 1 - \frac{\sum_{i}\left(\log(Q_{obs,i}) - \log(Q_{sim,i})\right)^2}{\sum_{i}\left(\log(Q_{sim,i}) - \log(\overline{Q_{obs}})\right)^2} \quad (2)$$

$$PerErr = \frac{\left(\overline{Q_{sim}} - \overline{Q_{obs}}\right)}{\overline{Q_{obs}}} \quad (3)$$

$$Total \quad Accuracy = R_{eff} \times R_{\log eff} \times (1 - |PerErr|) \quad (4)$$

Where $Q_{obs,i}$ is the observed streamflow and $Q_{sim,i}$ is the simulated flow at daily time step (i), and $\overline{Q_{obs}}$ and $\overline{Q_{sim}}$ are the long-term average of observed daily streamflow and simulated streamflow respectively.

To quantity the predictive uncertainty in the two watersheds, we used equation (5).

$$U = \frac{1}{T}\sum_{i}^{T}\left[Q_i(97.5\%) - Q_i(2.5\%)\right] \quad (5)$$

Where U is predictive uncertainty, T is total simulation time (days), i is time (day), Q is simulated values (mm/day or kgC/day), and 97.5%, and 2.5% are 95% upper and lower uncertainty limit of predicted daily values across soil parameter uncertainty. The selected behavioral parameters are used to predict the streamflow, ET and NPP, and estimate 2.5% and 97.5% uncertainty bounds for each estimate for each day. To calculate the 2.5% and 97.5% uncertainty limits, simulated flows (or ET and NPP) for each day are weighted by their normalized accuracy using equation (4). Since this study focuses on the comparison of predictive uncertainty between the two watersheds, this simple approach is valid. A detailed description and theoretic background of GLUE approach is provided in [*Freer et al.*, 1996].

We also investigate whether the effect of soil parameter uncertainty on different ecohydrologic model estimates are more important than the effect of climate warming for the two watersheds. We examine annual streamflow, summer flow (August flow), annual ET and annual NPP. In order to simulate climate warming effects, a soil parameter set with the highest streamflow accuracy (using equation (4)) is selected for each watershed respectively, and two climate warming scenarios are used. We also calculated the proportion of years in the total simulation period (63 years) that exceed the 95 % confidence limit of model estimates (using equation 5) associated with soil parameter uncertainty for the baseline (historic climate) simulations. In order to quantify the effect of soil parameter uncertainty and climate warming on annual model estimates, we compare this proportion across historic climate and 2 °C and 4 °C warming scenarios and for annual flow, summer flow and annual ET and NPP. We assume that if the proportion of years exceeding the 95% confidence limit of model estimates is larger than 5% then the estimated climate- warming effect is significant, even accounting for soil parameter uncertainty.

The climate warming scenarios are generated by adding 2 °C and 4 °C to historical daily air temperature data. Recent GCM predictions for the California Sierra Nevada over the next 50-100 years show air temperature to increase by 1.6 to 4.4 C° [*Maurer and Duffy*, 2005; *Cayan et al.*, 2008]. Using a simple, uniform temperature increase allows us to focus on the direct impact of increasing temperature on ecohydrologic responses and avoid the complex and highly uncertain downscaling of climate model outputs [*Wood et al*., 2002;*Tague et al*., 2009]. In this analysis, we focus on whether estimated model uncertainty ranges across behavioral soil parameter sets can enclose the model estimates under the two climate warming scenarios. To find the general trend of model estimates with a given annual precipitation under different climate inputs, we use a local polynomial regression fitting

algorithm, LOESS [*Cleveland and Grosse*, 1991], but do not claim the statistical meaning on the fitted lines.

2.3 Results

2.3.1 Comparison of model accuracy and predictive uncertainty between the transient snow watershed (TSW) and the snow-dominated watershed (SDW)

Model streamflow accuracy is compared between the two watersheds, and the predictive uncertainty of the model estimates across soil parameter uncertainty is estimated. Figure 2.3 shows the model accuracy (Equation 4) and the predicted streamflow uncertainty (Equation 5) using behavioral soil parameter sets in TSW and SDW. The behavioral parameter sets were selected from 5000 different soil parameter sets based on streamflow accuracy, or based on the best 1% parameter sets. We compare the cumulative distribution of non-behavioral parameters and behavioral parameters (Table 2.3). The nonparametric Kolmogorov-Smirnov d-static is used to estimate the difference. For both watersheds, selected behavior soil parameter sets have different distributions with non-behavioral soil parameters sets, especially, m and gw1 parameters for TSW, and gw1 and ae for SDW. Note our approach used to define behavioral sets means that TSW has the same number of behavioral soil parameter sets for both the case of accuracy based selection and the case of best 1% simulations. SDW has different numbers of behavioral parameters for the two different parameter selection approaches. Table 2.4 summarizes the model accuracy ranges and the calculated predictive uncertainty (equation 5) of the two watersheds. The model generally reproduced observed streamflow well, although peak flow was overestimated for

SDW and TSW in year 2008, and was underestimated for several peak flow events in year 2004 and 2005.

The uncertainty boundaries of SDW and TSW failed to enclose the measured streamflow in some periods (Figure 2.3). Unexplainable differences between observed and modeled streamflow may be due to uncertainty of model inputs or limitations in the model structure. The predictions for SDW had higher accuracy relative to those for TSW. SDW had slightly higher predictive uncertainty of daily flow estimate than TSW, but SDW had slightly lower predictive uncertainty of monthly flow estimates than TSW (Table 2.4 and equation (5)). For the 1% of soil parameter sets producing the most accurate streamflow predictions, the performance for each of the three accuracy measures (R_{eff}, R_{logeff} and PerErr) was better for SDW relative to results for TSW. For SDW, R_{eff} accuracy (0.74 to 0.88) was higher than R_{logeff} accuracy (0.58 to 0.77). However, for TSW, R_{eff} accuracy (0.56 to 0.73) was lower than R_{logeff} accuracy (0.62 to 0.77), suggesting that capturing peak flows for TSW was particularly problematic. The poor prediction of peak flow is likely due to an overestimate of the fraction of snowfall in total precipitation in the late fall and early winter. The poor prediction of the peak flow may also be due to the misrepresentation of variable soil depth within the watershed [*Merz and Plate*, 1997; *Freer et al*., 2002]. TSW has areas with locally shallow soil depths [*Bales et al.*, 2011]. Areas with shallow depths can generate the peak flow, by rapidly responding to snow melt or rainfall events. In our modeling study, we assumed that soil depth is uniform within the watershed because detail soil depths map at fine scales are not available. The model showed relatively high streamflow accuracy values at the monthly time scale (Table 2.4). The mean values of PerErr among the selected behavioral soil parameters for both watersheds are less than 1%. Based on this level of model performance, we argue that the calibrated model can be used to test the difference in

the sensitivity of seasonal and annual model estimates to soil parameter uncertainty between the two watersheds. We would caution the use of the model to estimate peak flows (and their sensitivity to soil parameters) until an improved method for partitioning incoming precipitation into rain versus snow is included in the model and spatially variable soil data can be provided. We emphasize however that for many model applications in climate change assessments, seasonal and annual flows are the key variable of interest and ecological fluxes (ET and NPP) are not highly sensitive to these errors in peak flow production processes.

Using a threshold accuracy value of 0.38 (the accuracy threshold obtained for the top 1% of parameters sets in TSW) to choose parameter sets for SDW led to a greater number of parameter sets (290, 5.8%) for SDW and thus increased model predictive uncertainty (Table 2.4). SDW had higher predictive uncertainty of daily and monthly flow estimates than TSW. Model prediction was not improved in terms of enclosing the observed streamflow. Therefore, the best 1% parameter sets are the most reasonable choice for SDW and we use those parameter sets for the following analysis.

2.3.2 The Impact of soil parameter uncertainty on long-term ecohydrologic predictions

When the best performing (highest accuracy) 1 % soil parameter sets for the two watersheds were used over a longer time period (63 years), TSW had substantially higher predictive uncertainty of annual ET and NPP than SDW. TSW has slightly lower predictive uncertainty of annual streamflow (Table 2.5). Figure 2.4 shows the sensitivity of predictive uncertainty of estimated annual streamflow, ET and NPP to annual precipitation in TSW and SDW. SDW always yields larger annual streamflow for a given annual precipitation inputs

relative to TSW (Figure 2.4a). The variation in estimated annual streamflow (expressed as standard deviation, SD) due to soil parameter uncertainty linearly increased with annual precipitation, and the slope of this relationship was steeper for TSW than for SDW. The estimated annual streamflow variation expressed as coefficient of variance (COV) across soil parameter uncertainty was larger in TSW than in SDW (Figure 2.4c). The estimated annual streamflow variation (COV) due to soil parameter uncertainty decreased with increasing annual precipitation in both watersheds (TSW and SDW). This implies that the relative effect of soil parameter uncertainty is larger in the drier years.

TSW always had larger annual ET for a given annual precipitation input relative to SDW. The estimated predictive uncertainty of annual ET across behavioral soil parameter sets was larger in TSW than SDW (Figure 2.4d and Table 2.5). In both TSW and SDW, estimated annual ET variation (SD and COV) across behavioral soil parameter sets was highest in years with intermediate precipitation. Estimated annual NPP and its variation across behavioral soil parameter sets and their relationship with annual precipitation between watersheds were similar to those of annual ET (Figure 2.4h, 2.4i and 2.4j). The predictive uncertainty for ET and NPP was greater for TSW relative to SDW (Table 2.5).

Figure 2.5 shows the mean and variation of estimated monthly streamflow, ET and NPP across behavioral soil parameters. SDW generally had higher mean monthly streamflow than TSW. Figure 2.5b shows the estimated monthly streamflow variation (expressed as standard deviation, SD) across behavioral soil parameter sets and across inter-annual variation in meteorological forcing (climate), including temperature and precipitation. For both SDW and TSW, the effect of inter-annual climate variability on streamflow variability in winter and spring was larger than the effect of soil parameter uncertainty (Figure 2.5b and 2.5c). However, soil parameter uncertainty and inter-annual climate variation effects on

monthly streamflow (SD, COV) were similar for late summer and fall flows (August, through November).

TSW generally had higher mean monthly ET and NPP than SDW (Figure 2.5d and 2.5g). However, TSW and SDW have similar seasonal patterns of mean ET and NPP, with highest mean ET and NPP typically occurring in June. Variation of monthly ET and NPP due to soil parameter uncertainty (SD or COV) is greatest during summer months (July and August) (Figure 2.5e, 2.5f, 2.5h and 2.5i). The effect of inter-annual climate variability monthly ET and NPP variation in winter, early spring and fall was more significant than soil parameter uncertainty effect (Figure 2.5e, 2.5f, 2.5h and 2.5i). However, the soil parameter uncertainty and climate variability effects were equally important in summer, including June, July and August (Figure 2.5e, 2.5f, 2.5h and 2.5i).

2.3.3 Comparison between climate-warming and soil parameter uncertainty effects on ecohydrologic predictions

To demonstrate the importance of accounting for soil parameter uncertainty in assessing climate warming impacts, we compare the effect of climate warming and soil parameter uncertainty on the model estimates of annual flow, summer flow, annual ET and annual NPP in TSW and SDW. Figure 2.6 and 2.7 show both the effect of 2°C and 4°C climate warming scenarios and soil parameter uncertainty on estimated ecohydrologic responses in TSW and SDW. For warming scenarios, we choose the best soil parameter set (having most accurate streamflow prediction) to simulate the annual streamflow, summer flow, annual ET and annual NPP. The predictive uncertainty boundary (or 95% confidence limit) of model estimates due to soil parameter uncertainty is calculated with GLUE [*Beven and Freer*, 2001]. In both TSW and SDW, soil parameter uncertainty had a larger influence on

estimated annual ecohydrologic estimates than the two warming scenarios. In other words, predictive uncertainty bounds for estimated annual streamflow due to soil parameter uncertainty enclose the variation of estimated annual streamflow caused by moderate temperature increases. However, the effect of warming on summer streamflow in the wetter years became larger than soil parameter uncertainty effect (Figure 2.7b) in SDW. The effect of soil parameter uncertainty on annual ET and NPP was still larger than the climate warming effect, but the effect of climate-warming increased in the wetter years (Figure 2.6c, 2.6d, 2.7c and 2.7d). Table 2.6 summarizes the proportion of years in which climate scenarios produce estimates outside the 95% confidence bounds derived from soil parameter uncertainty. Under the 2°C and 4°C warming scenario, summer streamflow estimates for SDW show a significant proportion of years (> 5%) in which estimates are outside uncertainty bounds (95%) that account for soil parameter uncertainty in historic estimates.

2.4 Summary and discussion

This study quantified the impact of soil parameter uncertainty on estimating ecohydrologic responses to climate variation and warming in two Sierra watersheds with distinctive snow regimes. We hypothesized that the impact of soil parameter uncertainty on the sensitivity of estimated ecohydrologic responses to climate would differ between these watersheds as well as the variable of interest. Our results show that for daily streamflow estimates, SDW is more sensitive to soil parameter uncertainty than TSW. For all other fluxes (annual ET and NPP), TSW is more sensitive to soil parameter uncertainty. The impact of soil parameter uncertainty on most monthly and annual fluxes, however, is small relative to the effect of historic climate variation, largely reflecting the impact of inter-

annual variation in precipitation. For 2°C and 4°C warming scenarios, August streamflow declines and annual ET and NPP increase for both watersheds. The magnitudes of these changes, however, are often small relative to soil parameter uncertainty effects, particularly for TSW.

In this study, behavioral soil parameter sets were estimated based on streamflow accuracy. Relative to TSW, SDW has slightly higher predictive uncertainty for daily streamflow but lower predictive uncertainty for monthly streamflow. Annual predictive uncertainty for streamflow was similar. We proposed a hypothesis to explain why the estimated predictive uncertainty of daily streamflow due to soil parameter uncertainty is greater for the SDW. The magnitude of groundwater level can lead to differences in soil parameter sensitivity. SDW tends to have shallower groundwater levels (near surface) due to lower ET and more concentrated infiltration than TSW. Model estimates of watershed mean groundwater table using the best soil parameter sets (the set with the highest flow accuracy) in both watersheds, show that the estimated groundwater level in SDW is always at least 0.3m shallower than in TSW. In RHESSys, as in many hydrologic models [*Ambroise et al.*, 1996], saturated hydraulic conductivity decays non-linearly with depth. Given this nonlinearity, we would expect that watersheds with high water tables would be more sensitive to soil drainage parameters.

We also note that differences in the predictive uncertainty of flow in the two watersheds can depend on how well behavioral soil parameter sets are constrained. TSW has lower prediction accuracy than SDW. Lower prediction accuracy in TSW may lead to less well-constrained soil parameter sets and contribute to increasing the predictive uncertainty values. As noted above, however, SDW has higher predictive uncertainty of daily flow even though it has higher predictive accuracy. Thus physical controls (shallower groundwater

level and the higher intensity of spring infiltration in SDW) suggest mechanistic differences between the watersheds that impact predictive uncertainty of daily streamflow estimates. Consequently even if both watersheds had similar accuracy, and had similarly constrained parameters we would expect SDW would have higher predictive uncertainty of daily streamflow when compared with TSW.

In contrast to daily streamflow, annual fluxes (ET, NPP) shows higher sensitivity to soil parameter uncertainty in TSW rather than SDW. (For annual streamflow estimates, watersheds show similar sensitivity to soil parameter uncertainty). TSW is generally more water limited (e.g. the soil water content falls below the field capacity earlier in the growing season than it does for SDW. Both watersheds however have little rainfall during the summer and consequently are vulnerable to water-limitation. In these water-limited environments, we expect that annual ET and NPP fluxes will be sensitive to soil parameters that influence storage. Model results confirm this and also show that soil parameter sensitivity is strongly influenced by seasonal and annual variation in climate forcing. Seasonal and inter-annual climate determines the conditions for each watershed under which water limitation is likely to occur and when soil parameters, and their uncertainty matter the most.

This interaction between climate forcing and the effect of soil parameter uncertainty can be seen at both annual and seasonal time scales. Figure 2.8 and 2.9 summarize how climate and soil parameter uncertainty interact at annual and seasonal time scales. Annually, the variation (COV) of annual streamflow due to soil parameter uncertainty decreases with increasing annual precipitation in both watersheds (Figure 2.4c, Figure 2.8a). For estimated annual ET and NPP (Figure 2.8b), the sensitivity to annual precipitation was highest with intermediate annual precipitation for both watersheds. In drier years, the variation of annual

ET due to soil parameter uncertainty is reduced because ET was limited by input (precipitation or snowmelt) rather than storage. In other words, for all acceptable soil parameters there is sufficient storage to capture the recharge that was ultimately lost as ET. In dry years, interception losses also play a larger relative role and are not sensitive to soil parameters. In wetter years, ET is often limited by colder temperatures and shorter growing season length which reduced the sensitivity to soil parameters. Seasonally, soil parameter uncertainty is important during the drier months (Figure 2.5g and 2.5j, Figure 2.9b). During the wet season, the effect of inter-annual climate variation is large relative to soil parameter uncertainty.

For annual ET (and NPP) fluxes sensitivity to soil parameter uncertainty is also determined by the phase of precipitation. TSW shows higher sensitivity of annual ET and NPP fluxes to soil parameter uncertainty even though the difference of annual precipitation between TSW and SDW is less than 1%. Other studies[Goulden et al., 2012; Goulden and Bales, 2014] have similarly found that ET is sensitive to the amount of snow for Sierra Nevada watersheds using ET estimates inferred from remote sensing and simple water balance. In this study, when the proportion of snow in total precipitation is increased (SDW versus TSW), the sensitivity of ET and NPP estimates to soil parameter uncertainty have a shallower relationship with annual precipitation This again reflects the reduced importance of soil storage parameters in the colder, less water-limited climate of SDW (Figure 2.4g and 2.4j, Figure 2.8b).

The interactions between the effect of soil parameter uncertainty and climate forcing shown in this paper are similar to results from other studies. *Zhu and Mackay* [2001] showed in Lubrecht Experimental Forest in western Montana that using detailed soil map information has a large effect on estimating NPP when the semi-arid watershed experienced

water-limitation in the growing season. *Shields and Tague* [2012] found that summer rather than winter ET is particularly sensitive to soil parameter uncertainty for a non-snow dominated western US watershed. Their work is similar to our results that show maximum sensitivity of NPP and ET in intermediate years. *Tromp-van Meerveld and Mcdonnell* [2006] showed from field measurements at the hillslope scale that soil depth (or total water storage) controls the spatial pattern of transpiration in periods of intermediate wetness, while in wetter and drier periods, differences of soil depth do not correlate with the measured transpiration.

These results indicate that proper soil parameterization, is particularly important for capturing summer streamflow, annual ET and annual NPP across a range of precipitation forcing. Accurate climate forcing on the other hand is particularly important during wetter periods, for both annual and seasonal streamflow predictions. Our results also suggest that model calibration in different climate conditions may result in increasing (or decreasing) model predictive uncertainty. In this study, drier years or intermediate years tend to have the highest sensitivity of modeled streamflow, ET and NPP estimates to soil parameter uncertainty. Therefore, if wet year data are used to constrain the soil parameter uncertainty for streamflow predictions, model uncertainty may increase because streamflow estimates in wet years are less sensitive to soil parameter uncertainty and constraining the behavioral soil parameter sets through calibration may become less effective. This result can also be explained as different levels or types of information in data for constraining model parameter and falsifying model structures [*Wagener et al*., 2003].

Previous model uncertainty research in the climate change impact analysis *[Wilby and Harris*,2006; *Kay et al.*, 2010;*Jung et al*., 2012] demonstrated that model parameter uncertainty is minor compared with other sources of uncertainty (future greenhouse gas and

aerosol emission, general circulation model structure, downscaling method and hydrologic structure uncertainty). Their study sites, however, focused on watersheds larger than 1000km^2. Our study demonstrates that the soil parameter uncertainty at a small watershed scales (<2km^2) can have a substantial impact on ecohydrologic estimates. At small catchment studies, initial soil moisture and soil properties are essential key factors in controlling streamflow generation [*Merz and Plate*, 1997]. Modeling studies that focus on a larger areas may show less sensitivity to soil parameter uncertainty because ecohydrologic estimates with increasing scale may be more dependent on topography, geology and climate rather than soil properties [*Zhu and Mackay*, 2001].

In this study, the effect of soil parameter uncertainty is also large when compared with the effect of a moderate warming scenarios (2 °C and 4 °C increases) on ecohydrologic fluxes in both TSW and SDW. In general, the effect of warming is greater for summer flow, annual ET and annual NPP than for annual flow. For all fluxes however changes with warming fall within the uncertainty bounds associated with soil parameters. Only for summer flow for SDW are there years where declines in summer flow with warming extend beyond the effect of soil parameter uncertainty. These results highlight the importance of reducing soil parameter uncertainty. Where additional data is not available in study sites, we recommend that model estimates should include uncertainty bounds that account for soil parameter uncertainty. Using additional data, including soil moisture data, ET and carbon flux data and stable isotope tracer data may help to further reduce soil parameter uncertainty in future research. Research at the current Sierra Critical Zone Observatory (CZO) project site offers a good example of this type of research effort. Ongoing data collection includes distributed snow depth [*Bales et al.*, 2011], hillslope-scale ET and carbon fluxes [*Goulden et*

al., 2012], and distributed microclimate, soil moisture and sapflow measurements [*Son and Tague*, 2012] that will contribute to reducing soil parameter uncertainty.

Figures

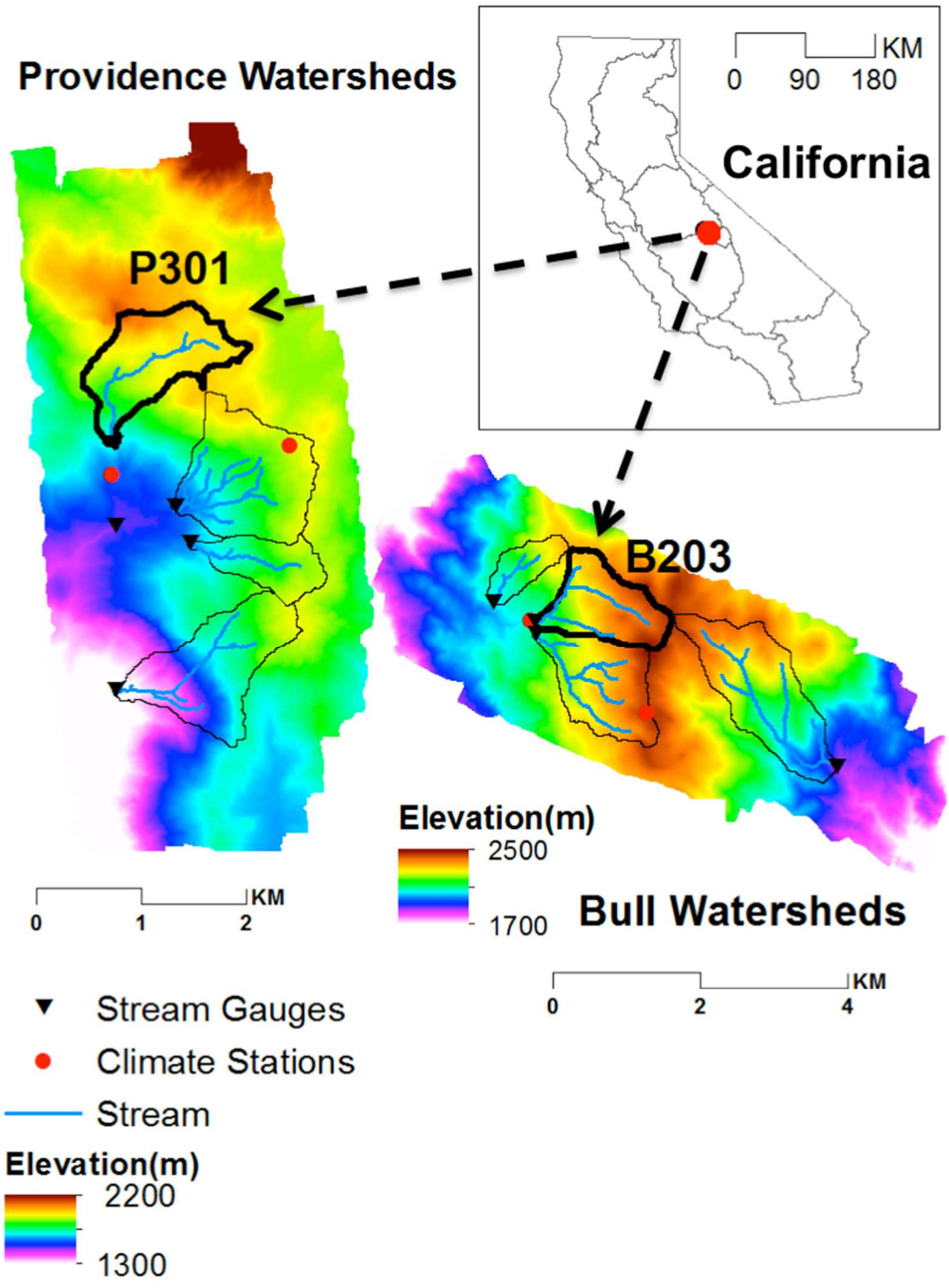

Figure 2.1. The location and elevation gradients of study sites: Providence watersheds and Bull watersheds.

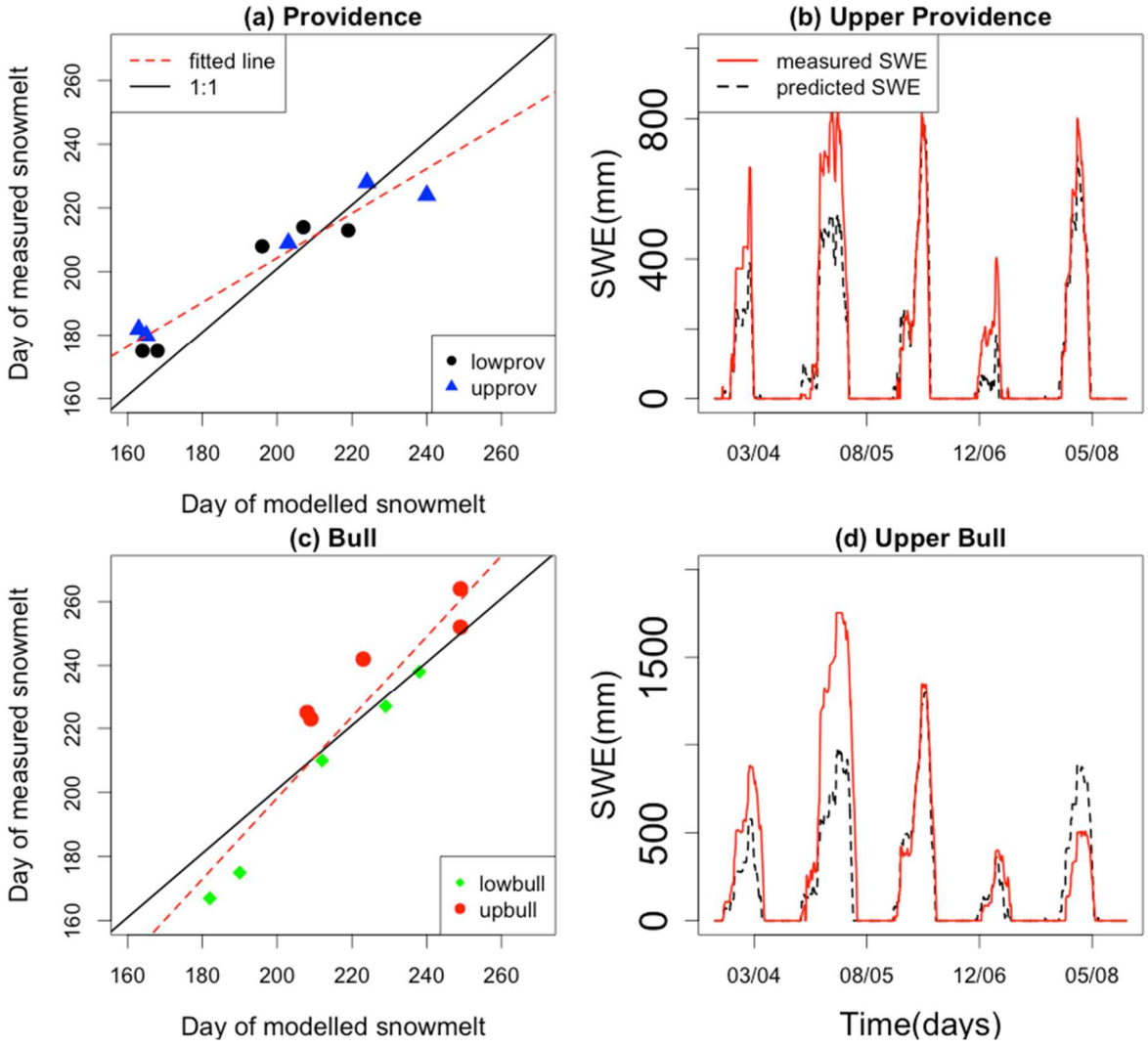

Figure 2.2. Comparison of predicted Snow Water Equivalent (SWE) and measured snow depth and SWE data in the Providence watersheds and Bull watersheds: (a) the timing of complete snow melt at Providence climate station, (b) SWE estimate at Upper Providence climate station, (c) the timing of complete snow melt at Bull climate station, and (d) SWE estimate at Upper Bull climate station.

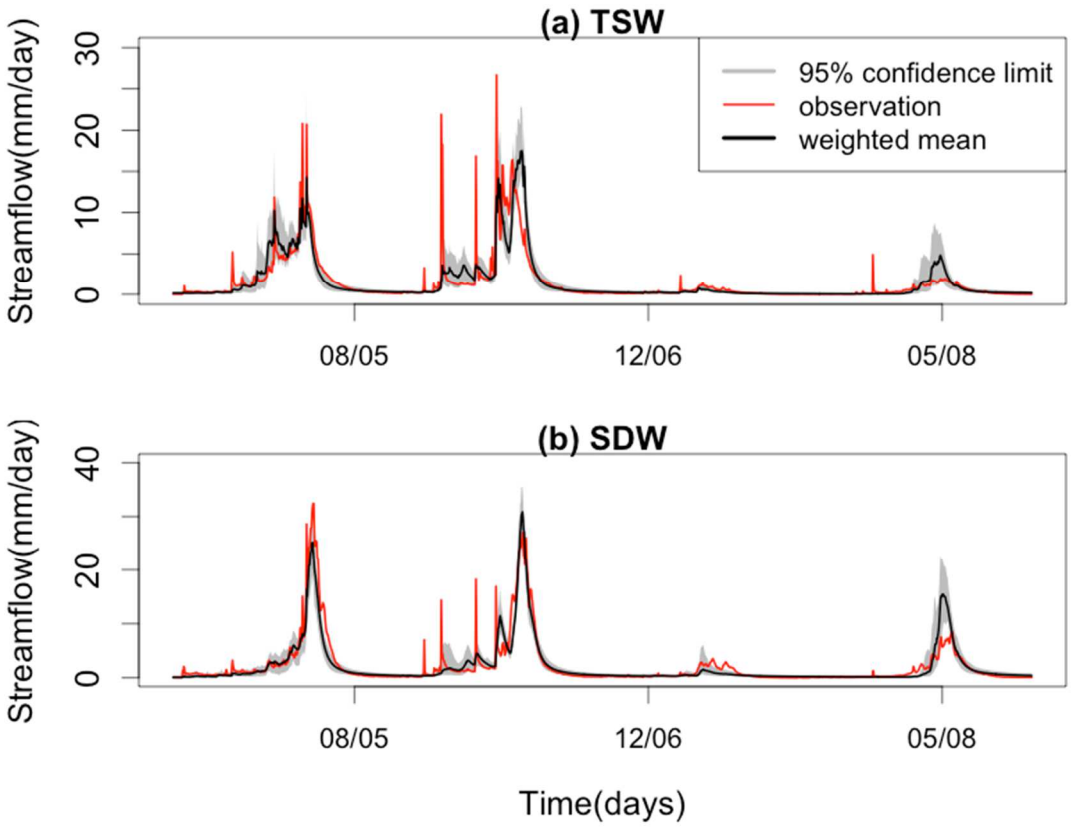

Figure 2.3. Streamflow predictions for selected behavioral soil parameter sets for TSW and SDW: (a) comparison of predicted daily streamflow (accuracy-based weighted mean streamflow and 95% lower and upper boundary of streamflow) with measured streamflow of TSW and (b) comparison of predicted daily streamflow with measured streamflow of SDW. For uncertainty boundary calculation, the best performing 1% of total simulation (5000) was used for TSW and SDW.

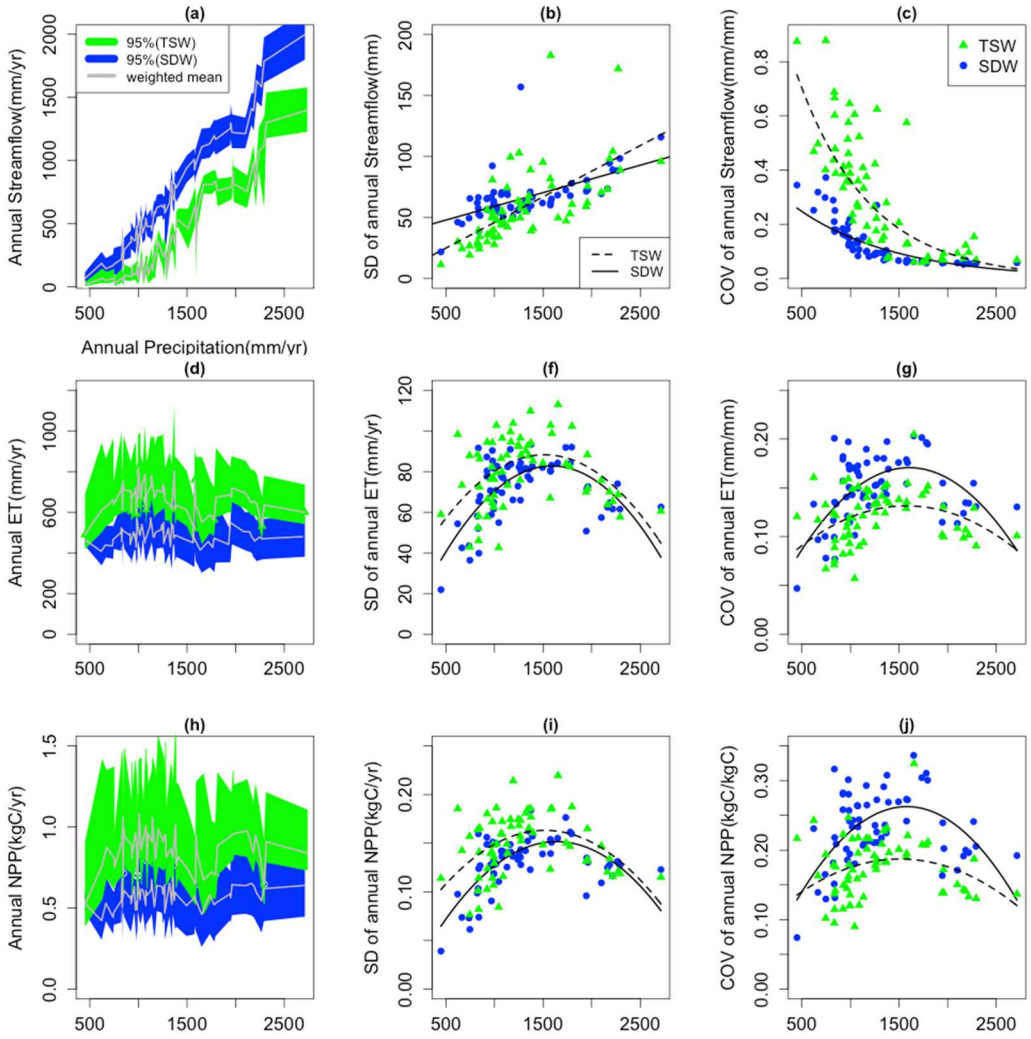

Figure 2.4. The predictive uncertainty of estimated annual streamflow, ET and NPP across soil parameter uncertainty in TSW and SDW; (a) estimated annual streamflow with 95% uncertainty boundary across behavioral soil parameter sets, (b) the relationship between annual precipitation and estimated annual streamflow variation (expressed as standard deviation, SD) across behavioral soil parameter sets, (c) the relationship between annual precipitation and estimated annual streamflow variation (expressed as coefficient of variance, COV) across behavioral soil parameter sets, (d) estimated annual ET with 95% uncertainty boundary across behavioral soil parameter sets, (e) the relationship between annual precipitation and estimated annual ET variation (SD) across behavioral soil parameter sets, (f) the relationship between annual precipitation and estimated annual ET variation (COV) across behavioral soil parameter sets, (g) estimated annual NPP with 95% uncertainty boundary across behavioral soil parameter set, (h) the relationship between annual precipitation and estimated annual NPP variation (SD) across behavioral soil parameter sets, and (i) the relationship between annual precipitation and estimated annual NPP variation (COV) across behavioral soil parameter sets. The fitted lines are all statistically significant (p-value<0.05).

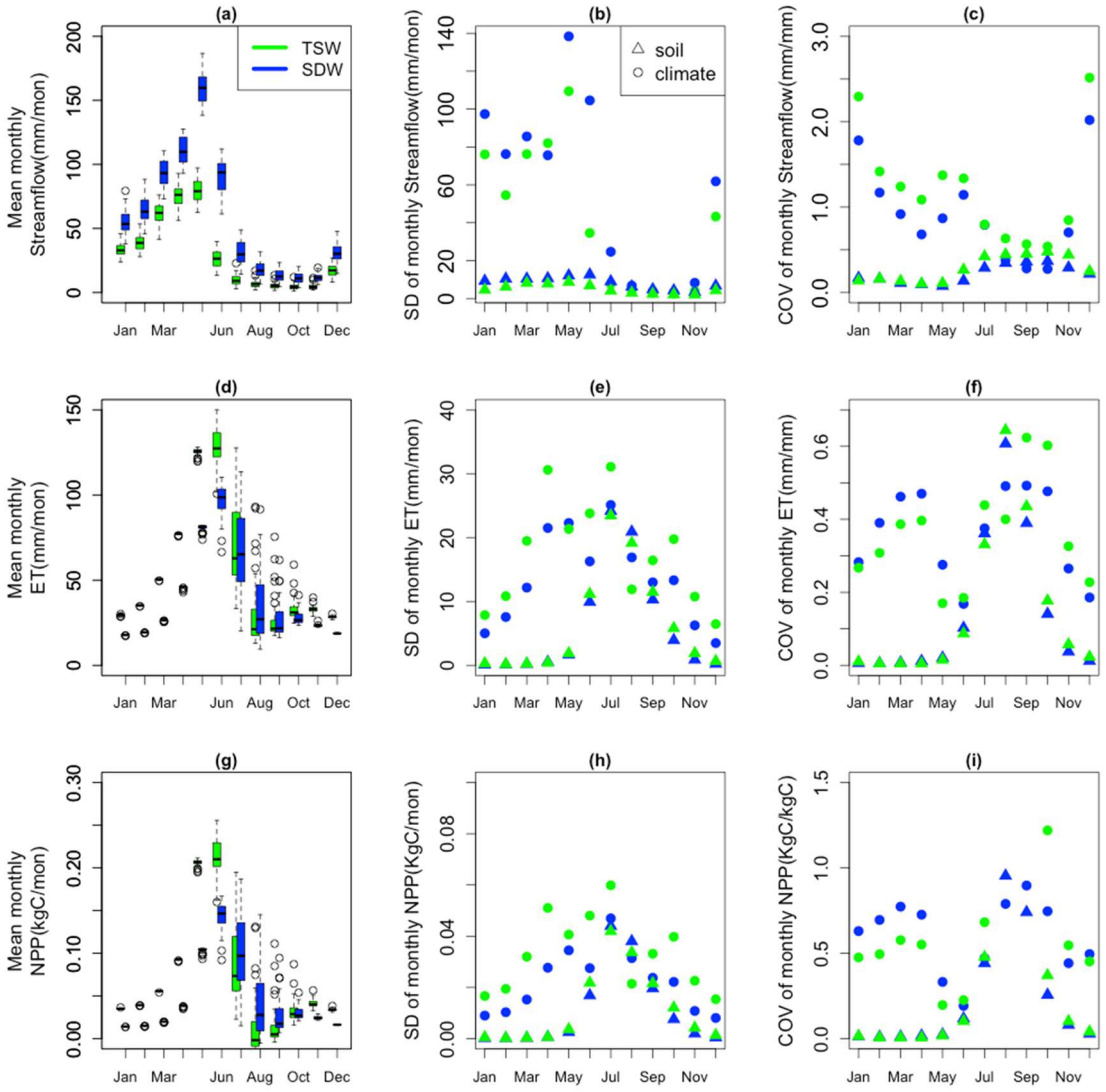

Figure 2.5. The predictive uncertainty of estimated monthly streamflow, ET and NPP across soil parameter uncertainty in TSW and SDW; (a) estimated mean monthly streamflow across behavioral soil parameter sets, (b) the effect of soil parameter uncertainty and inter-annual climate variability on estimated monthly streamflow variability (expressed as standard deviation, SD), (c) the effect of soil parameter uncertainty and inter-annual climate variability on estimated monthly streamflow variability (expressed as coefficient of variance, COV), (d) estimated mean monthly ET across behavioral soil parameter sets, (e) the effect of soil parameter uncertainty and inter-annual climate variability on estimated monthly ET variability (SD), (f) estimated mean monthly NPP across behavioral soil parameter sets, and (g) the effect of soil parameter uncertainty and inter-annual climate on estimated monthly NPP variability (SD), and (i) the effect of soil parameter uncertainty and inter-annual climate on estimated monthly NPP variability (COV).

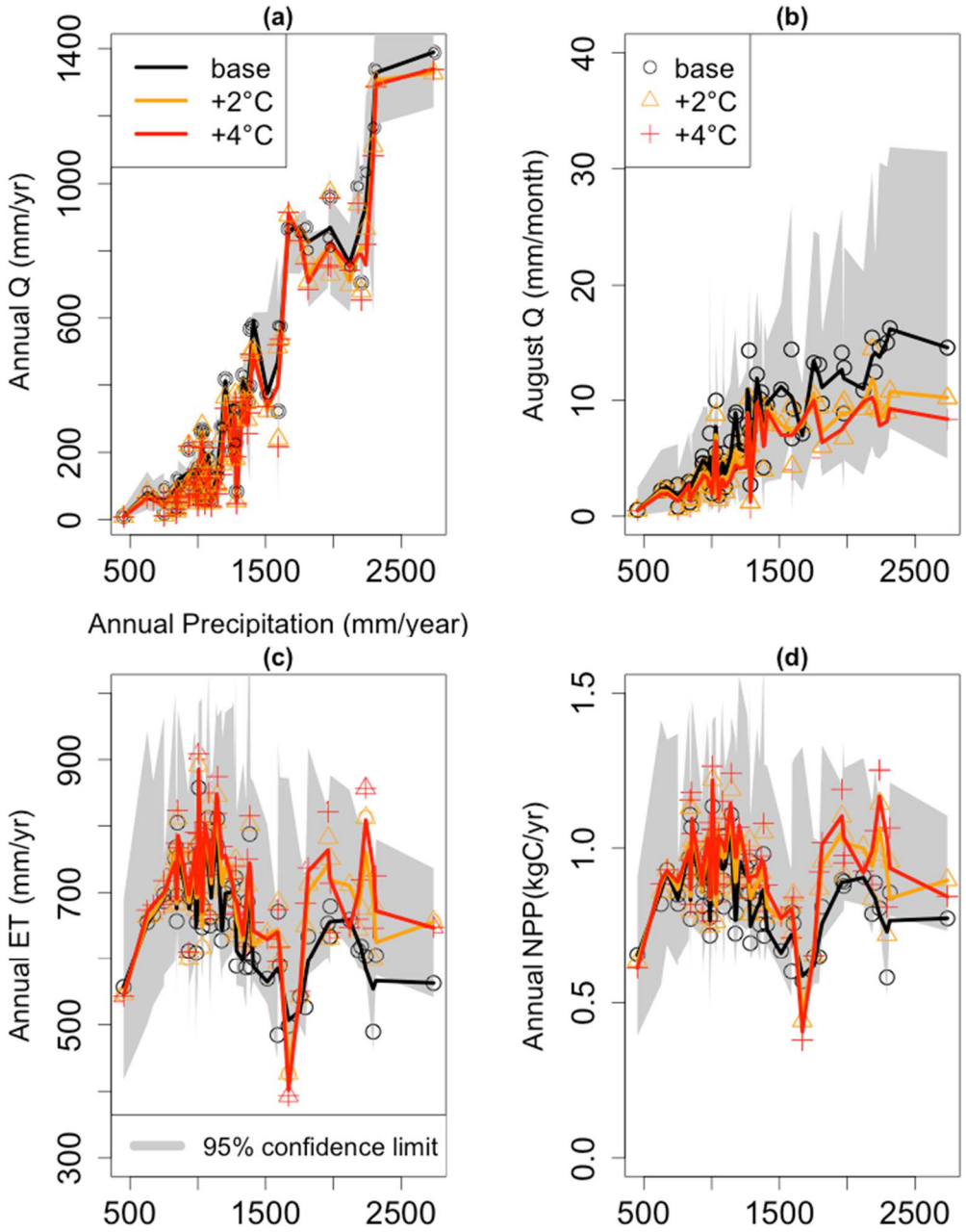

Figure 2.6. Comparison between climate warming and soil parameter uncertainty effects on ecohydrologic responses in TSW for: (a) annual streamflow (Q), (b) summer (August) streamflow (Q), (c) annual ET and (d) annul NPP. The three lines (black, orange and red) were created by using LOESS (local polynomial regression fitting algorithm), and the interpolated line is used for only guiding visually the general pattern of model estimates and is not necessarily statistically significant. Gray shaded area refers to estimated model uncertainty range across behavioral soil parameters.

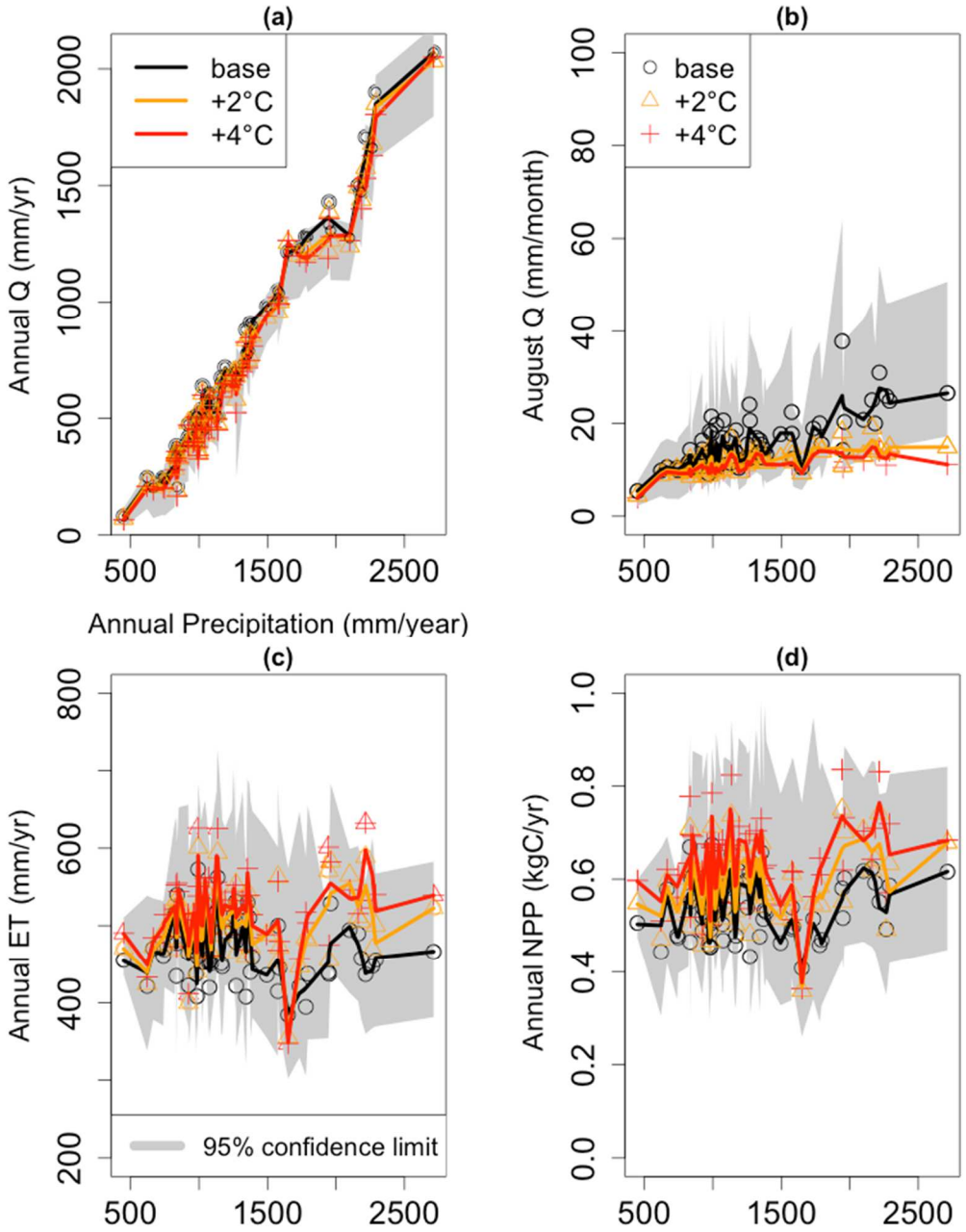

Figure 2.7. Comparison between climate warming and soil parameter uncertainty effects on ecohydrologic responses in SDW for: (a) annual streamflow(Q), (b) summer (August) streamflow, (c) annual ET and (d) annul NPP. The three lines (black, orange, and red) were created by using LOESS that is local polynomial regression fitting algorithm and interpolated line is used for only guiding visually the general pattern of model estimates regardless of statistical meaning. Gray shaded area refers to estimated model uncertainty range across behavioral soil parameters. For uncertainty boundary calculation, 1% of total simulation (5000) was used.

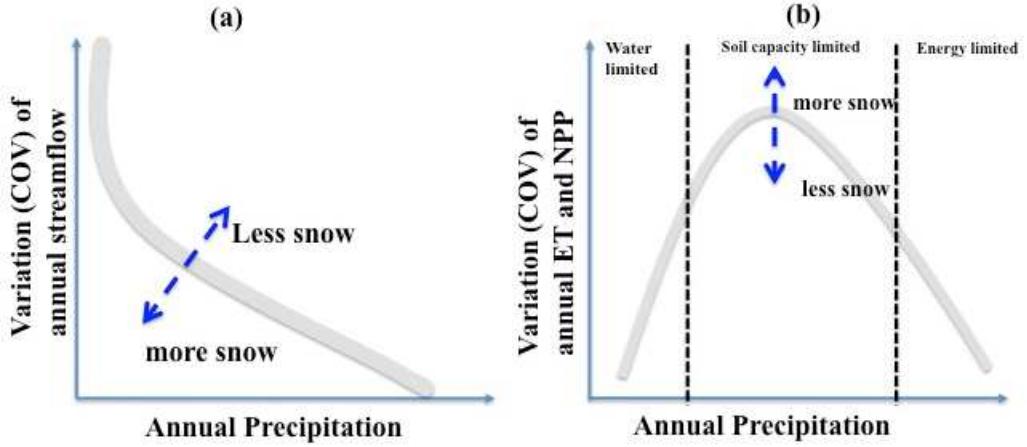

Figure 2.8. Conceptual model for evaluating the sensitivity of estimated predictive uncertainty of annual streamflow, ET and NPP to annual precipitation in two Sierra watersheds: (a) sensitivity of the annual streamflow variation across soil parameter uncertainty to annual precipitation, (b) sensitivity of annual ET and NPP variation across soil parameter uncertainty to annual precipitation.

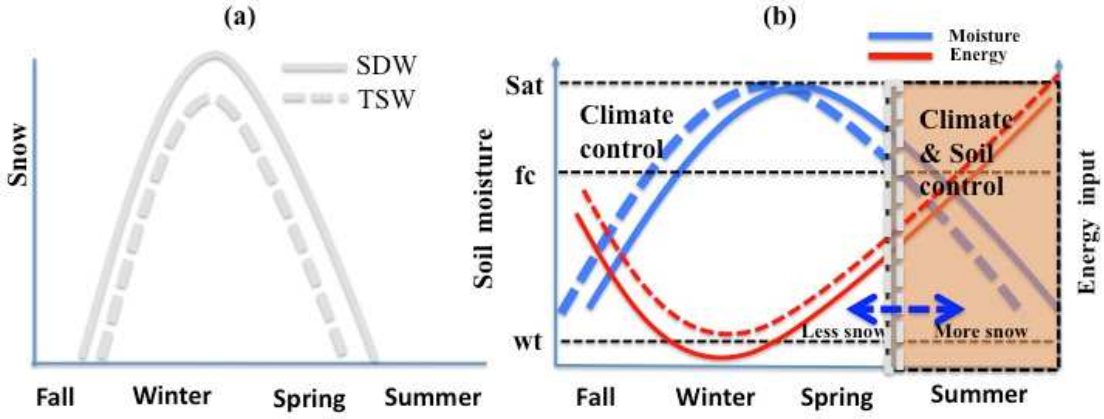

Figure 2.9. The key controls on the sensitivity of seasonal modeled streamflow, ET and NPP to soil parameter uncertainty and inter-annual variability: (a) seasonal snow pattern in TSW and SDW, (b) the seasonal pattern of soil moisture and energy input in TSW and SDW and the effect of inter-annual climate variability and soil parameter uncertainty on the seasonal ecohydrologic estimates (streamflow, ET and NPP)

Tables

Table 2.1. Basic hydrologic properties of P301 and B203 (Some values in this table were from [Hunsaker et al., 2012]).

Watershed	P301 (TSW)	B203 (SDW)
Elevation	1795 to 2102m	2185 to 2488m
Aspect	SW	SW
Slope	0.4 to 31.8 (10.7)	0.4 to 24.7(11.3)
Vegetation	Mixed Sierra conifer (Dominant tree species: white fir) LAI distribution:0 to 4.6 (2.0) Effective rooting depth: 0.76 to 2m	Mixed Sierra conifer (Dominant tree species: Red fir) LAI distribution: 0 to 3.1(1.1) Effective rooting depth: 0.5 to 1m
Soil	Dominant Soil types: Shaver (66%) Strongly weathered quartz diorite Permeability: Moderately rapid Hydrologic soil group: B	Dominant Soil types: Cagwin (80%) Highly weathered granitic rock Permeability: Rapid Hydrologic soil group: A
Precipitation /Runoff	Precipitation type: Snow-rain transition Mean annual Precipitation (2005 to 2007): 1513mm Runoff ratio(R/P): 0.20	Precipitation type: Snow-dominated Mean annual Precipitation (2005 to 2007): 1517mm Runoff ratio(R/P): 0.53
Temperature	Daily average temperature (°C) of (2004 to 2007) (mean ± SD): Min: 4.5 ± 0.8 Max: 13.0 ± 1.0 Mean: 8.6 ± 0.9	Daily average temperature (°C) of (2004 to 2007) (mean ± SD): Min: 3.3 ± 1.1 Max: 11.2 ± -0.7 Mean: 6.8 ± 0.8
Drainage pattern	Wetness index: 4.1 to 15.3(7.0)	Wetness index: 4.0 to 16.0(7.2)

Table 2.2. Calibrated snow-related parameters for the Providence and Bull watersheds.

	Snow-related parameters		
Watershed	Temperature laps rates[1] (tmax /tmin) (°C/m)	Temperature threshold for rain vs snow[2] (°C)	Temperature melt coefficient[3] (m/°C)
Providence	0.0063/-0.0064	-3-3	0.005
Bull	0.0068/-0.0060	-3-3	0.005

1: Since fine-spatial scale air temperature is not available in the two watersheds, air temperature within a watershed is spatially interpolated with the given elevation and the calculated temperature lapse rates.

2: To partition total precipitation into snow and rain, we use the air temperature as a proxy variable, and the proportion of snow and rain in the total precipitation is linearly interpolated based on the minimum and maximum temperature values. 3: Temperature melt coefficient accounts for snow melt due to latent heat and sensible heat.

Table 2.3. Calibrated soil-related parameters, parameter ranges, and model sensitivity[7] to each parameter for TSW and SDW.

Soil parameters (Units)	Used parameter ranges (Minimum /maximum)	Value of d-static in TSW	Value of d-static in SDW
Ksat_h[1] (m/day)	2/300	0.56	0.30
Ksat_v[2](m/day)	2/300	0.21	0.19
m[3](/)	0/4	0.18	0.06
gw1[4](/)	0/0.3	0.44	0.41
ae[5](m)	0.09/0.79	0.13	0.47
psi[6](1/m)	0.09/0.25	0.22	0.21

1: horizontal saturated hydraulic conductivity; 2: vertical saturated hydraulic conductivity; 3: Decay coefficient of Ksat with depth; 4: Proportion of deep drainage into deep groundwater storage through preferential flow path from net precipitation input; 5: air entry pressure; 6; pore size index; 7: we use non-parametric Kolmogrov-Smirnov d-static is applied as a measure for the difference in the distribution of behavioral/non-behavioral soil parameter sets. The value of d ranges from 0 to 1, and the value of d close to 1 indicate high sensitivity, while a value of d close to 0 indicates low sensitivity.

Table 2.4. Model streamflow accuracy and predictive uncertainty for TSW and SDW.

Watershed	Time scale	Model accuracy			
		R_{eff} (eq.1)	R_{logeff} (eq.2)	PerErr (eq.3)	Accuracy (eq.4)
TSW	Daily	0.56-0.73(0.64)[1]	0.62-.77(0.71)	-18.0-19.7(-0.1)	0.38-.52(0.42)
	Monthly	0.71-0.90(0.81)	0.64-.80(0.73)	-18.0-19.7(-0.1)	0.49-0.65(0.56)
SDW	Daily	0.74-0.88(0.82)	0.58-0.77(0.67)	-12.9-11.5(-0.5)	0.49-0.60(0.52)
	Monthly	0.84-0.94 (0.87)	0.61-0.80(0.73)	-12.9-11.5(-0.5)	0.55-0.69(0.61)

		Predictive uncertainty (mm)	
		1% sampled	Accuracy-based[2]
TSW	Daily	1.47	1.47
	Monthly	68.6	68.6
SDW	Daily	1.92	2.61
	Monthly	65.0	74.5

1: Parentheses values are mean model accuracy values among selected behavioral soil parameter sets in comparison between predicted streamflow and measured streamflow. 2:The minimum streamflow accuracy (equation 4) for TSW is 0.37. When the same threshold value (0.37) is applied for selecting behavioral soil parameter sets for both watersheds, the number of selected behavioral parameter sets for SDW is 290.

Table 2.5. Predictive uncertainty of estimated annual streamflow, ET and NPP (using eq. 5).

Variables (units)	TSW	SDW	
	1% sampled & accuracy-based	1% sampled	Accuracy-based[1]
Annual Streamflow (mm/year)	205.3	220.3	390.0
Annual ET (mm/year)	303.4	236.0	273.3
Annual NPP (kgC/year)	0.58	0.43	0.50

1: The minimum streamflow accuracy (equation 4) for TSW is 0.37. When the same threshold value (0.37) is applied for selecting behavioral soil parameter sets for both watersheds, the number of selected behavioral parameter sets for SDW is 290.

Table 2.6. Effect of climate warming and soil parameter uncertainty on estimating ecohydrologic responses to inter-annual climate variability.

	Annual flow		Summer flow		Annual ET		Annual NPP	
Watershed	TSW	SDW	TSW	SDW	TSW	SDW	TSW	SDW
2 °C warming	3(0.048)	1(0.016)	0(0)	**6(0.095)**	2(0.032)	2(0.032)	2(0.032)	2(0.032)
4 °C warming	2(0.032)	1(0.016)	0(0)	**9(0.143)**	2(0.032)	2(0.032)	2(0.032)	2(0.032)

Table show the number of years (and proportion of total years (63 years) in parenthesis) where model estimates under 2°C and 4°C warming scenarios exceed the 95% confidence limit for simulations using historic climate. The 95% confidence limit of annual flow, summer flow, annual ET and annual NPP due to soil parameter uncertainty is calculated with GLUE for historic climate simulations [*Beven and Freer*, 2001]. When climate-warming effect is larger than soil parameter uncertainty effect, values in the table are highlighted.

3. Hydrologic responses to climate warming for a snow-dominated watershed and a transient snow watershed in the California Sierra

Abstract

Climate warming will have substantial impacts on hydrological fluxes in the California Sierra, but differences in the impacts of warming on fluxes in snow-dominated watersheds (SDWs) and transient snow watersheds (TSWs) are not well understood. To improve our understanding of these differences, a process-based model, Regional Hydrologic-Ecologic Simulation System (RHESSys) was applied to a TSW and a SDW in Sierra National Forest, California. This study investigated the effect of climate warming (2° C and 4° C) on the model estimates of snow water equivalent (SWE), streamflow, evapotranspiration (ET) and moisture deficit (MD) in the two watersheds. Modeling results showed that SDW has greater sensitivity to climate warming than TSW. Estimated changes in inter-annual and seasonal SWE, ET, MD and streamflow are greater in SDW compared to TSW when the warming scenarios are applied. In the both watersheds, leaf area index (LAI) and wetness index [Beven and Kirkby, 1979] are primary factors controlling spatial patterns of seasonal ET under both of historical climate conditions and climate warming scenarios. Climate warming increases the spatial variability in monthly ET, especially during the summer period. For the 2° C warming scenarios, the average air temperature and magnitude and the timing of monthly SWE for SDW are similar to those for TSW under historical climate conditions. However, SDW under 2° C warming scenarios generates higher annual streamflow (including summer flow) due to shallower groundwater storage, and experiences

less water-limitation due to lower ET (lower LAI), relative to TSW under historical climate conditions. These modeling results suggests that vegetation structure and subsurface properties may be as important as air temperature in explaining hydrologic response to climate warming in small Sierra Nevada watersheds.

3.1 Introduction

Climate warming in the western mountains, United States has altered snow, soil moisture, vegetation water use and streamflow. However, the magnitude and timing of these effects varies both between and within watersheds[*Howat and Tulaczyk*, 2005; *Christensen et al*., 2008; *Tague and Grant*, 2009]. Complex interactions among topography, soil, vegetation, and geology cause the hydrologic variables to respond differently to climate warming.

Elevational controls on snow processes and energy distribution are key factors controlling the sensitivity of hydrologic responses to climate warming. However, there has been poorly understood the difference of hydrologic responses to climate warming between snow-dominated watersheds and transient snow watersheds [*Jefferson*, 2011]. *Safeeq and Grant* [2012] demonstrated that climate warming reduces the ratio of summer flow to annual precipitation more in snow-dominated watersheds than in transient snow watersheds. *Jefferson* [2011] showed that the effect of climate warming on streamflow change was detected in snow-dominated watersheds but not in transient snow watersheds. However, *Nolin and Daly* [2006] showed that transient snow watersheds in the Pacific Northwest region are more sensitive to climate warming than the snow-dominated watersheds.

The discrepancies between these finding suggest that climate warming's effects on transient snow watersheds and snow-dominated watersheds vary with other hydrologic properties, such as vegetation and geology; it is likely that these underlying and often unexamined differences in hydrologic properties confound the results [*Peel and Bloschl*, 2011].

Hydrologic models are used to predict the changes in snow regime, vegetation water use and streamflow for future climate conditions. Studies using the hydrologic models have improved our understanding of how hydrologic processes may be altered given predicted climate change [*Tague and Grant*, 2009; *Jasper et al*., 2006]. This study uses the Regional Hydrologic-Ecologic Simulation System (RHESSys) [*Tague and Band*, 2004]-physical process-based hydrologic model- to better understand difference in hydrologic response to climate warming between a TSW and a SDW. Using a process-based model also allows us to understand how the spatial pattern of soil moisture, ET and net primary productivity (NPP) within watersheds may be altered by climate change. Mountain watersheds have steep topographic gradients, and therefore the spatial patterns of hydrologic variables (snow, soil moisture, ET and NPP, etc.) may vary with climate change*[Jasper et al., 2006; Christensen et al*., 2008]. The RHESSys study of *Christensen et al*. [2008] showed that the sensitivity of annual transpiration to climate variation (precipitation and air temperature) varies along the elevation gradients. *Jasper et al*. [2006] also used a distributed hydrologic model (WasiM-ETH) to show that the degree of soil water depletion in future climate conditions varies with land use, soil texture, and topographic condition.

This study uses RHESSys to predict the effects of climate warming on two small Sierra Nevada watersheds (Figure 3. 1): P303, a transient snow watershed (TSW), and B203, a snow-dominated watershed (SDW). Specifically, this study investigates the impacts of

climate warming on: (1) seasonal and inter-annual variation of hydrologic fluxes in TSW and SDW and (2) the spatial structure of seasonal ET and its relationship with physiographic parameters in TSW and SDW. This study applies two climate warming scenarios (2 ° C and 4 ° C) to RHESSys for the two watersheds. SDW under climate warming is compared with TSW under historical climate conditions to demonstrate the confounding effect of other hydrologic properties on each watershed's hydrologic responses to climate warming. SDW typically maintains an air temperature about 2° C cooler than TSW (Table 3.1), and the two watersheds have similar total annual precipitation. In theory, a 2° C warming would prompt SDW to behave similarly to TSW under historical climate conditions if the difference in the air temperature between the two watersheds is the dominant explanation for the different hydrologic responses to warming. For this paper we assume that snow parameters (e.g. parameters that influences melt responses to the environment), soil drainage parameters and vegetation parameters (e.g. LAI and rooting depth) for each watershed are constant at the decadal time scale. By holding vegetation and soil properties constant, the model allows us to consider the impact of temperature warming alone on hydrologic responses and determine whether the difference of temperature can explain the difference in hydrologic responses to climate warming between the two watersheds. Previous studies use "space-for-time" substitution approach, which assumes that climate is main controller for hydrologic behaviors, including ET and streamflow [*Singh et al*., 2011; *Goulden and Bales*, 2014]. In particular, ecology studies assume that climate controls vegetation distribution, and vegetation will expect to move uphill due to climate warming. This study tests whether this assumption is valid.

3.2 Study sites and model calibration

3.2.1 Study sites

The study sites are the Providence sub-watershed (P303, 1.32km^2) and the Bull sub-watershed (B203, 1.4km^2) located in the King River Basin (Figure 3. 2), and part of King River Experimental Watershed and Southern Sierra Critical Zone Observatory (SSCZO). P303 is classified as transient snow watershed (TSW). B203 is classified as a snow-dominated watershed (SDW)[*Hunsaker et al*., 2012] . In both watersheds, precipitation mostly occurs between October and April. Snow in SDW accumulates earlier, with higher peak accumulations, and melts later than in TSW (Figure 3. 2). The difference in averaged daily temperature between the watersheds is about 2° C and annual precipitations are similar (Table 3.1). Each watershed has two climate stations (Upper and Lower Providence climate stations for TSW, Upper and Lower Bull climate stations for SDW). One of stations is located near or in top of watersheds and the other station is located near the bottom of watersheds. The climate stations measure 15-min precipitation, air temperature, relative humidity, global solar radiation, wind speed and direction, snow depth and SWE. Each watershed has two flumes at the outlet of the watershed to measure low and high flows.

The elevation of TSW ranges from 1730 to 1990m and the elevation of SDW ranges from 2185 to 2490m (Figure 3.2, Table 3.1). TSW is more steeply sloping than SDW. SDW has slightly higher mean wetness index [*Beven and Kirby*, 1979] than TSW. The two watersheds are covered with Sierran mixed conifer forest with some mixed chaparral and barren land cover. Sierran mixed conifer is composed of white fir (Abies concolor), Red fir (Abies magnifica), ponderpine pine (Pinus ponderosa), Jeffrey pine (Pinus Jeffrey), black oak (Quercus kelloggii), suger pine (Pinus lambertiana) and Incense cedar (Calocedrus

decurrens). The dominant tree of TSW is white fir but the dominant tree of SDW is red fir. A 10m LAI map was derived from LIDAR point cloud using a deterministic approach [*Richardson et al*., 2009](Table 3.1). TSW has denser tree cover (or higher LAI) than SDW. The dominant soil type of TSW is Shaver (66%) and its SDW is Cagwin (80%). Soil types in both watersheds are highly permeable and have high percentages of sand.

3.2.2 RHESSys model parameterization and calibration

The Regional Hydro-Ecologic Simulation System (RHESSys) is the physically based-spatially explicit model used to investigate climate warming's effect on hydrologic fluxes in TSW and SDW, two distinct Sierra Nevada watersheds. RHESSys is under continuous development, and in this study, version 5.15.r326 was used. A detailed description of the model equations is provided in [*Tague and Band*, 2004]. RHESSys has been applied to study climate change impacts in many watersheds across North America [*Mackay et al.*, 2003; *Hwang et al*., 2009;Tague and Peng, 2013], Europe[*Zierl et al.*, 2007] and Asia[*Kim et al.*, 2007], and the model successfully reproduced observed streamflow, evapotranspiration (ET) and carbon fluxes in these studies.

RHESSys models hydrological processes, including snow accumulation and melt, soil infiltration, evapotranspiration, and both shallow and deep groundwater flow. To calculate the snow accumulation rate, an estimation of the snowfall in the total precipitation is required. When the measurement of snowfall is available, snowfall data can be used as a climate input data. Otherwise, the partitioning of total precipitation in rain and snow is estimated using daily average temperature. Therefore, we expect that when air temperature increases, the amount of snow in total precipitation will be reduced. To account for the

uncertainty of the temperature threshold value used to define the phase of precipitation, dual temperature threshold values are used (equation 1)[*Marks et al.*, 2013].

$$\begin{aligned} Rain &= 1 && T>t1 \\ Rain &= 1-\frac{t}{t1-t2} \\ & && t2<T<t1 \quad (1) \\ Snow &= 1-Rain \\ Snow &= 1 && T<t2 \end{aligned}$$

Where T is daily averaged air temperature (°C), t1 is upper threshold temperature (°C) and t2 is lower threshold temperature (°C).

RHESSys uses a quasi-energy balance snowmelt model. Snowmelt is computed using radiation-driven melt, and melts due to the combination of sensible and latent heat, and advective heat-driven melt, occurring as rain falls on snow. Snowmelt from the combination of sensible and latent heat and advection occurs only when the snow pack is isothermal. The snowmelt due to sensible and latent heat flux is based on an empirical and linear relationship with air temperature[*Coughlan and Running*, 1997b]. Solar radiations (direct and diffuse shortwave radiation, and longwave radiation) are computed based MT-CLIM [*Running et al.,* 1987]. Absorbed direct and diffuse shortwave radiation on snowpack is computed using Beer's law and snowpack age-based albedo [*Laramie and Schaake*, 1972]. Longwave radiation on snowpack is estimated using air temperature[*Croley*, 1989]. According to the snowmelt equations implemented in RHESSys, we expect that when air temperature increases, snowmelt will be accelerated due to the increasing of the combination of sensible and latent heat, and longwave radiation contribution during the melt period.

The model has four vertical storages: vegetation (canopy and litter), surface detention storage, soil storages (unsaturated zone, rooting zone and saturated zone), and deep groundwater storage. Vegetation water storage incorporates multiple layers, including upper

vegetation layer, lower vegetation layer and litter layer. Using Beer's law, it is possible to calculate radiation distribution through vertical vegetation layers. RHESSys also accounts for sunlit versus shaded leaves and canopy gaps in its radiative transfer routines. To calculate the vegetation interception, LAI is used to determine the size of a vegetation layer's detention storage. Net throughfall through canopy and snowmelt is added to surface detention storage, and infiltrated to soil. Soil infiltration is computed using Philip's equation[*Philip*, 1957]. The drainage rate of infiltrating water from the unsaturated zone to the saturated zone is limited by soil field capacity. To calculate the soil field capacity and unsaturated hydraulic conductivity, the Clapp and Hornberger model[*Clapp and Hornberger*, 1978] is used. Preferential flow through soil macropores and bedrock fractures is computed by assuming that a fixed percentage of infiltrated water bypasses the soil zone and infiltrates to deep groundwater storage. Lateral shallow groundwater flow is calculated using transmissivity and local slope. Deep groundwater flow is calculated using the linear storage model.

The RHESSys uses Penman-Monteith equation[*Monteith*, 1965] to compute evapotranspiration (ET), which includes transpiration, evaporation of intercepted water, soil and litter evaporation. To effectively account for the environmental control on stomatal conductance in the transpiration, the model uses the Jarvis model [*Jarvis*, 1976]. In this study, vegetation is assumed to be constant over time; for example, rooting depth is constant over time, and LAI is limited by maximum LAI, and only varies with season. Model estimates of ET in RHESSys account for the interaction among atmospheric process, soil water availability and tree physiology. Warming increases atmospheric demand by increasing the capacity of air to hold moisture and changes the timing of water inputs to the soil by changing snow melt.

RHESSys has hierarchic model structures that considers of patch, zone, hillslope and watershed. Patches are the finest spatial model units related to snow, soil and vegetation processes. The 10m LIDAR DEM was used to derive the patch map. Each patch has a unique elevation value. The zone map defines climate processes, including precipitation, air temperature, solar radiation, etc. To account for the fine-scale variability of the climate processes within the watersheds, the zone map was set to be same as the patch map. The hillslope map and watershed boundary are derived using the multiple flow direction algorithm (r.watershed in GRASS6.4).

Each watershed was assigned "mixed conifer" as the vegetation type, as spatial information about vegetation species is not available. Associated vegetation parameters for the mixed conifer vegetation type were taken from RHESSys parameter libraries (https://github.com/RHESSys/ParamDB), and vegetation parameters are based on [*White et al.*, 2000]. A set of allometric equations [*White et al.*, 2000] was used to initialize carbon and nutrient stores in vegetation. The rooting depths for TSW and SDW were estimated based on [*Hunsaker et al*., 2012]: 2m for TSW and 1m for SDW. Soil properties are assumed to be spatially homogenous at watershed scale, as soil data are limited to parameterize soil properties at fine scales. Initial soil properties for each soil type are estimated based on existing RHESSys parameter libraries and then subsequently refined through calibration, described in more detail below.

The two snow parameters including the temperature threshold values and empirical temperature melt coefficient were calibrated by comparing the SWE model estimates with the measured snow depth (or measured SWE in the Upper Providence station and the Upper Bull stations)(Table 3.2). The temperature threshold values for both watersheds are the same (Table 3.2). Empirical temperature melt coefficient for the both watershed are also the same

(Table 3.2). The spatial variability of air temperature within watersheds was estimated with the temperature lapse rate. The lapse rate for minimum and maximum air temperature were calculated using the ratio of the difference of the daily minimum and maximum air temperature data to the difference of the elevations in the two stations respectively. The estimated temperature lapse rates of the two watersheds are very similar (Table 3.2). In this study, it was assumed that the snow-related parameters do not change with climate warming. This assumption may be valid because the estimated snow parameters for the both watersheds are similar or same (Table 3.2).

Figure 3. 3 show the comparison of model estimates of SWE and observed snow depth (or SWE) in the two climate stations of TSW and SDW respectively. To compare the model prediction of SWE with measured snow depth at the lower and upper station, we calculated the day of complete snowmelt in the four climate stations. Comparison between model estimate and measured values in the day of complete snowmelt results in R^2 of 0.95, 0.9 at the Providence and Bull stations respectively. These high values of R^2 imply that the model reproduced the timing of observed snowmelt (Figure 3. 3). However, the model at the Upper Providence station underestimated SWE in the year 2004 and 2007, and the model at the Upper Bull station underestimated the SWE in year 2004, and 2005, and overestimated SWE in the year 2008. The comparison of modeled SWE and measured SWE at the two station results in R^2 of 0.87 and 0.73. The lower model accuracy in the Upper Bull station (Figure 3.3d) may be related to measurement errors in SWE[*Johnson and Schaefer*, 2002]. For example, the differences of the first day of snow accumulation in year 2007 and 2008 based on the measured SWE values and measured snow depths at the Upper Bull station are 29 and 65 days each year. The peak SWE in year 2008 at the Upper Bull station is also lower than those at the Upper Providence station. In some years the model prediction of SWE did

not match observed snow data. One major problem in SWE prediction may be related to estimating the fraction of snow in the total precipitation. In RHESSys, a fixed dual daily temperature threshold is used to partition the precipitation into snow and rain, while the temperature threshold may vary with events, season and year[*Marks et al.*, 2013]. Previous studies showed that hourly humidity-based methods and physical precipitation-phase partitioning methods are a better predictor for the precipitation phase than daily temperature-based methods [*Marks et al.*, 2013]. This study however focuses on how different snow processes in the two watersheds may affect the sensitivity of hydrologic responses to climate warming. Because the modeled SWE is able to mimic the difference in the timing and magnitude of snow accumulation and melt between the two watersheds, the error of the SWE prediction will not influence this study' conclusion.

After estimating the snow-related parameters, six soil parameters (m, Ksat_h, Ksat_v, ae, po and gw1) were calibrated to reproduce the observed streamflow (Table 3.3). The six soil parameters characterize the main soil drainage properties of the both watersheds. In this study, soil parameters are assumed to remain relatively stable at decadal time scales (Figure 3. 1). The calibrated soil parameter sets with short streamflow records (5 years) can represent the drainage properties of each watershed for longer periods (63 years). The predictive performance of the model is evaluated using a combination of three objective functions (multiple objectives). The definitions of these objective functions are:

$$R_{eff} = 1 - \frac{\sum_{i} \left(Q_{obs,i} - Q_{sim,i}\right)^2}{\sum_{i} \left(\overline{Q_{obs}} - Q_{sim,i}\right)^2} \quad (2)$$

$$R_{\log eff} = 1 - \frac{\sum_{i} \left(\log(Q_{obs,i}) - \log(Q_{sim,i})\right)^2}{\sum_{i} \left(\log(\overline{Q_{obs,}}) - \log(Q_{sim,i})\right)^2} \quad (3)$$

$$PerErr = \frac{\left(\overline{Q_{obs}} - \overline{Q_{sim}}\right)}{\overline{Q_{obs}}} \quad (4)$$

$$\text{Total accuracy} = R_{eff} \times R_{\log eff} \times |1 - PerErr| \quad (5)$$

Where $Q_{obs,i}$ is the observed streamflow and $Q_{sim,i}$ is the simulated flow at any give time step (i), and $\overline{Q_{obs}}$ and $\overline{Q_{sim}}$ are the long-term average of streamflow. Note that the total accuracy (equation 5) combine different aspect of flow variability; high flows ($R_{eff,}$ [*Nash and Sutcliffe*, 1970]), low flows ($R_{loggeff}$) and total volume error of flows (PerErr).

Son and Tague [2014] showed that in both drier year, and summer periods, the effect of soil parameter uncertainty tends to be more significant in estimating hydrologic responses to climate than the effect of climate warming. To overcome the limited model calibration of soil parameters with using only observed streamflow, this study accounts for soil parameter uncertainty in predicting ET and streamflow through the use of Generalized Likelihood Uncertainty Estimation (GLUE) approach [*Beven and Freer*, 2001]. To select the behavioral soil parameter sets, same number of behavioral soil parameter sets are applied for the two watersheds; the 10 best behavioral soil parameter sets (the highest streamflow accuracy based on equation 5) among 500 simulations are selected. Figure 3. 4 shows the comparison of streamflow predictions with behavioral soil parameter sets and measured streamflow for TSW and SDW. In general, the model reproduced the measured streamflow of the two watersheds. The overall accuracy of the daily streamflow prediction is higher for SDW (0.57-0.65) than for TSW (0.28-0.39) even though snow predictions in TSW are slightly better than in SDW (Table 3.3 and Figure 3. 3 and 3.4). In SDW, the model showed high

accuracy in daily flow prediction and the high flow is better predicted than low flow (R_{eff}=0.82-0.86 and R_{logeff}= 0.70-0.80). In TSW, the model captured the seasonal pattern of observed streamflow (Table 3.3), and the model had better performance for low flows (R_{logeff}= 0.67-0.76) than high flows (R_{eff}=0.47-0.56). For both watersheds, the model failed capturing the observed small peak flow. The poor prediction of peak flow may be due to an overestimate of the fraction of snowfall in total precipitation in the late fall and winter as well as misrepresentation of variable soil depth within the watershed. TSW has areas with locally shallow soil depths [*Bales et al.*, 2011]. The area with shallow depths can generate the peak flow rapidly responding to snow melt or rainfall event. In this study, soil depth is assumed to be uniform within the watershed because detail soil depths map at fine scales is not available. The model showed larger percentage error of streamflow prediction (PerErr=-23-18) in TSW than in SDW. The existence of deep weathered bedrock in TSW alters the flow path through deep percolation, and the watershed might have more complex flow process compared to relative simple subsurface lateral flow over hard bedrock in SDW. The poorer streamflow prediction of TSW compared with those of SDW may be partially due to the inaccurate representation of subsurface topography and processes. The model showed relatively high streamflow accuracy values at the monthly time scale(Table 3.4). The model with highest streamflow accuracy for both watershed has less than 3% in PerErr. The model performance are similar to performance statitics obtained for other model applications in this region. The selected set of behavioral soil parameters also reflect the different flow drainage pattern of two watersheds (Table 3.3): for example, model parameters for TSW have higher gw1 than those for TSW. Based on this level of model performance, we argue that the calibrated model can be used to test the difference in the sensitivity of seasonal and annual model estimates to climate warming between the two watersheds, because the model

successfully distinguishes the difference in observed flow drainage pattern between the two watersheds.

3.2.3 Impact of climate warming on hydrologic fluxes of TSW and SDW

This study aims to investigate the impact of climate warming on hydrologic fluxes (snow, evapotranspiration (ET), moisture deficit (MD) and streamflow) in TSW and SDW. The investigation examines the following hydrologic variables: inter-annual variation of hydrologic fluxes, seasonal ecohydrological fluxes, spatial structure of seasonal ET, and primary factors controlling seasonal spatial ET. To investigate the inter-annual variability of the hydrologic fluxes of the two watersheds, a long historical climate data (>50 years) is required. In the Providence and Bull watersheds, basic climate data have been collected since year 2002. In order to extend our meteorological record to drive model scenarios, this study used the longer climate data (year 1941 to 2009) of the Grant Grove station where the station is located at 20km away from the Bull watersheds. The Grant Grove station has a similar temporal pattern of precipitation and temperature to the Providence and the Bull climate stations. The longer climate data for the Providence and the Bull climate stations were estimated by comparing the local climate station data with Grove Grant station data. By fitting the air temperature data of local climate station to the data of the Grove Grant station, a linear regression model was estimated for air temperature of local climate stations. The linear regression model was applied to generate the longer air temperature data of each local climate station; the correlation between minimum daily temperature and maximum daily temperature of Providence and Grant Grove stations results in R^2 of 0.89 and 0.85. The correlation between minimum daily temperature and maximum daily temperature of Bull and Grant Grove stations results in R^2 of 0.82 and 0.73. To generate the longer daily

precipitation data for the Bull and Providence stations, mean annual precipitation of the Bull and Providence stations was divided by mean annual precipitation of the Grove Grant station for the period of 2003 to 2007, and 2002 to 2006 respectively. The ratios of the two values were computed. The respective ratios (1.22 and 1.21) were applied to generate the longer daily precipitation data of each local climate station. To simulate projected climate warming scenario based on recent GCM prediction for California Sierra[*Maurer and Duffy*, 2005; *Cayan et al.*, 2008], this study adds a uniform 2 C° and 4 C° temperature increase to the observed meteorological record. We assume that the temperature increase with elevation is constant[*Oyler et al.*, 2015]. This simple approach focus on the direct impact of increasing temperature on model estimate and avoid the complex and highly uncertain downscaling of climate model output[*Wood et al.*, 2002; *Tague et al.*, 2009].

This study also examines the relationship among annual precipitation, annual ET, annual moisture deficit, summer streamflow and annual streamflow and how the relationship varies between TSW and SDW, and how climate warming might alter these relationships. Moisture deficit (MD) is defined as potential evapotranpiration (PET) minus actual evapotranspiration (ET) (index of plant water stress, [*Tague et al.*, 2009]). PET is calculated using Penman-Monteith equation [*Monteith*, 1986]. In the PET calculation, the canopy conductivity (1/canopy resistance) is calculated with maximum species-level stomata conductivity times estimated LAI values from LIDAR image. The estimated moisture deficit is used to determine the change in vegetation water stress imposed by climate warming.

To examine the dominant factors in controlling the spatial seasonal ET both in TSW and SDW, univariate linear regression models are developed to identify the relationship between physiographic parameters and seasonal ET estimates. Four physiographic parameters are considered: 1) elevation, 2) aspect, 3) LAI and 4) wetness index [*Beven and Kirkby*, 1979].

Values for four physiographic parameters and monthly ET are taken from each patch within the watershed boundaries. The relationship between the physiographic parameters and monthly ET is quantified using Pearson correlation coefficient (R). Table 3.4 shows the correlations (measured by Pearson correlation coefficient, R) of the physiographic parameters in TSW and SDW. For both watersheds, the correlation between all parameters is statistically significant except for the relationship between aspect and LAI in SDW. Among parameters, elevation is most correlated with wetness index (R=-0.23) compared with elevation's correlation with other parameters. In TSW, LAI is also highly correlated with elevation (0.19), while in SDW, LAI is highly correlated with wetness index (0.16).

3.3 Results

3.3.1 Climate warming's effects on inter-annual hydrologic responses in TSW and SDW

Figure 3.5 shows the relationship between annual precipitation and model estimates of annual streamflow, summer flow, annual ET and annual MD in TSW and SDW, and the effect of warming on the relationship. For the two watersheds, increases in annual precipitation leads directly to linear increases in the estimated annual streamflow. SDW has a higher runoff ratio than TSW (Figure 3. 5a, Table 3.1), which may be due to lower vegetation water use (lower LAI and shallower rooting depths) [*Hunsaker et al*., 2012] and Table 3.1). Shallower groundwater storage of SDW also attributes to the higher runoff yield given precipitation. Summer flow estimates of both watersheds have positive relationships with the annual precipitation, and SDW has higher magnitude and variability of summer flow than TSW. Annual ET estimates in TSW increase non-linearly with the increasing

annual precipitation. Annual ET estimates in SDW are more or less constant with the increasing precipitation. Annual MD estimates in TSW decrease with increasing precipitation with a steeper slope than those in SDW. These results suggest that TSW is a more water-limited watershed than SDW.

Climate warming reduces annual peak SWE, annual flow and summer flow, and increases annual ET and annual MD for the two watersheds (Table 3.5). The warming effects on these four variables are larger in SDW than in TSW. For both watersheds, 2 °C and 4 °C warming significantly reduced annual peak SWE compared with historical climate. In TSW, 2 °C and 4 °C warming results in reduction in mean annual peak SWE of 116mm (55%)and 172mm (82%), respectively; In SDW, 2 °C and 4 °C warming results in reduction in mean annual peak SWE of 222mm (56%) and 324mm (81%), respectively. For TSW, the changes of summer flow and annual ET with 2 °C and 4 °C are also statistically significant compared with those with historical climate. The changes of annual flow and annual MD with 4 °C warming are statistically significant relative to the model estimates with historical climate conditions (Table 3.5). For SDW, the change of the four variables with 2 °C and 4 °C warming are statistically significant relative to historical climate conditions (Table 3.5). Warming effects on summer flow, annual MD and annual ET are also larger in wetter years than drier years (Figure 3.5). SDW under 2 °C warming still has higher annual streamflow, and summer flow and has lower sensitivity of annual ET to annual precipitation compared to the TSW under historical climate conditions.

3.3.2 Climate warming's effects on seasonal hydrologic responses in TSW and SDW

Figure 3.6 shows the effect of climate warming on monthly SWE, ET, MD and streamflow in the two watersheds. In TSW, peak monthly SWE occurs in March, and climate warming decreases snow accumulation and accelerates snowmelt (Figure 3.6a). In TSW, 2 °C and 4 °C warming results in reduction in mean peak monthly SWE for 72mm (78%) and 90mm(96%), respectively; In SDW, 2 °C and 4 °C warming results in reduction in mean monthly peak SWE for 206mm(74%) and 262mm(95%), respectively. With a 4°C warming, most precipitation occurs as rain rather than snow for both TSW and SDW. In TSW, Peak monthly ET occurs in May, and 2°C and 4 °C warming do not change this timing but increase monthly ET in the winter and early spring while decreasing monthly ET in the late spring and summer. Peak monthly MD occurred in August. Similarly, 2°C and 4 °C warming do not alter this timing, but warming increases the monthly MD from May to November, and decreases the monthly MD in all other months. Peak monthly streamflow occurs in March, and do not change this timing at the monthly time step, while at the daily time step, there is 31 and 43 day shift in timing of flow (measured as center of mass of flow) for 2 °C and 4 °C warming scenarios. 2 °C warming does increase peak monthly streamflow from 66mm to 72mm (9%). Warming increases the monthly streamflow in January to March, and decreases the monthly streamflow in the remaining months.

The effects of warming on monthly hydrologic fluxes in SDW are larger than those in TSW. For a 2°C warming, SDW has the same timing but slightly smaller magnitudes of monthly SWE as TSW under historical climate conditions. A 2°C warming in SDW shifts the timing of peak monthly ET from June to May, but the change in the magnitude of peak

monthly ET is less than 5%. A 2°C warming increases monthly ET from October to May, but decreases monthly ET in all other months. With a 2°C warming, SDW has similar temporal monthly ET patterns as well as the same timing of peak monthly ET, compared with TSW under historical climate conditions. TSW however has larger monthly ET across all years than SDW. 2°C warming shifts the timing of SDW's peak monthly streamflow to be same as TSW under historical climate conditions; however, SDW still has larger monthly streamflow than TSW.

3.3.3 Climate warming's effects on spatial structure of seasonal ET and its relationship with physiographic parameters

Figure 3.7 shows the effect of climate warming on the spatial structure of monthly ET in TSW and SDW. The spatial structure of monthly ET is measured with standard deviation (SD) and coefficient of variance (COV). Spatial SD and COV of monthly ET are computed using values of monthly ET taken from each patch within the watershed boundaries. The spatial SD of the monthly ET in TSW has different temporal patterns than those in SDW (Figure 3. 7b). In TSW, the highest SD of monthly ET occurs in July, and high SD values are maintained in the spring and summer (from March to August). In SDW, the highest SD of spatial ET occurs in August, and SDW has a lower SD of spatial ET in the spring and winter compared to TSW. In TSW, 2 °C and 4°C warming decreases SD of spatial ET in the spring and increases the spatial SD of ET in the summer. However, in SDW, 2 °C and 4°C warming increases SD of spatial ET in the winter, spring and summer. SDW under 2 °C warming has similar temporal patterns of SD of spatial ET to TSW under historical climate conditions and both watersheds have the highest SD in July. SDW under 2 °C warming

however has higher SD of spatial ET in the summer and lower SD of spatial ET in the spring than TSW under historical climate conditions.

Spatial patterns of monthly ET and the effect of warming on these patterns were also explored with the coefficient of variance (COV) (Figure 3.7b). Both watersheds have the highest COV of spatial ET in August under historical climate conditions. Climate warming decreases COV of spatial ET in the winter and spring, but increases its values in the summer for both watersheds. The highest COV of spatial ET occurs in the August under the two warming scenarios. SDW under 2 °C warming has similar temporal patterns of COV of spatial ET and higher COV values, compared with TSW under historical climate conditions.

Figure 3.8 shows the relationship between four physiographic parameters and spatial monthly ET in TSW and SDW and the warming effect on their relationship. In TSW, elevation has negative correlation with the spatial ET in the winter and spring, and has positive correlations with the spatial ET in the summer (Figure 3. 8a). Lower elevations tend to have higher ET due to higher temperatures. Aspect has negative correlation with spatial ET in most months, such that southwest locations tend to have higher ET (Figure 3.8b). Because slopes with southwest aspect tend to receive more radiation, and have earlier snowmelt, southwest slopes will tend to have higher ET in the winter and spring. As a season changes to summer, effect of aspect becomes minor. Wetness index always has positive correlation with spatial ET, and in summer, wetness index has the highest correlation value with spatial ET among the four physiographic parameters. LAI has positive and the highest correlation values with spatial ET in winter, spring and fall. The correlation between ET and LAI decreases in the summer. Lower correlation between ET and LAI in the summer reflects that vegetation experiences water-stress conditions in the summer.

The relationship between physiographic parameters and spatial monthly ET in SDW is very similar to those in TSW. Elevation and aspect have a negative correlation with spatial ET in the winter and the spring, and the correlations value becomes close to zero in the summer. Wetness index always has positive correlation with spatial ET, and correlations are higher in summer than other seasons. Similar to TSW, LAI has a positive correlation with ET and the highest correlation value, across all physiographic parameters, with spatial ET in the winter, the spring and the fall. As with the TSW, the correlation between spatial ET and LAI decreases in the summer.

The effects of warming on the relationship between monthly ET and physiographic parameters are larger in SDW than in TSW. Under 2 °C and 4°C warming, the correlation between wetness index and spatial ET in SDW increases in the spring but decreases in the summer. Effect of warming on these relationships in TSW is minor. The correlation values between LAI and spatial ET in SDW increase in the winter and early spring, but the values decrease in late spring and the summer. In TSW, the correlation values slightly decreases or remains constant. Warming reduces the correlation between LAI and summer ET in both watersheds. In SDW, the increase of available water for plant due to earlier snowmelt and change in the precipitation phase from snow to rain can explain the increase in correlation values between monthly ET and LAI in the winter and earlier spring. The increase in water-limitation due to the higher vapor deficit in atmosphere and higher moisture deficit in soil lead to the decreased correlation values in the summer for both watersheds. While SDW under 2°C warming has higher correlation value in the monthly ET and LAI than TSW under historical climate conditions, especially in winter and spring, the two watersheds has similar temporal pattern in the relationship between monthly ET and LAI.

3.4 Summary and Discussion

This study used RHESSys to examine the potential difference in hydrologic changes between TSW and SDW due to climate warming. As expected, modeling results showed that increasing air temperature reduces snow accumulation and accelerates snowmelt, increases annual ET, and decreases annual streamflow and summer flow in both TSW and SDW. These results are consistent with previous modeling and empirical studies in snow dominated mountain regions [*Christensen et al*., 2008;*Tague et al*., 2009;*Godsey et al*., 2014;*Berghuijs et al.*, 2015]. The reductions of annual streamflow and summer flow result from the reduction of SWE, and the increase of spring ET. Since average air temperature of SDW about 2°C colder than those of TSW, and SDW generally has more of precipitation falling as snow under historical climate conditions, we expect that SDW will show higher sensitivity to climate warming than TSW. Modeling results confirmed that SDW has higher sensitivity to climate warming than TSW. The relationship between annual ET (or MD) and annual precipitation suggests that TSW is more water-limited compared to SDW. When the warming scenarios are applied, larger changes in mean monthly and annual peak SWE for SDW are observed, compared to TSW. This suggests that SDW is more temperature-limited when compared to TSW. The empirical study of *Goulden and Bales* [2014] also support our results. *Goulden and Bales* [2014] developed an empirical water balance model based on flux tower ET data and MODIS vegetation product (NDVI) in upper King River Basin where our two watersheds are located. Their modeling study showed that above 2400m, estimated ET is limited by cold temperatures, while at lower elevations, estimated ET is limited by water availability. Consequently the sensitivity of ET to warming is more significant at the higher elevations than at the lower elevations.

Previous studies using empirical approach improve our understanding of the sensitivity of ET and streamflow to climate warming in various sites [*Safeeq and Grant*,2012; *Nolin and Daly*, 2006; *Jefferson*, 2011]. However, empirical approaches have difficulty in assessing the effect of climate warming on individual watersheds due to the confounding effect of other hydrologic properties [*Peel and Bloschl*, 2011]. To demonstrate these compounding effects, this study examined whether the differences of air temperature between TSW and SDW can explain the different hydrologic responses to climate warming (Table 3.6). On average SDW is 2 ° C colder than TSW. Thus we might expect that SDW under a 2C warming will behave similarly to TSW under historical climate conditions. When 2° C warming is applied to SDW, monthly SWE is similar that of TSW under historical climate conditions. However there are signficant differences in hydrological behavior between the two watersheds. With a 2° C warming, SDW still has higher annual streamflow and summer flow than TSW under historical climate conditions. Even though warming increases annual ET in SDW in wet periods, the slope of the annual ET versus annual precipitation curve in SDW is still small compared this slope in TSW. In the model implementation used here, vegetation parameters (e.g. LAI and rooting depth) were held constant and both LAI and rooting depth are lower in SDW. Lower LAI for trees in SDW means that they experience less frequent water-stress conditions compared with those in TSW even after snow processes and atmospheric demand for ET became similar with a 2 °C warming. To examine how a shift in LAI in SDW might alter these results, we perform additional simulation to test the effect of LAI on the responses of annual ET and annual MD to precipitation in SDW. Figure 3.11 and Table 3.7 show the effect of doubling LAI in SDW under 2° C warming scenario on annual ET and annual MD. A doubling of LAI in SDW

leads to an LAI is SDW similar to the LAI in TSW. Doubling the LAI in SDW under 2° C warming increases annual ET, and slope of the annual ET versus annual precipitation curve becomes similar to the slope in TSW under historical climate condition. Doubling the LAIs in SDW increases annual MD, and yields values that are similar to annual MD in TSW. Thus once difference in LAI are accounted for, SDW for the 2° C warming scenario are similar to hydrologic fluxes for TSW under baseline conditions. However, SDW under 2° C warming with mean LAI value similar to TSW still has a lower mean annual ET (119mm, 15%) than TSW under historical climate conditions. Shallower rooting depth in SDW may attribute to the lower ET. In this study, 2m rooting depth was applied to TSW, while 1 m rooting depth was applied to SDW. These results suggest that the differences in vegetation structures between the two watersheds can partially explain the different ET response to climate warming.

When doubling LAI and 2° C warming are applied to SDW, SDW still generates higher annual flow and summer flow than TSW under historical climate conditions (Table 3.5). The difference of subsurface properties between the two watersheds may explain the remaining flow difference. Even though the two watersheds both have the same granitic geology, TSW has more deeply weathered bedrock than SDW [*Dahlgren et al.*, 1997]. TSW therefore has higher percolation in deep groundwater storage through preferential flow paths than SDW. Calibrated drainage parameters in RHESSys for the two watersheds reflect these geologic distinctions (Table 3.2); SDW has higher Ksat_h value, and lower gw1 than TSW. SDW with relatively shallow regolith depths therefore can generate faster subsurface flow. Due to the difference of subsurface properties and vegetation structures, SDW under 2 °C warming still generates higher annual flow and summer flow compared with TSW under

historical climate conditions. Previous studies also demonstrated that the geological difference can explain the sensitity of hydrologic responses to climate warming. *Tague and Grant* [2009] demonstrated showed that watersheds with slow draining, deep groundwater, such as those of the High Cascades in Western Oregon, have four times greater reduction of August streamflow under 1.5 °C warming scenarios than neighboring fast draining watersheds dominated by Western Cascade geology. Similarly *Safeeq and Grant* [2012] tested the observed streamflow sensitivity to climate variability between watersheds in the western United States. They concluded that watersheds dominated by deep groundwater are more sensitive to climate warming than watersheds dominated by shallow groundwater.

For seasonal hydrologic fluxes, SDW under 2°C warming scenario behaves similarly to TSW under historical climate conditions, compared with annual hydrologic fluxes. For example, the two watersheds have the same timing of monthly SWE, and peak monthly ET, MD and streamflow. The temporal pattern in SD of monthly ET in SDW under climate warming is similar to those in TSW under historical climate conditions. The similar response of the two watersheds can be attributed to similarities in the temporal distribution of water and energy in the two watersheds: in both watersheds, winter precipitation in annual precipitation is dominant, and solar radiation and air temperatures follow similar seasonal patterns.

This modeling study showed that LAI is the dominant control on the spatial ET for most of the year, and wetness index becomes important during the summer in the both watersheds, and these patterns remain under future warming conditions (Figure 3.8). High correlations between LAI and spatial ET reflect the dominant atmospheric control on ET, and high correlations between wetness index and spatial ET reflect the water stress control on ET[*Emanuel et al.*, 2010]. On the other hand, previous studies showed that elevation and

aspect ctonrols on spatial patterns of vegetation water use and distribution [*Christensen et a*l., 2008; *Istanbulluoglu et al.*, 2008]. In mountain watersheds, elevation is highly correlated with air temperature and precipitation, and aspect is also highly correlated with solar radiation distribution. However, the two watersheds in this study have a low spatial variability (less than 1%) of precipitation along elevation gradients. Low temperature gradient is also observed due to small elevation range, compared with other studies [*Christensen et a*l., 2008;*Tague et al*., 2009]. In regions drier than our sites, aspect may play a key role in controlling the vegetation water use and growth through large solar irradiance difference[*Istanbulluoglu et al.*, 2008]. *Goulden and Bales* [2014] showed that the effect of local aspect on estimated ET (NDVI-based ET) is more substantial in the lower elevation (<1000m) in the Kings River Basin where the water limitation is a key control on vegetation behaviors. Aspect within both watersheds tends to have a unimodal distribution rather than bimodal distribution. For our study sites, less water-limited conditions and spatial pattern of aspect within the watersheds can explain the low correlation between aspect and spatial ET in this watershed.

Spatial patern of ET also vary seasonally and respond to warming. This modeling study showed that spatial variances (SD and COV) of monthly ET are highest in the summer and that climate warming increased the spatial variances, although this effect is small relative to differences between months or between watersheds. The increased variances may be related to limited soil moisture in the dry summer periods, and under climate warming. The field measurement of soil moisture supports this pattern. *Kerkez et al*. [2012]'s soil moisture sampling study that conducted in a sub-watershed (P301) of Providence watershed showed that soil moisture variation (COV) increases in the summer period. According to the relationsip between wetness index and spatial ET (Figure 3.8), summer ET is highly

correlated with wetness index that reflects spatial distribution of surface moisture conditions within a watershed. *Emanuel et al.* [2010]'s modeling study also showed in the northern Rocky Mountains that summer ET is dependent on the available soil moisture. Increased spatial variance of predicted ET under climate warming implies that evapotranspiration monitoring in future may require dense sampling networks in order to accurately characterize the vegetation responses to climate.

In summary, this study demonsrated that SDW with 2°C warming is not equivalent to TSW with historical climate condition; This result implies that hydrology does not simply move uphill under climate warming, which is opposed to the assumption of previous studies in ecology[*Goulden and Bales*, 2014;*Blois et al.*, 2013]. This result showed potential limitation of using "space-for-time" substiution approach for climate impact studies. This result also suggests that forest structure and subsurface properties may be as important as the difference in air temperature in explaining hydrologic response to warming in the two Sierra Nevada watersheds. Our modeling study demonstrated that vegetation (e.g. LAI) and topography (e.g. wetness index) are primary factors controlling spatial patterns of seasonal ET under both of historical climate conditions and climate warming scenarios, and the spatial variability of seasonal ET increases under warming scenarios, especially during the summer. These results provide information about where and when forest will experience water stress both in current and future conditions and can guide management adpations to these risks.

Figures

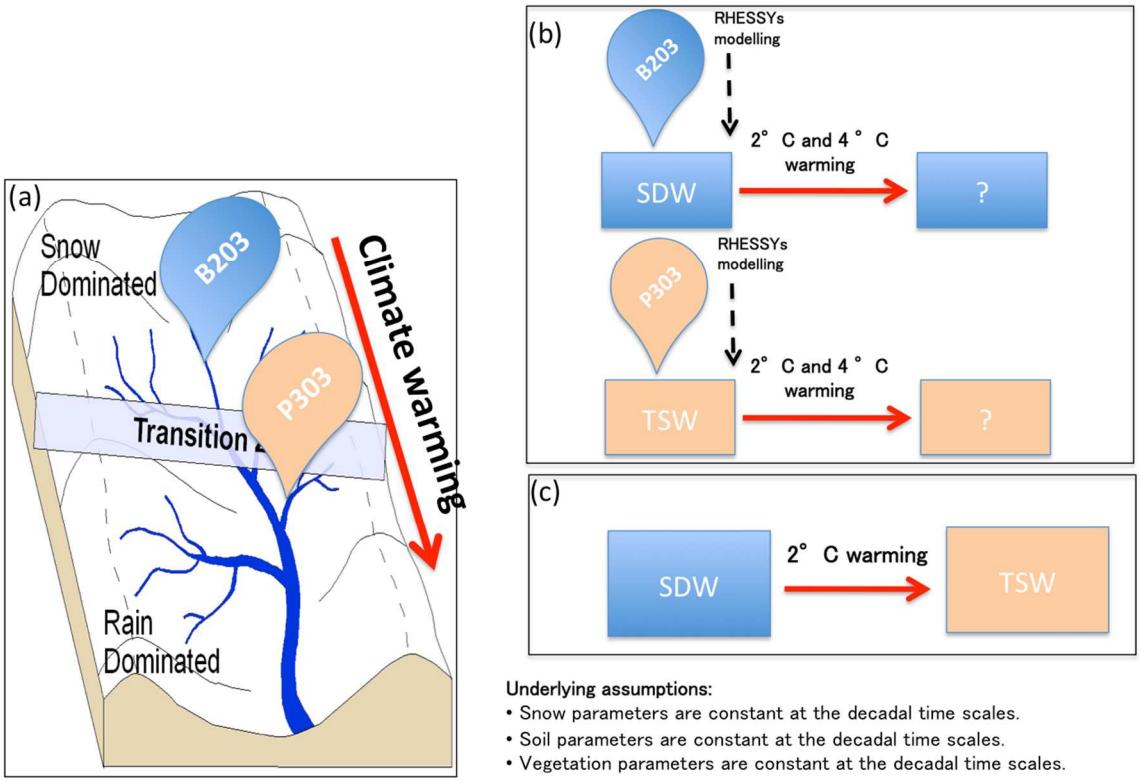

Figure 3.1. A framework for examining the effect of climate warming on hydrologic responses in the two small Sierra Nevada watersheds: (a) P303 is located in transient snow zone, and B203 is located in snow-dominated zone. (b) 2 °C and 4 °C warming scenarios are applied to the two watersheds, and are compared the two watersheds' hydrologic responses to the two warming scenarios, and (c) to isolate the effect of climate warming relative to other hydrologic properties (vegetation and geology, etc), the TSW under historical climate conditions is compared with SDW under 2 °C warming.

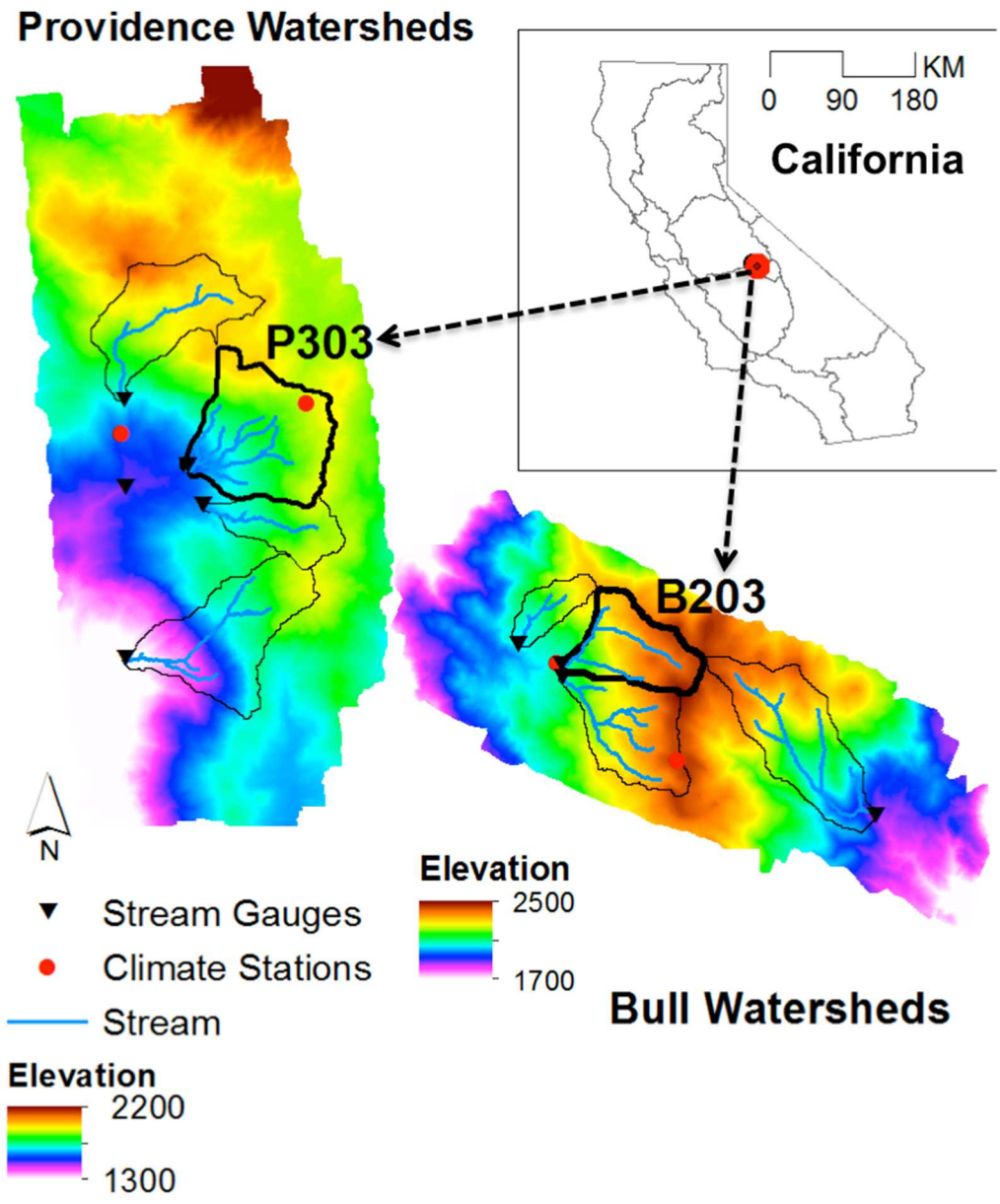

Figure 3.2. Study sites: (left) Providence watersheds, (right) Bull watersheds: (circle) climate stations.

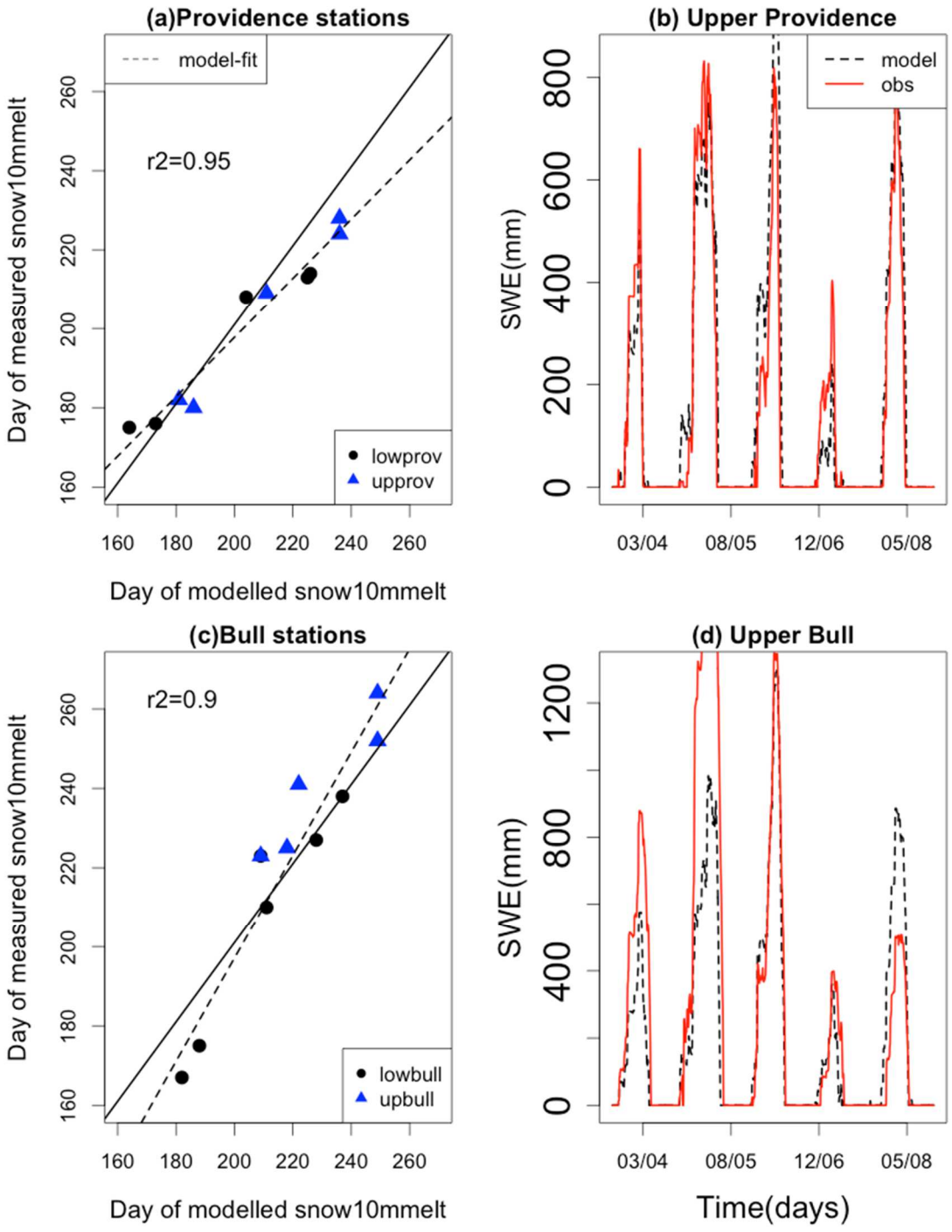

Figure 3.3. Comparison of observed snow depth/ SWE with predicted SWE at the climate stations: (a) comparison of day of snowmelt in Providence climate stations, (b) comparison of SWE in Providence climate stations, (c) comparison of day of snowmelt in Bull climate stations, and (d) comparison of SWE in Bull climate stations.

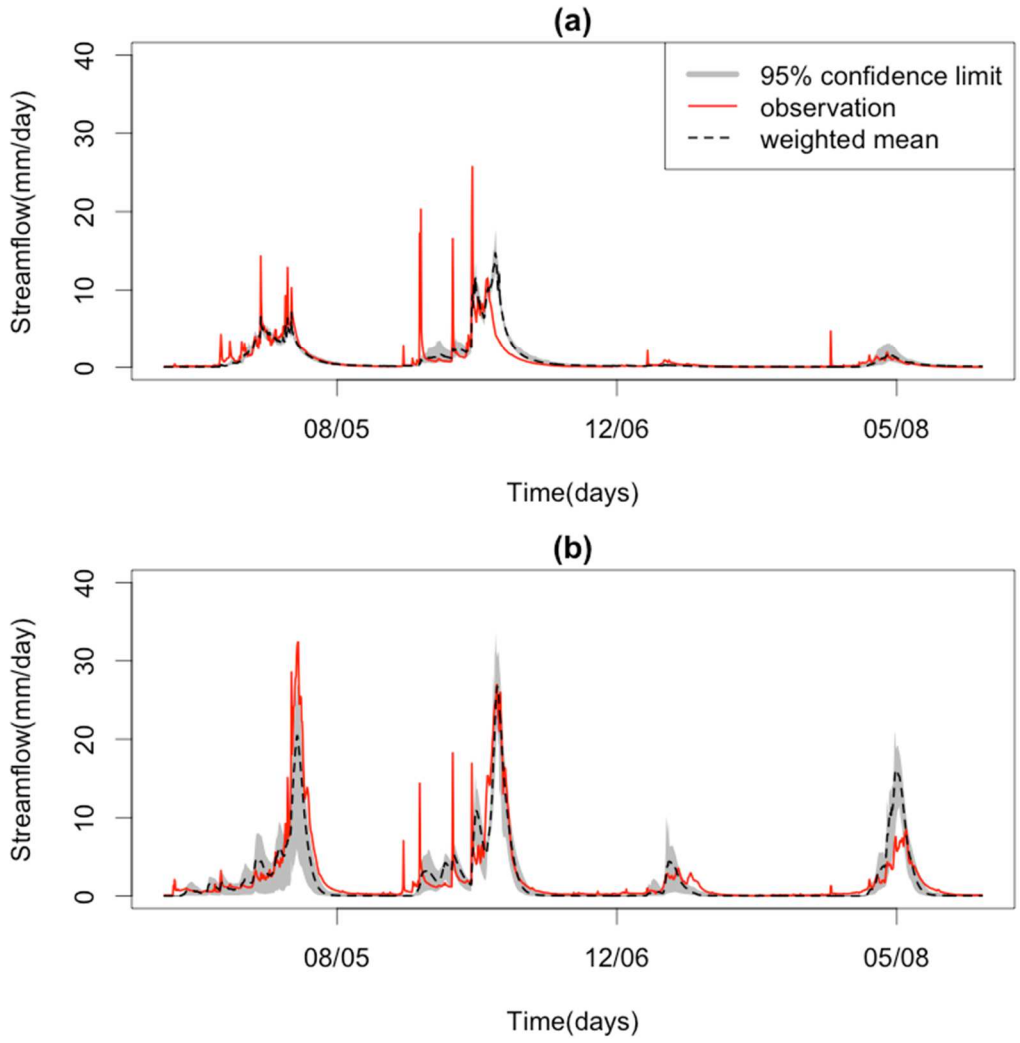

Figure 3.4. Comparison of observed streamflow with predicted streamflow at TSW and SDW gauging stations: (a) TSW and (b) SDW, gray area represents the 95% confidence limit.

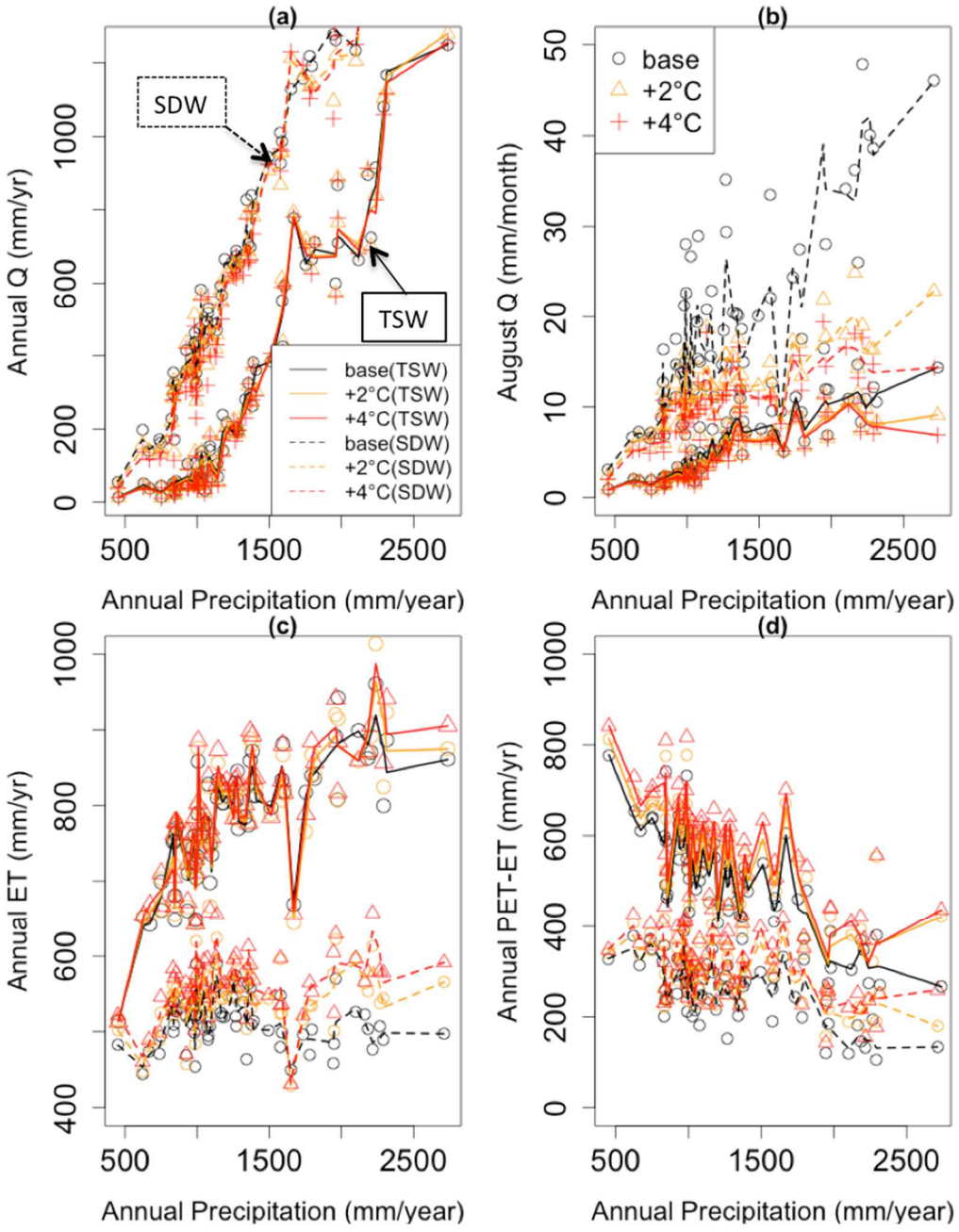

Figure 3.5.The relationship among annual precipitation, annual streamflow, August streamflow, annual moisture deficit (PET-ET) and annual ET of TSW and SDW during climate warming scenarios: (a) annual flow, (b) August (summer) flow, (c) annual ET, and (d) annual moisture deficit (PET-ET), and the three lines (black, orange, and red) were created by using LOESS (local polynomial regression fitting algorithm), and the interpolated line is used for only guiding visually the general pattern of model estimates and is not necessarily statistically significant.

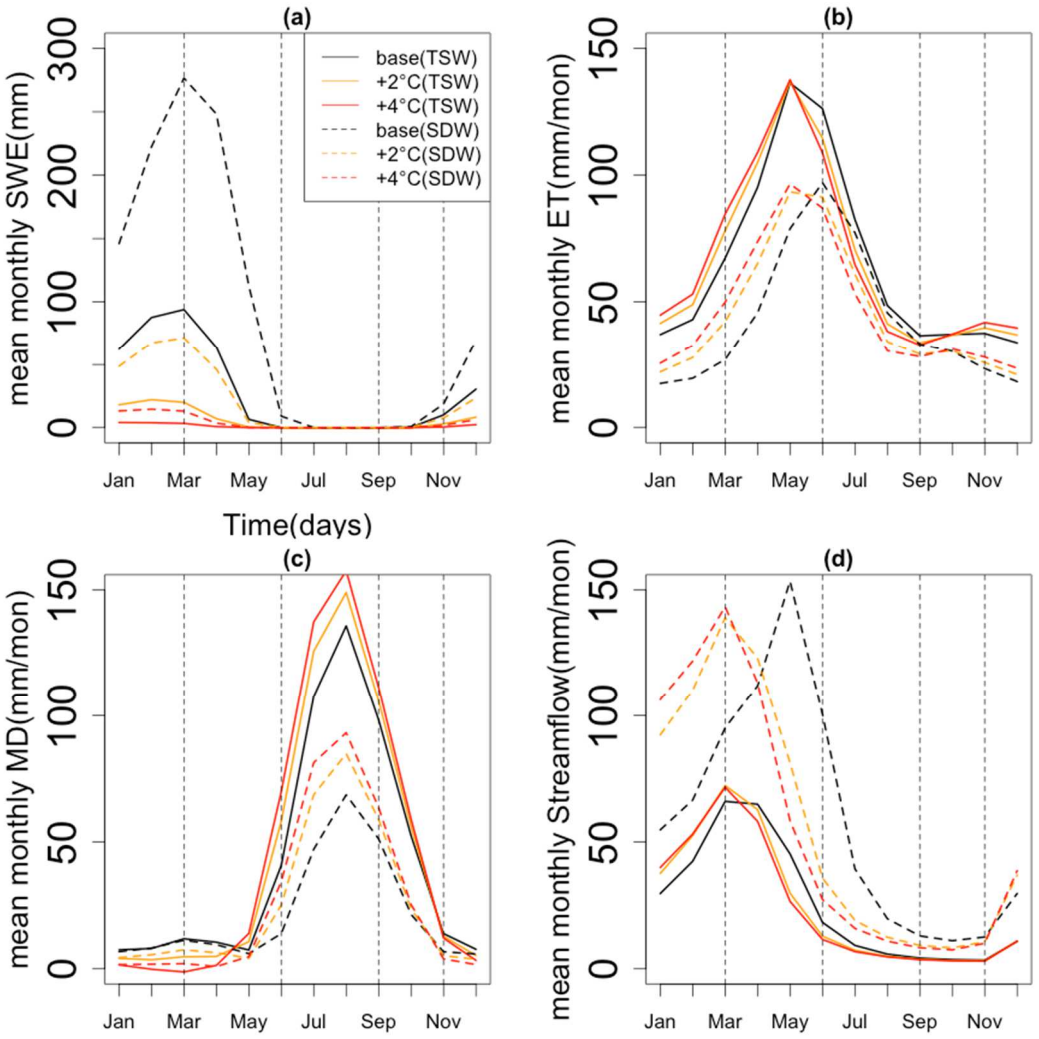

Figure 3.6. Climate-warming effect on long period (63 years) seasonal hydrologic fluxes of TSW and SDW: (a) monthly mean flow across 63 years, (b) monthly mean ET across 63 years, (c) monthly mean moisture deficit across 63 years, and (d) monthly mean streamflow across 63 years.

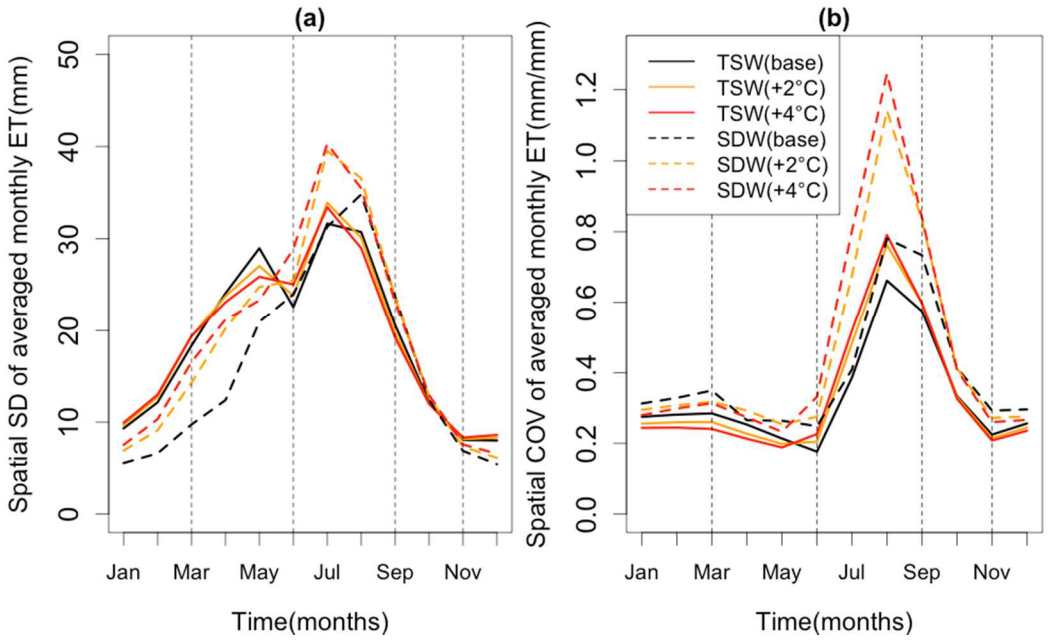

Figure 3.7. Spatial mean, standard deviation (SD), coefficient of variance (COV) of monthly ET across 63 years for TSW and SDW with climate warming: (solid line) TWS and (dotted line) SDW: (a) spatial mean of averaged monthly ET, (b) spatial standard deviation (SD) of averaged monthly ET a (c) spatial variance (COV) of averaged monthly ET.

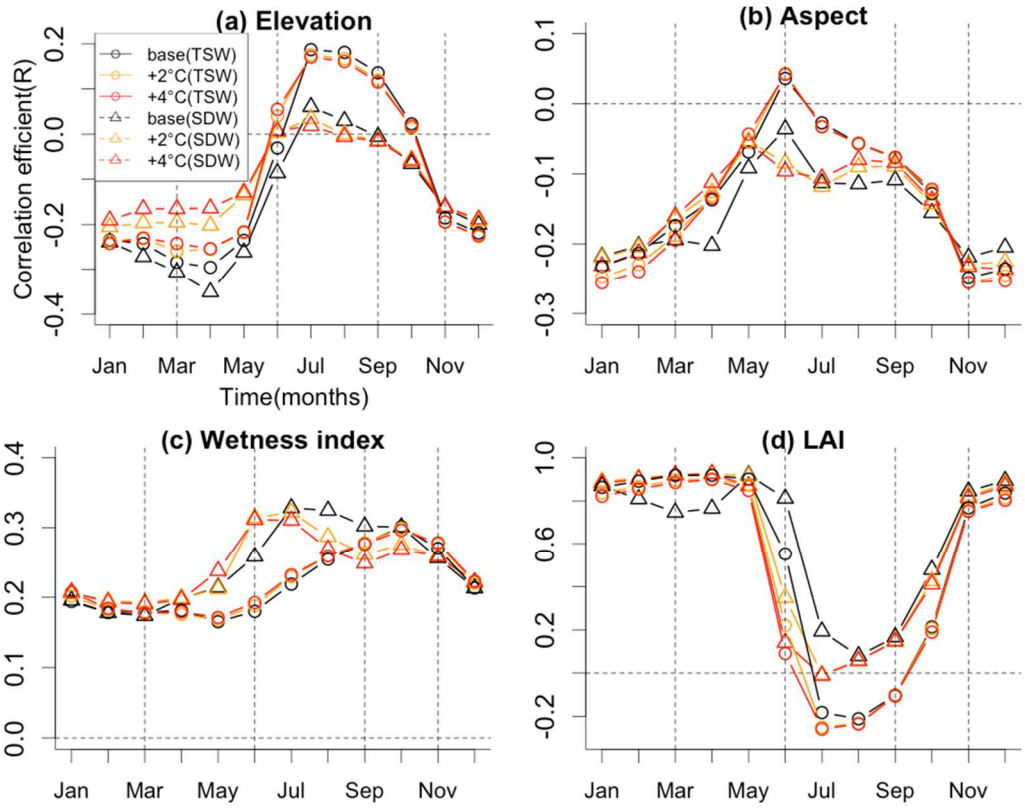

Figure 3.8. The relationship between physiographic parameters and the spatial pattern of monthly ET (expressed as Pearson correlation coefficient (R)): (a) elevation, (b) aspect, (c) wetness index and (d) LAI.

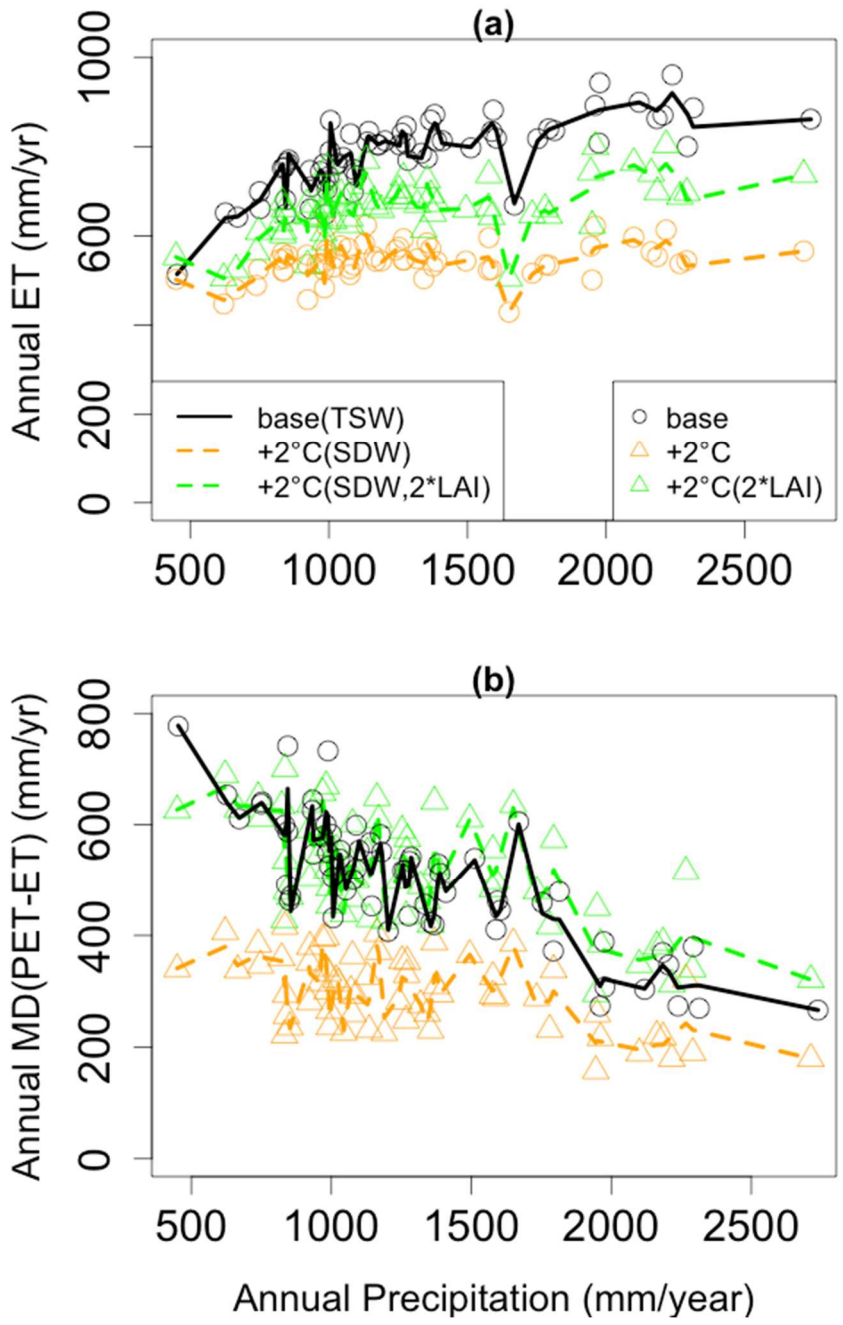

Figure 3.9 The relationship between annual precipitation, annual evapotranspiration (ET) and annual moisture deficit (MD) in TSW and SDW: (a) annual ET and (b) annual MD (PET-ET). I applied two scenarios for SDW including 2°C warming and doubled LAI value. Using LOESS (local polynomial regression fitting algorithm created the three lines (black, orange, and green).

Tables

Table 3.1. Basic hydrologic properties of the P303 and the B203 [Hunsaker et al., 2012]

Watershed	P303 (TSW)	B203 (SDW)
Elevation	1730 to 1990m	2185 to 2490m
Aspect	SW	SW
Slope	1.3 to 30.3 (12.73)	0.9 to 24.9(11.38)
Vegetation	Mixed Sierra conifer (Dominant tree species: white fir) LAI distribution:0.3 to 6.2 (3.2)	Mixed Sierra conifer (Dominant tree species: Red fir) LAI distribution: 0.2 to 5(1.6)
Soil	Dominant Soil types: Shaver (66%) Strongly weathered quartz diorite Permeability: Moderately rapid Hydrologic soil group: B	Dominant Soil types: Cagwin(80%) Highly weathered granitic rock Permeability: Rapid Hydrologic soil group: A
Precipitation /Runoff	Precipitation type: Snow-rain transition Mean annual Precipitation (2005 to 2007): 1513mm Runoff ratio(R/P): 0.20	Precipitation type: Snow-dominated Mean annual Precipitation (2005 to 2007) :1517mm Runoff ratio(R/P): 0.53
Temperature	Daily average temperature (°C) of 2004 to 2007 (mean ±SD): Min: 4.5 ±0.8 Max: 13.0 ±1.0 Mean: 8.6 ±0.9	Daily average temperature (°C) of 2004 to 2007 (mean ±SD): Min: 3.3 ±1.1 Max: 11.2 ±-0.7 Mean: 6.8 ±0.8
Drainage pattern	Wetness index: 4.1 to 13.8(7.2)	Wetness index: 4.1 to 15.9(7.2)

Table 3.2. Calibrated snow and soil parameters.

Snow parameters			
Watershed	Temperature laps rates (tmax /tmin)[1] (°C/m)	Temperature threshold for rain vs snow[2] (°C)	Temperature melt coefficient (m/°C)[3]
TSW	0.0063/ -0.0064	-3 to 3	0.005
SDW	0.0068/ -0.0060	-3 to 3	0.005

Soil parameters[4]						
Watershed	m (/)	Ksat_v (m/day)	Ksat_h (m/day)	ae (1/m)	po (/)	gw1 (/)
TSW	0.02/0.34 (0.20)	54.1/272.8 (272.8)	4.8/196.8 (64.2)	0.11/0.77 (0.19)	0.1/0.22 (0.22)	0.11/0.25 (0.25)
SDW	0.17/0.40 (0.17)	14.0/294.4 (122.8)	6.6/280.7 (234.8)	0.10/0.68 (0.14)	0.1/0.24 (0.14)	0.02/0.09 (0.03)

1: Since fine-spatial scale air temperature is not available in the two watersheds, air temperature within a watershed is spatially interpolated with the given elevation and the calculated temperature laps rates; 2: To partitioning total precipitation into snow and rain, I use the air temperature as a proxy variable, and the proportion of snow and rain in the total precipitation is linearly interpolated based on the minimum and maximum temperature values;3: Temperature melt coefficient accounts for snow melt due to latent heat and sensible heat; 4: Six soil parameters are calibrated: Ksat_v: vertical saturated hydraulic conductivity; Ksat_h: horizontal saturated hydraulic conductivity; m: decline coefficient of Ksat with depth; gw1: the percentage of preferential flow from the soil surface to deep groundwater storage; ae; air entry pressure; po: pore size index. Parentheses values are the best soil parameter sets or highest model accuracy values in comparison between predicted streamflow and measured streamflow.

Table 3.3. Model accuracy of streamflow prediction for TSW and SDW.

Watershed	Time scale	Streamflow accuracy measures (Equation 1-4)[1]			
		R_{eff}	R_{logeff}	PerErr	Total accuracy
TSW	Monthly	0.64/0.79(0.73)	0.64/0.75(0.75)	-23/18(-2.6)	0.41-0.53(0.53)
	Daily	0.44/0.57(0.54)	0.64/0.75(0.75)	-23/18(-2.6)	0.28-0.39(0.39)
SDW	Monthly	0.89/0.92(0.91)	0.72/0.82(0.82)	0.98/7.7(0.6)	0.63/0.74(0.74)
	Daily	0.82/0.86(0.82)	0.70/0.80(0.79)	0.98/7.7(0.6)	0.57-0.65(0.65)

1: Minimum and maximum values of streamflow accuracy for 10 best soil parameters at monthly and daily scale (high streamflow accuracy) in the two watersheds are presented. Parentheses values are highest model accuracy values in comparison between predicted streamflow and measured streamflow.

Table 3.4. Correlation[1] between physiological parameters in TSW and SDW.

Parameters (TSW/SDW)	Elevation[2]	Wetness Index[2,3]	LAI[4]	Aspect[2]
Elevation	**1.00/1.00**	**-0.23/-0.23**	**-0.19/-0.07**	**0.13/-0.09**
Wetness index	**-0.23/-0.23**	**1.00/1.00**	**0.09/0.16**	**0.06/0.12**
LAI	**-0.19/-0.07**	**0.09/0.16**	**1.00/1.00**	**0.11**/-0.00
Aspect	**0.13/-0.09**	**0.06/0.12**	**0.11**/-0.0	**1.00/1.00**

1: Correlation between physiological parameters is measured by Pearson's correlation coefficient, and if the correlation between the two parameters is statically significant (p-value<0.05), then values are displayed in bold. 2: LIDAR 10-m DEM is used to derive the topographic parameters including elevation, wetness index and aspect. Here, the transformed aspect was used (Urban et al., 2000); A'=cos(45-A)+1. This transform has the maximum value (2) in northeast and the minimum value (0) in southwest. 3: Wetness index is calculated with the algorithm of [Beven and Kirkby, 1979]. 4: LAI is derived from LIDAR 10m vegetation products.

Table 3.5. Change of annual water budget in TSW and SDW under climate warming scenarios.

	TSW	
	H.C.[1] / 2°C	H.C. / 4°C
Annual Peak SWE (mm)	211[2]/95 (116, -55%)***	211/39(172, -82%)***
Annual Streamflow (mm)	304/302 (2, -0%)*	304/293(11, -4%)***
Summer Streamflow (mm)	5.8/5.0 (0.8, -14%)***	5.8/4.7(1.1, -19%)***
Annual ET (mm)	781/784* (3, +0%)	781/792***(11, +1%)
Annual MD (mm)	502/541***(39, +8%)	502/566***(64, +13%)
	SDW	
	H.C. / 2°C	H.C. / 4°C
Annual Peak SWE (mm)	399/177(222, -56%)***	399/75(324, -81%)***
Annual Streamflow (mm)	708/678 (30, -4%)***	708/662(46, -7%)***
Summer Streamflow (mm)	19.8/12.4***(7.4, -37%)	19.8/10.9***(8.9, -45%)
Annual ET (mm)	514/544***(30, +6%)	514/560***(46, +9%)
Annual MD (mm)	257/298***(41, +16%)	257/315***(58, +23%)

H.C: Historical Climate, 2: Annual mean values, 3: Wilcox matched pairs test was to test the significance change of annual streamfow, summer Streamflow, annual ET and annual MD under historical climate, 2 warming and 4 warming scenarios. Asterisks indicate a significant difference according to climate warming:*p>0.05; **p<0.05;***p<0.01. Parenthesis shows absolute difference and percentage change for each flux between historical climate conditions and warming scenarios.

Table 3.6. Comparison between SDW under 2°C warming and TSW under historical climate conditions in terms of hydrologic responses to climate.

Question: Does SDW under 2°C warming behave similar to TSW under historical climate condition?			
Variable	Spatial scale /time scale	SDW ≈TSW	Comments
Snow	Mean watershed/month	Yes	The timing of peak monthly SWE is same and TSW has slightly higher peak monthly SWE than SDW.
ET	Mean watershed/annual	No	SDW has lower annual ET than TSW, and SDW experiences water-limitation less often than TSW.
	Mean watershed /month	No	The two watersheds have same timing of peak monthly ET, but TSW has lower monthly ET than SDW.
	SD of watershed /month	No	The highest spatial variance (SD) in monthly ET occurs in July for the two watersheds, but SDW has higher SD than TSW.
	COV of watershed /month	No	Two watersheds have similar temporal pattern of COV in monthly ET but SDW has higher COV.
	Patch level/ month in the relationship with physiographic parameters	No	LAI and wetness index are main factors controlling the seasonal ET in the both watersheds, but 2 °C warming does not make the relationship between physiographic parameters and ET in SDW to be similar to those in TSW under

			historical climate.
MD	Mean watershed/annual	No	SDW always has lower MD than TSW.
	Mean watershed /month	No	The two watersheds have same timing of peak monthly ET, but TSW has higher monthly MD.
Streamflow	Mean watershed/annual	No	The two watersheds have similar relationship between annual flow and annual precipitation, but SDW always has higher annual streamflow.
	Mean watershed /month	No	The two watersheds have same timing of peak monthly streamflow, but SDW has higher monthly streamflow.
August Streamflow	Mean watershed/annual	No	The two watersheds have similar relationship between summer flow and annual precipitation, but SDW has higher summer streamflow.

Table 3.7. Comparisons of annual water budget between TSW under historical climate conditions and SDW under 2°C climate-warming scenarios and under change in vegetation structure.

	TSW	SDW
	Historical climate conditions	2°C warming+ 2*LAI
Annual Streamflow (mm)	304	562 (85%)[1]
Summer Streamflow (mm)	5.8	10 (72%)
Annual ET (mm)	781	662 (15%)
Annual MD (mm)	502	517 (3%)

1: Parentheses show the percentage ratio of each flux for SDW to each flux for TSW

4. A top-down soil moisture and sap flux sampling design to capture the effect of inter-annual climate variation on ecohydrologic response of a transient snow watershed

Abstract

This paper presents a top-down approach for soil moisture and sap flux sampling based on a physical distributed model, Regional Hydro-Ecologic Simulation System (RHESSys), given the goal of understanding ecohydrologic response to inter-annual climate variation in transient snow watersheds. RHESSys was initially calibrated with existing snow depth and streamflow data. Calibrated model estimates of snow, soil moisture and transpiration were used to estimate the five hydrologic similarity indicators at the patch level (30m) that represent seasonal trajectories of snowmelt, root-zone soil moisture storage and transpiration. The Partitioning Around Medoids (PAM) clustering algorithm was used to define the distinctive cluster based on the calculated five hydrologic similarity indictors. Through clustering analysis and field surveys, six clusters were found and the representative site per cluster was identified. For each representative site, soil moisture sensors (5TE) were installed at the two depths (30cm and 90cm) and at the five soil pits. A sapflux sensor at the averaged-size white fir tree for each site was also installed. The model-based clustering analysis suggests that the elevation gradient and flow drainage pattern may control the spatial patterns of soil moisture and transpiration. The comparison of model-based calculated hydrological similarity indicators with measured data based values shows that spatial patterns of field-sampled soil moisture data typically fell within uncertainty bounds of model-based estimates for each cluster. There were however several notable exceptions. The model failed to capture the soil moisture and sapflux dynamics in the riparian zone site

(C6), and in a site (C4) where lateral subsurface flow may not follow surface topography. Future research will investigate these differences between modeled and observed patterns in order to identify and test refinements to model inputs, parameters or structure that might reduce these errors. In particular, the future research will examine improvement related to the use of finer-scale representations of microclimate, topography, vegetation, and soil properties.

4.1 Introduction

Recent studies have shown that mountain watersheds of the Western US, warmer temperatures in the past several decades have lead to reductions in snow accumulation, earlier melt and corresponding changes in the timing of streamflow [*Stewart et al*., 2004, 2005]. Hydrologic models suggest that these changes will intensify with increasing warming projected for both California and Pacific Northwest[*Regonda et al.*, 2005]. The magnitude of these changes, however, varies substantially between and within mountain regions. Latitude and elevational climate gradients, for example, control the sensitivity of snow accumulation and melt to warming [*Bales et al.*, 2006]. Previous work [*Tague and Grant*, 2009] has also emphasized the importance of subsurface drainage characteristics as a control on sensitivity of streamflow to climate warming. Local (headwater stream scale) estimates of climate driven changes to streamflow must account for spatial variation in these different controls. Subsurface drainage characteristics are often particularly challenging to estimate and hydrologic models typically calibrate against observed streamflow to infer these properties. In addition to streamflow, vegetation is expected to respond to climate variation and change. Increased rates of vegetation mortality observed throughout the Western US [*van Mantgem*

et al., 2009] may be linked with increased water stress. Vegetation water use (and potential stress) is likely to change with both increasing temperature and changes in the timing of water inputs [*Case and Peterson*, 2005; *van Mantgem and Stephenson*, 2007]. Spatial variation in vegetation water use, however, is a function of multiple controls, including soil and topographic characteristics that determine the amount and timing of available moisture [*Christensen et al*., 2008].

For all of these processes, soil moisture plays a central role in partitioning water and energy fluxes and influences hydrological processes and vegetation growth [*Albertson and Montaldo*, 2003; *Rodríguez-Iturbe and Porporato*, 2004]. Soil moisture has very high spatial and temporal variability [*Western and Blöschl*, 1999; *Penna et al.*, 2009] and mountain watersheds, in particular, show high spatial heterogeneity in soil moisture patterns [*Grant et al.*, 2004; *Penna et al.*, 2009]. In mountain watersheds, steep topographic gradients, complex soil and vegetation patterns and seasonally varying energy and moisture inputs (including rainfall vs snow) contribute to this heterogeneity. However, there are relatively few studies of soil moisture patterns in snow-melt dominated watersheds due to inherent difficulties in conducting field research [*Grant et al.*, 2004]. In contrast, the role of soil moisture in hydrologic process and vegetation growth in rainfall dominated watersheds has been relatively well studied [*Seyfried et al.*, 2009].

Numerous strategies have been used to link point measurements of soil moisture with plot to watershed scale spatial patterns. Soil moisture measurements are typically sparse relative to soil moisture distributions at hillslope and watershed scales. Previous studies have used a variety of statistical approaches including time stability analysis, geostatistics and EOF analysis [*Vachaud et al.,* 1985; *Perry and Niemann*, 2007; *Western and Blöschl*, 1999] or combined soil moisture measurements with remote sensing images using Kalman filtering

[*Walker et al.,* 2001; *Margulis et al.,* 2002] to overcome the limitations of relatively few point measurements. In an idealized setting, a randomized soil moisture sampling design with high spatial frequency can be used to examine watershed scale controls on soil moisture and hydrologic or ecologic response to moisture inputs. Very few studies [e.g. *Western and Blöschl*, 1999] have taken this bottom-up approach because soil moisture sampling is typically limited by cost, feasibility and accessibility – these limitations are particularly relevant in mountain environments. In complex mountain environments, where soil moisture sampling is likely to be limited, an alternative, topdown approach may be needed. A top-down approach uses an a-priori model of how soil moisture is likely to vary in space and time. This model is then used to strategically allocate limited sampling resources.

Measurement of vegetation water use may be useful as part of a top-down sampling approach. Patterns of vegetation water use and the sensitivity to climate are tightly coupled with soil moisture. Vegetation water use is strongly linked to soil moisture patterns and the potential for increased vegetation water stress with warming will in part depend on how soil moisture regimes change. Measurements of vegetation water use can be particularly useful as indicators of water availability because whole tree sap-flux reflects root-zone storage, and may integrate over very fine-scale (<meter) soil moisture heterogeneity. The vegetation water use is likely to be a good indicator of soil moisture states in water limited periods.

This study used a physically based model, Regional Hydro-Ecologic Simulation System (RHESSys, [*Tague and Band*, 2004]), to develop an a-priori model of soil moisture and vegetation water use and further uses this model to develop a strategic sampling design that emphasizes watershed scale responses to inter-annual climate variation. Specifically this study asks: (1) Based on a physically based distributed model, what are optimal soil

moisture and sapflux monitoring locations, given the goal of capturing within watershed spatial patterns of inter-annual (climate driven) variation in soil moisture dynamics?, (2) How does measured soil moisture and sapflux compare with estimates from a physically based distributed model? .

4.2 Methodology

4.2.1 Top-down approach sampling design for soil moisture and vegetation water use

A top-down sampling approach is used here to overcome the limitations that prevent a bottom-up statistically rigorous characterization of soil moisture and vegetation water use patterns. This sampling design is specifically targeted to define distinctive soil moisture and vegetation water use patterns within snow-melt dominated catchments in response to climate variability. This study uses a combination of physically-based modeling and cluster analysis to achieve this goal (Figure 4.1). The general approach involves: 1) physically based model calibration using existing measured snow and streamflow; 2) model estimation of long-term spatial patterns of key hydrologic indicators of snow, soil moisture and tree water use dynamics; 3) spatial clustering of these indicators to define an index of "hydrologic similarity" that can be mapped spatially and used to define N-distinctive soil moisture/vegetation water clusters across the watershed; 4) selecting optimal locations of soil moisture and sap-flow sampling based on clustering analysis; 5) using results from sampling to refine hydrologic model parameters; and finally, 6) using the revised model to estimate how the spatial pattern of soil moisture and vegetation water use is likely to evolve

under different climate warming scenarios. This study covers (1) to (4) and the (5) and (6) will be investigated in future research.

4.2.2 Watershed descriptions

Providence watersheds, located in the King River Experiment Watershed (KREW), is part of the larger Kings River Project that is working to develop forest management techniques for sustainable forest ecosystems in the Sierra Nevada (Fig.4.2). The watershed is also one of the Sierra Critical Zone Observatory (CZO) sites. The Providence watershed is located in rain-snow transition zone, and thus offers an ideal site for investigating how inter-annual climate variability will change the spatial distribution of snow melt and associated soil wetting-drying, plant water use and streamflow. Elevation ranges from 1500 to 2000m. The vegetation is mainly composed of mixed conifer with small areas of meadow and shrub. During winter, precipitation is a mixture of rainfall versus snow and its ratio varies with elevation. The major soil type is Shaver (47%) and Cerle-Cagwin (26%) soils. This study focuses on the Providence Creek (P300). Two meteorological stations are located near or in the study watersheds (Figure 4.2). The stations have measured precipitation, wind speed, direction, relative humidity, solar radiation, air temperature, and snow depth at a 15 min interval since 2002. 15min-streamflow has been measured at the outlet of P303 since year 2003. This paper present an approach to strategically extend this baseline data collection as part of the CZO project through additional measurements, with a focus on capturing spatial variation of soil moisture and tree transpiration at the watershed scale. Detail information about the data collection in the Sierra CZO site refers to the work of *Bales et al*. [2011].

4.2.2 Model calibration

The hydrologic model used for this study is RHESSys, a physically based, spatially explicit model that was designed to simulate climate and vegetation change impacts on hydrology and ecosystem carbon and nutrient cycling. Previous applications of RHESSys have shown that it can successfully model both hydrologic and carbon cycling behavioral in mountains of western North America [e.g *Tague and Grant*, 2009; *Mackay et al.,* 2003]. A study by *Zierl et al*. [2007] compared RHESSys estimates of streamflow and carbon flux with measured data for 15 EUROFLUX sites in mountain catchments across Europe. RHESSys captured significant cross-site differences in water and carbon fluxes as well as distinctions between managed and undisturbed forests and tree species. RHESSys also adequately reproduced the amplitude and phase of growing season evapotranspiration and net primary productivity for most sites, with R^2 values between observed and modeled monthly actual evapotranspiration and net primary productivity above 0.8 for most sites. Another application of RHESSys highlights that the model is able to capture significant differences in the sensitivity of streamflow to warming scenarios due to differences in subsurface drainage rates [*Tague and Grant*, 2009]. RHESSys was also applied to the upper Merced River basin to show that the model produced reasonable predictions of percent snow covered area when compared with MODIS data and good correspondence between observed and modeled streamflow [*Christensen et al*., 2008]. Strong model performance and the ability of the model to represent coupled vegetation and water fluxes support the selection of RHESSys for this study.

A 30-m DEM was used to derive the watershed boundary and estimate topographic parameters (slope, aspect and flow paths). Soil Survey Geographic (SSURGO, USDA Natural Resources Conservation Service) was used to define soil type. Initial soil properties

for each soil type were based on existing RHESSYs parameter libraries (available at https://github.com/RHESSys/ParamDB). Vegetation within Providence watershed is classified as mixed conifer. Associated vegetation type parameters were also taken from RHESSYs parameter libraries. A Landsat-TM (07/07/2007) image was used to estimate the leaf area index (LAI), following [*White et al.*, 1997]. Meteorological data (daily maximum and minimum temperature, precipitation) from 2002 to 2005 were available in the P303 watershed (Figure 4.2). Table 4.1 summarizes the number of assumption used in initial model implementations.

RHESSys was initially calibrated with measured snow depth and streamflow. The model calibrations focus on the two model sub-routines; snow and streamflow. To estimate the snow-related parameters, the measured snow depth data were used in the Upper Providence and Lower Providence climate stations. The calibrated parameters were the snowmelt coefficient (0.0005 m/day) and the temperature threshold ranges for precipitation phase (-1 to 6 °C). Since SWE estimate of model are compared with measured snow depth, the model calibrations focus on the timing of snow accumulation and melt rather than absolute amount of snow. We calculated the day of complete snowmelt in the two climate stations. The comparison in the day of complete snowmelt between model and observation yields R^2 of 0.93 in the two stations (Figure 4.3a).

Following the calibration of snow-related parameters, the soil-related parameters were calibrated: anisotropic saturated hydraulic conductivity (Ksat_h, Ksat_v), decay of Ksat_h and Ksat_v with depth (m), the fraction of infiltrated water that directly drains to deep groundwater stores (gw1). In this study, the linear coefficient of deep groundwater storage (gw2) was fixed as zero to reflect deep groundwater losses that are not captured by the stream gauge. Soil parameters sets were calibrated by comparing predicted streamflow with

observed daily streamflow at the outlet of P303 because the measured streamflow at the P300 gauging station is not available, when this study is conducted. As well, the major soil type (Shaver, 66%) of P303 is same as those (47%) of P300. Since soil parameters are uncertain and difficulty to obtain a single optimized parameter set, this study used the Generalized Likelihood Uncertainty Estimation (GLUE) approach [*Beven and Freer*, 2001], which assume to have multiple behavioral parameters sets with respect to the measured streamflow. 500 different soil parameters sets were sampled using uniform distribution across specified parameter ranges because the prior distribution of soil parameters is not available. Table 4.2 shows parameters ranges used in this study. To better obtain the behavioral parameters, this study used multi-objective functions (combining the three efficiency coefficients, R_{eff}, R_{logeff} and PerErr).

$$R_{eff} = 1 - \frac{\sum_{i} \left(Q_{obs,i} - Q_{sim,i}\right)^2}{\sum_{i} \left(\overline{Q_{obs}} - Q_{sim,i}\right)^2} \tag{1}$$

$$R_{\log eff} = 1 - \frac{\sum_{i} \left(\log(Q_{obs,i}) - \log(Q_{sim,i})\right)^2}{\sum_{i} \left(\left(\overline{\log(Q_{obs})} - \log(Q_{sim,i})\right)\right)^2} \tag{2}$$

$$PerErr = \frac{\left(\overline{Q_{obs,}} - \overline{Q_{sim}}\right)}{\overline{Q_{obs}}} \tag{3}$$

$$\text{Total accuracy} = R_{eff} \times R_{\log eff} \times |1 - PerErr| \tag{4}$$

Where $Q_{obs,i}$ is the observed streamflow and $Q_{sim,i}$ is the simulated flow at any give time step (i), and $\overline{Q_{obs}}$ and $\overline{Q_{sim}}$ are the long-term average of streamflow. Note that the total accuracy (equation 4) combine different aspect of flow variability; high flows ($R_{eff,}$ [*Nash*

and Sutcliffe, 1970]), low flows (R_{logeff}) and total volume error of flows (PerErr). The model accuracy was calculated using the three days time step. A daily time step model cannot account for within 24hour patterns of snowmelt and of routing time to the stream and this can lead to discrepancies at a daily time step but these timing issues should be resolved at a slightly larger (3-day) time step.

If the total accuracy was larger than 0.4, then the parameters were classified as behavioral parameter sets, otherwise, they were classified as non-behavioral parameter sets. The ensemble of streamflow estimates is computed as the weighted average of estimated flow from each selected behavioral soil parameter sets. The weight is based on streamflow accuracy (Equation 4). The behavioral parameters sets for P300 were selected based on the P303 catchment simulation results. The calculation of ensemble of soil moisture and transpiration also follows the same approach used for computing streamflow estimate. Figure 4.3(b) shows the comparison of selected behavioral model estimates with observed streamflow at the P303 gauging station. The model generally reproduced observed streamflow. For selected behavioral parameters, R_{eff} accuracy (0.59 to 0.82) was higher than R_{logeff} accuracy (0.63 to 0.90). The PerErr accuracy ranges from -22.2 to 26.9. The mean value of PerErr is close to zero. Considering high spatial heterogeneity of climate, soil, topography and vegetation in mountain watersheds, model performance is acceptable.

4.2.3 Clustering analysis

Following initial calibration, RHESSys was used to estimate the spatially explicit indicators of hydrologic similarity. The indicators used are summarized in Table 4.3. Selected indicators focus on inter-annual variation in snow, soil moisture and transpiration; and in particular spatial-temporal differences during the post-snowmelt drying period –since

this is likely to be the period most impacted by climate driven changes in snow accumulation and melt – and is most relevant from a vegetation water use – drought stress perspective. This study also looked at the pattern of post-snow melt drainage in order to improve model representation of soil moisture controls on streamflow.

As discussed above, meteorological data from stations within the study site can be used to drive hydrologic model for calibration and comparisons with observed data. However the short period of record (4 years) precludes the use of this data for RHESSys model estimation of longer-term average estimates of spatial-temporal patterns. To derive estimates of longer-term patterns of eco-hydrologic fluxes, this study used climate data from Grant Grove Climate station (water years 1941-2009) located approximate 40 km from the site. The climate data from Grant Grove station was adjusted by comparing the data (daily minimum and maximum air temperature and precipitation) with lower Providence climate data for water years 2003 to 2005. For each 30m patch, the hydrologic similarity indicators were estimated by running RHESSys for water years 1941-2009 (Table 4.3). To determine the sampling location, this study conducted clustering analysis with Partitioning Around Medoids (PAM) algorithms in the R Language clustering package [*Maechler et al.*, 2013].

The annual mean and coefficient of variance (COV) of the five hydrologic similarity indicators was calculated based on the model estimates of snow, root zone soil moisture and transpiration of each patch (Table 4.3). To define the similarity and dissimilarity between estimated indictors, the PAM defined the number of clusters and a Medoid per cluster. The Medoid is the representative object of a cluster for which the average dissimilarity to all the objects of the cluster is minimal. The dissimilarity is computed using the Euclidean distance between the objects. The number of clusters is computed by iteratively changing the Medoid and number of clusters and grouping of the objects until averaged dissimilarity within a

cluster is smaller than the smallest averaged dissimilarity between clusters. We tried to choose the number of clusters based on the both of PAM dissimilarity and resources available for sampling. In the end, this study uses six clusters.

Based on the resources available for sampling, this study uses six clusters. The PAM algorithm suggests a Medoid (representative location) per cluster. Efforts were made to sample at this representative location per each cluster. However, sampling at the suggested location was frequently infeasible in the field (rock outcrops or limited open space for installing solar panel near to sampling site were common issues). Thus, multiple approximate Medoids per cluster that have HIS values within 5% of the Medoid were generated. Through multiple sites visits, the representative sites per cluster were selected.

At the selected sites, the five soil pits were selected within 30m patch, and the locations of soil pits were selected by considering the vegetation coverage, and slope. Decagon Echo-5TE sensors were used to measure the soil moisture. 5TE sensor also measures electrical conductivity and soil temperature. The measurement was recorded at 30min intervals. The sensors were installed at the two different vertical depths (30 and 90cm) in the five soil pits. To characterize and estimate the soil properties within a patch and between sites, four soil samples per site were collected, and the soil texture and soil hydraulic parameters (porosity, saturation hydraulic conductivity, etc) were estimated. To measure tree-level sapflux at the selected site, a sapflux sensor at the averaged-size white fir tree per plot was also installed. Used sapflux probe is compensation heat pulse type [*Green et al.*, 2003]. Each probe set consists of a linear heater and two temperature sensors that are installed radially into the tree stem. One temperature sensor is placed 5mm upstream from the heater while the other one placed 10 mm downstream. The heat sensor injects the heat every 30min, and the lapse time (tz) is measured when the two temperature sensors have equal temperature after heat is

injected in the tree stem. The raw heat pulse velocity (V_z) is calculating based on the lapse rate (Equation 5). The raw heat pulse velocity is corrected for the probe-induced effects of wounding (Equation 6). The heat pulse velocity (V_c) is converted to the sap flow (J_s) (Equation 7).

$$V_z = (x_d + x_u)/2tz \quad (5)$$

$$V_c = 0.394 + 1.12V_z + 0.088V_z^2 \quad (6)$$

$$J_s = (0.441F_m + F_l)V_c \quad (7)$$

Where x_d(mm) is downstream of heat (10mm), and x_u (mm) is upstream of heater (5mm), and 0.441 is thermal properties of the woody matrix [*Becker and Edwards*, 1999], and F_m and F_l is the volume fractions of wood and water (0.25 and 0.5). A detail description of calculating sapflow can be referred to the work of [*Green et al.*, 2003].

4.3 Results

4.3.1 Clustering analysis

To select the sampling location, this study conducted clustering analysis based on the estimated hydrologic similarity indices. Figure 4.6 shows clustering analysis results of each hydrologic similarity index (HSI). Each HSI shows the different spatial patterns that reflect the differences in dominant controls on ecohydrologic the behavioral captured by the different HSIs. For each HSI, the follow variables were computed for each cluster, mean elevation, mean wetness index [*Beven and Kirkby*, 1979], mean LAI (results not shown). For most HSI the environmental variables (elevation, wetness index and LAI) that lead to different clusters are clear. HSI-1, the index associated with snow melt, has two clusters that represent different elevations zone. Higher elevation tend to have larger number of snow

melt days due to higher snow accumulation and slower snowmelt, while lower elevation tend to have shorter snow melt day. All HIS associated with root zone soil moisture showed a strong relationship with flow drainage. HSI-2, the index associated root-zone saturation has the eight clusters that follow flow drainage pattern; each cluster has distinct wetness index. HSI-3, the index associated root-zone field capacity was similar to the clusters using HSI-2 but it has more numbers of clusters than the case of HSI-3. HSI-4, the index associated root-zone wilting point creates two clusters, and the clusters follow he flow drainage pattern. Cluster 1 has lower wetness index than cluster 2. HSI-5 also has two clusters, and each cluster has distinct LAI value and wetness index. For example, Cluster-1 has lower wetness index and higher LAI values than Cluster-2. Therefore, each cluster represents where vegetation experiences water limitation. When all five HSIs are combined, six clusters were identified. Elevation and wetness index appeared to be the strongest landscape variables associated with clusters (Figure 4.5 and Table 4.5). Cluster-1 has the highest elevation, and Cluster-6 has the lowest elevation. Cluster-1 and Cluster-2 have the low values of wetness index, and Cluster-5 and Cluster-6 have high values of the wetness index. The resulting clustering map suggests that elevation gradient and flow drainage pattern is the primary controls on the spatial pattern of ecohydrologic responses to inter-annual climate variability.

Figure 4.6 shows the two statistical properties of the selected five HSIs for six clusters: annual mean and annual variance (COV). Cluster-1 has highest mean annual # of snowmelt days, but Cluster-6 had the lowest # of snowmelt days. However, Cluster-1 has the lowest annual variation of # of snow melt days. The # of days of snowmelt can be explained by elevation. Cluster-5 has the highest moisture indices (HSI-2 and 3) and low annual variance of HSI-2 and HSI-3. Cluster-3 also has higher moisture index relative to other sites. Cluster-

3 has the highest annual variance of HSI-2, but had low annual variance of HSI-3 relative to other sites. Cluster-6 has low inter-annual mean and variation of moisture (HSI-2 and 3). Cluster-3, Cluster-4 and Cluster-5 has higher annual mean transpiration (HSI-5) than other clusters. Cluster-3 and Cluster-5 had higher inter-annual transpiration variation than other clusters. Transpiration patterns roughly followed soil moisture patterns but showed significantly less inter-annual variation (much lower CV).

4.3.2 Spatial and temporal variability of measured soil moisture and sapflux

Soil moisture and sapflux data were collected at the selected six sites. All sites show strong seasonal patterns; soil moisture rises after autumn rainfall, and maintains high values during winter and starts to decline from spring, and has lowest values in summer (Figure 4.7). However, each site has a different magnitude of seasonal soil moisture, and seasonal moisture at each site varies between years. The soil moisture also varies between 30cm and 90cm. In most periods, deeper soils (90cm) tend to have higher soil moisture level than shallower soils (30cm). This is likely due to lower evapotranspiration losses from deeper soils, and contributions of lateral water from the upslope area. The rank of mean soil moisture level is as follows; C5>C4>C3>C6>C1>C2. The highest moisture content at the C5 site can be explained by its relatively large upslope contributed area (Table 4.5). Other sites have very small upslope contributed area. C5 also has the highest clay content that allows more moisture to be held in the soil (Table 4.5). On the other hand, C1 has very low moisture content, even though C1 is expected to have high moisture due to longer snow presence. This pattern was also observed from other CZO soil moisture data sets [*Bales et al.*, 2011] ; Higher moisture contents were observed at the lower elevation than at the higher elevations. Higher clay content at the lower elevation may contribute to the higher moisture

[*Bales et al.*, 2011]. The moisture level at C6 is low even though C6 is located in riparian zone. Low soil moisture level at C6 may be explained by the steep slope, and high sandy content (Table 4.5). Soil moisture at C4 rises after snowmelt is completed even though the upslope area is very minor at the site (Table 4.5). This rise suggests lateral contributions of moisture. However, the small upslope area above C4 does not suggest substantial lateral contributions that would lead to the late rising of the soil moisture at C4, relative to other sites. The soil moisture patterns of C4 suggest that it may receive lateral contribution from locations not in its immediate upslope area and suggest that surface topography may not always represent the subsurface topography. This pattern disappears in year 2012 (Figure 4.7b). Thus, the extent of lateral contribution areas at C4 may vary depending on the moisture level or groundwater level. In the dry year, 2012, the upslope contributing area and C4 may disconnect due to lower moisture level.

Figure 4.8 shows the normalized daily sapflux data in the selected three sites. Sapflow sensors failed at other three sites. This study only reports sapflux here due to high uncertainty in estimating tree-level volumetric with single sensor. Since this study focuses on capturing the different timing of tree water use given environmental conditions, the use sapflux data is sufficient. The measured sapflux data shows a strongly seasonal pattern at the all three sites; sapflux rate increases in autumn, and decreases in winter, and increases again in spring and early summers, and decreases again in summer. However, the timing of rising and declining of sapflux varied with sites, especially in the summer period. At C1, summer sapflux declines rapidly. Summer sapflux is mainly limited by reduced moisture (Figure 4.9b). However, at C2 and C6, sapflux rate maintains high values compared to C1, even though measured soil moisture at 30cm and 90cm declines, and the difference of soil

moisture level between the two sites and C1 is small (Figure 4.8). This result suggests that tree may excess deeper soil water than 1m.

4.3.3 Validation of suggested sampling design

To validate the model estimates used in creation of the sampling design, the modeled HSI values were compared with the measured HSI values. Model estimates of HSI values are based on 63 years climate records, while the measured data are only available for the two years. Therefore, direct comparison between modeled HSI values and observed HSI values is not feasible. Instead, the comparison focus whether the average observed HSI values for the two years are located within the distribution of modeled HSI values, and on whether the order of observed HSI values between the six sites matches with the order of modeled values between the sites. Figure 4.9 shows the distribution of annual precipitation and the comparisons between modeled annual mean value of three HSI values and observed values for year 2011 and 2012 for validating our sampling design. Year 2011 and year 2012 represent a relatively wet and dry year, respectively (Figure 4.9a). Note that the comparison of HSI-1 values is not included because the snow data were not collected at the six sites. For HIS-2, measured values of HIS for year 2011 and 2012 are all zero even though model estimates for HIS-2 is greater than zero (results not shown). Figure 4.9b shows the comparison of modeled HSI-3 values with measured values for year 2011 and 2012. Higher value of HSI-3 reflects higher soil moisture value. In general, measured values fall in the distribution of model estimates. At C3, modeled annual mean values of HSI-3 are overestimated relative to the measured value. At C5, model values are underestimated relative to the measured values. The order of measured value is similar to model estimate except that C3 and C4 have reverse order. Model estimate of HSI-4 values was also

compared with measure values (Figure 4.9c). Higher HSI-4 reflects lower soil moisture value. At most sites, measured values fall in the distribution of model estimates except for C5 and C6. The order of measured value is similar to those of model estimates except for C6. Measured values of HSI-4 at C6 are lower than other sites, but the model estimates are higher, and are similar to C1 and C2.

Model estimated HSI-5 values were compared with measured values (Figure 4.9d). Note that only three sites results for year 2011 are shown here because sensors at other sites were broken. Higher values for HSI-6 reflect that transpiration maintain higher rates over the summer period. At C1, measured value falls in the distribution of model estimates, but at C2 and C6, modeled transpiration in any year decline much earlier than measured transpiration in year 2011. These results suggest the problem with initial model implementation and assumptions (Table 4.3).

4.4 Discussion and summary

In the mountains of the Western US, a warming climate is likely to lead to profound changes in soil moisture dynamics due to changes in the timing and magnitude of snow melt that is often the major water input. How ecosystems will respond to these climate driven changes in mountain environment remains a key question in climate change research [*Diaz et al.,* 2008; *Bales et al.,* 2006]. Characterizing soil moisture dynamics, however, is complicated by soil moisture dependence on multiple interacting controls that vary with scale, time and location.

This study presents a strategic sampling design framework for guiding the soil moisture and sapflux measurements based on the model estimates of spatial and temporal pattern of

snow, soil moisture and transpiration. Model outputs were used to define clusters of hydrologic similarity. Model-based clusters analysis showed that elevation and flow drainage may control the spatial pattern of soil moisture and tree water use. Comparison of model-based calculated values with measured soil moisture showed that model reproduced the general spatial pattern of measured soil moisture. However, model failed to capture the soil moisture and sapflux dynamics in the riparian zone site (C6), and at site (C4). At C6, model underestimated the measured transpiration due to shallow rooting depth (1m), even though tree may excess deeper soil water than 1m. High observed soil moisture at site (C4) suggest that these are location where lateral subsurface flow does not follow surface topography, and thus is not captured well by the original model implementation.

Using hydrologic model for soil moisture and sapflux sampling has several advantages. First of all, the model can be used to generate the hypothesis prior to data collection. For example, the clustering analysis of model-based HSI values suggested that elevation and flow drainage pattern may control the spatial pattern of soil moisture and tree transpiration behavioral (Figure 4.5). An alternative and commonly used approach for sampling design is to use environmental layers (elevation, landuse, soil and vegetation maps) to define the sampling strategy. However, it is difficult to determine which environmental layer can be related to patterns of interest (e.g timing of vegetation water stress, or seasonal soil moisture depletion) prior to sampling. To demonstrate the limitation of using environmental layers for soil moisture sampling, five layers (elevation, aspect, wetness index, slope and LAI) were used to partition the watershed via PAM algorithm. The resulted clustering map and the distribution of each layer per cluster showed that each layer is equally important for clustering the watershed (Figure 4.10). This results show that using environmental layers defines clusters but does not associate these with testable hypothesis prior to data collection.

In contrast to using environmental layers, the clustering analysis of mode-based HSI values provides a testable hypothesis: elevation and flow drainage pattern may be the primary controls on spatial pattern of soil moisture and tree transpiration behavioral.

Another advantage of model-based sampling design is directly related to the variable of measurement. This study used five hydrologic similarity indices. Three indices describe soil moisture behavioral and one index describes tree transpiration. Soil moisture and tree transpiration are the actual variables that are measured in the sampling design. Lastly, using the combination of model and clustering analysis more explicitly line data collections to specific sampling goal prior to data collection. In this study, the sampling goal was to capture the watershed soil moisture and vegetation responses to inter-annual climate variation. Through clustering analysis using model-based calculated hydrologic similarity indices, we can identify the six clusters, and a representative site per cluster for data collection.

Both measured soil moisture showed a distinctive seasonal pattern, which is similar to previous analysis of soil moisture data at the Providence watersheds [*Bales et al.*, 2011]. Soil moisture sampling sites of *Bales et al*. [2011]were mostly located where the lateral flow drainage is minor. In this study, the model-based strategy was specifically designed to more fully capture the watershed-scale soil moisture and tree water use patterns. Consequently the collected data have a greater range of soil moisture variability across locations. For examples, the C5 site has large upslope drainage area (based on surface topography), and measured soil moisture also showed high moisture, especially at the deeper soil (90cm). The C4 has small upslope drainage area (based on surface topography) but has rising moisture level due to lateral flow contribution occurred in the late spring period when snowmelt is already completed. Since soil moisture measurements are collocated with

sapflux sensors, we can improve our understanding of how soil moisture and tree water use are interacted; the vegetation water use is limited by available moisture in summer, and the tree at the C6 may excess deeper soil water than 1m. Our work builds on existing soil moisture as part of the Sierra CZO. Data from the CZO provides detailed plots scale measurements, which contribute to an understanding of relatively fine-scale soil moisture variation. What is lacking is a modeling-measurement that can be used to clearly scale this information to hillslope to watershed scales, where gradients in snow accumulation and melt are likely to be strong drivers and will respond to a changing climate. Our study fills this gap. This study also suggests the first step for integrating process based modeling, space-time statistical analysis and measurements. A closer link between hydrologic models and field-measurement is often called for within the hydrologic community but few studies use models to guide measurements [*McDonnell et al.*, 2007]. The next step will be the integration of the measured soil moisture and sapflux data with RHESSys.

The comparison of model-based HSI values with measured values (Figure 4.9) show potential limitation of current model structure and parameterization. Figure 4.11 show a framework for improving ecohydrologic predictions using measured soil moisture and sapflux data at the plot scale and the catchment scale. The initial model implementation used for collecting soil moisture and sapflux data has several simplified assumptions (Table 4.3): 1) spatial uniform soil properties, 2) spatial uniform rooting depths, 3) spatial interpolation of air temperature with simple lapse rate approach, 4) spatial uniform precipitation and 5) 30m resolution topographic map and LAI map. We can hypothesize that using local parameter values including microclimate, topography, soil and vegetation (rooting depths) may improve the prediction of soil moisture and sapflux data at the plot scale. The comparison of measured soil moisture and sapflux data with model estimate can identify

specific parameters or processes where improvements are needed. If the model estimate is improving using local parameters, local value of the parameter in the model need to be incorporated, and the parameter values across catchment should be estimated to represent catchment responses (e.g. streamflow). For example, initial model estimates of transpiration underestimate HSI- 5 value at C2 and C5, which means that summer transpiration of model estimate stops earlier than measured data. Current model initialized the root depth as 1m, and spatially homogeneous. We expect that root depth spatially vary and are deeper than 1m. Therefore, accounting for more realistic local value of rooting depth may be important to reduce model error. As well, LIDAR-based tree height product may be used to estimate rooting depths across catchment when tree height can be assumed to reflect the distribution of rooting depths. The refined model can be tested with measured streamflow at the watershed scale as well as measured soil moisture and sapflux data within the watershed. They will be investigated in future research.

Figures

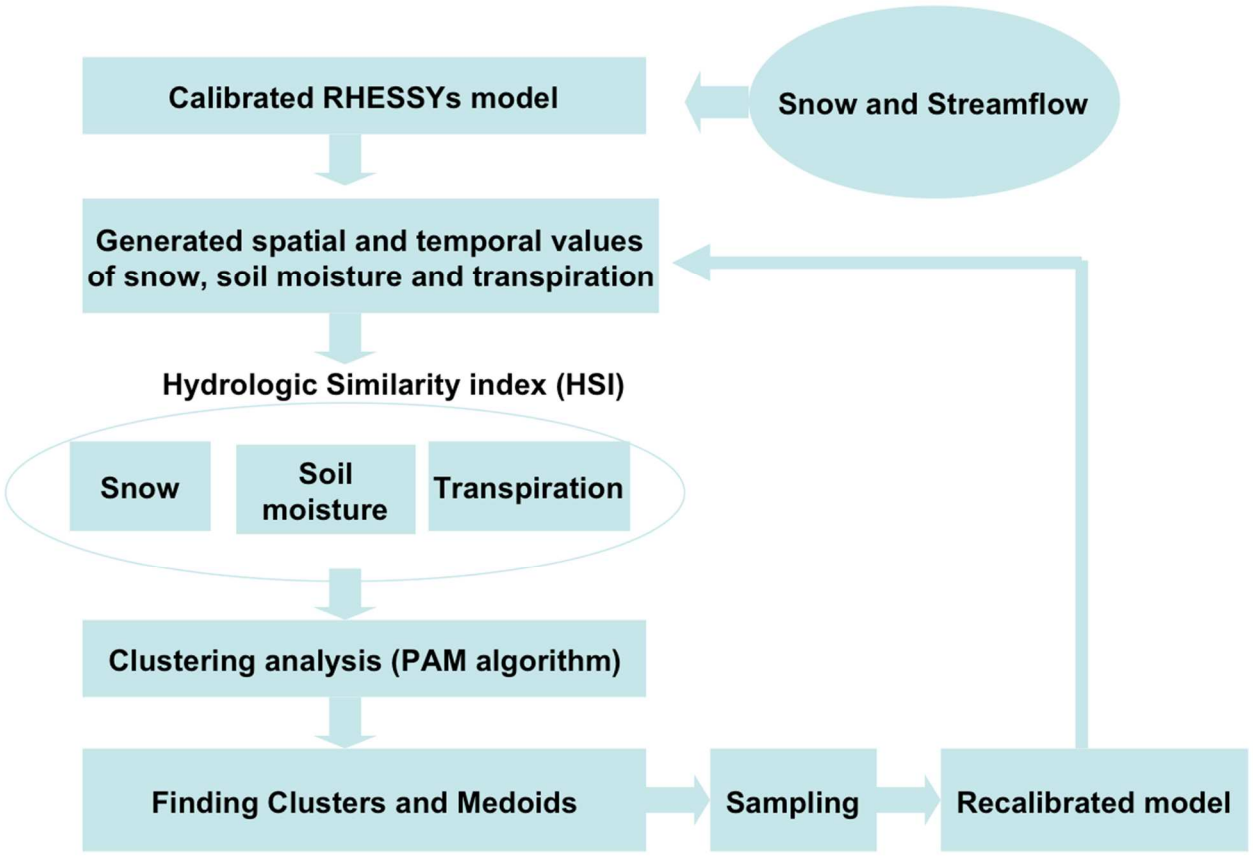

Figure 4.1. Top-down sampling design approach for capturing the spatial pattern of soil moisture and transpiration at the watershed scale.

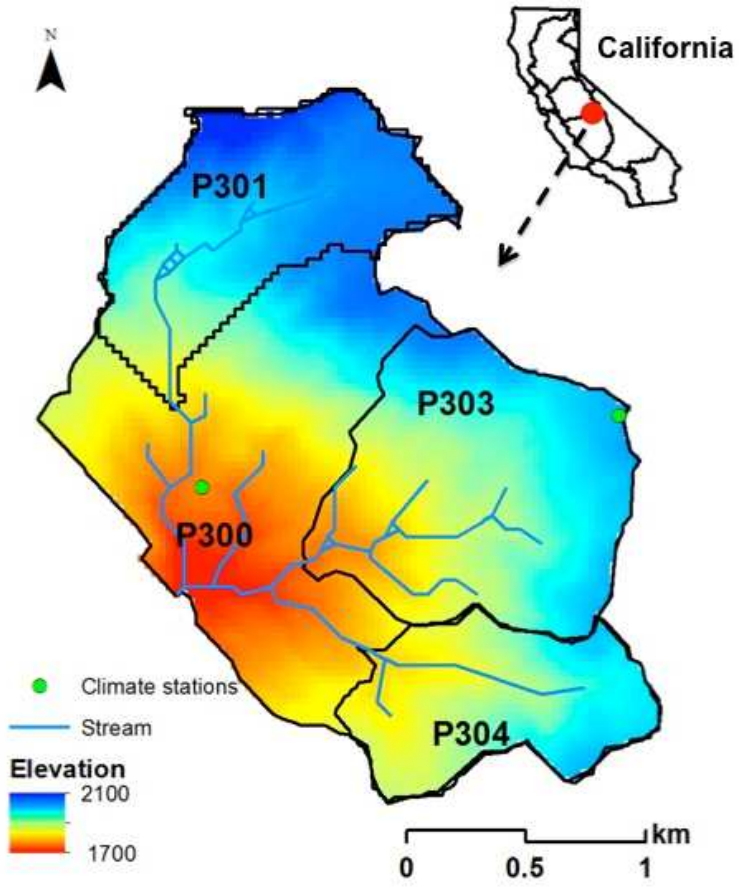

Figure 4.2. Study catchments in Providence site: two meteorological stations (upper, and lower). The P301, P303 and P304 watersheds drain into the P300 watershed.

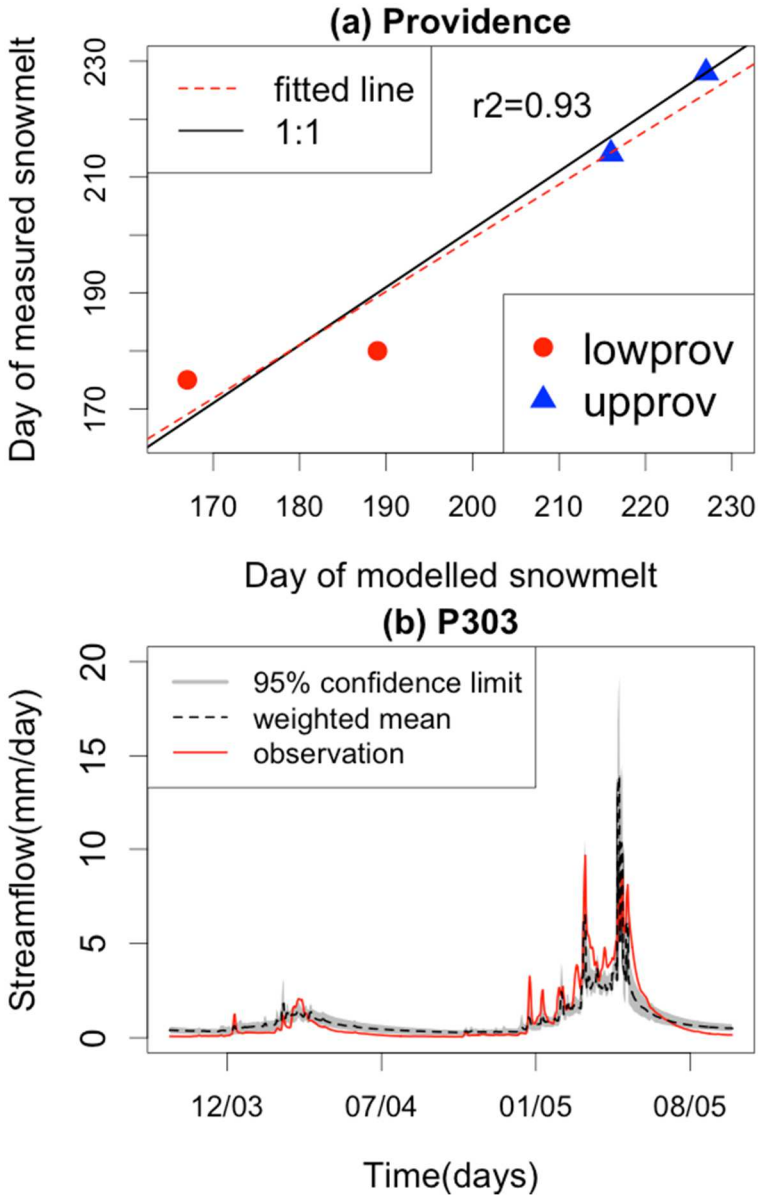

Figure 4.3. Model calibration of snow and streamflow: (a) the comparison of the estimated day of complete snowmelt between measured snow depth and modeled SWE in Lower Providence and Upper Providence station, (b) the comparison of measured streamflow and modeled streamflow; 39/500 behavioral soil parameters (accuracy(eq.4)> 0.4) are used to generate the 95% confidence limit of streamflow.

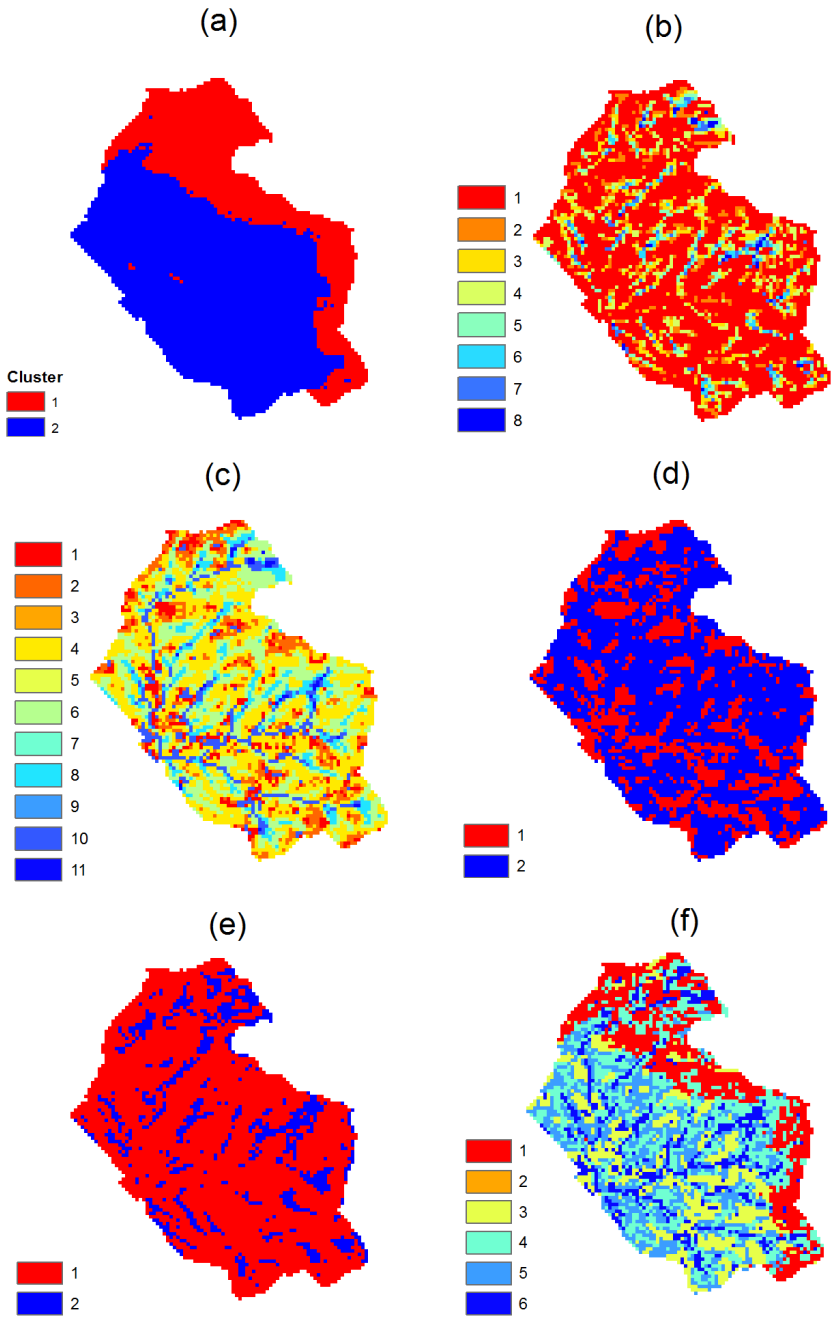

Figure 4.4. Clustering analysis results with different hydrologic similarity indicators: (a) HSI-1, (b) HSI-2, (c) HSI-3, (d) HSI-4, (e) HSI-5, and (f) including all five indicators

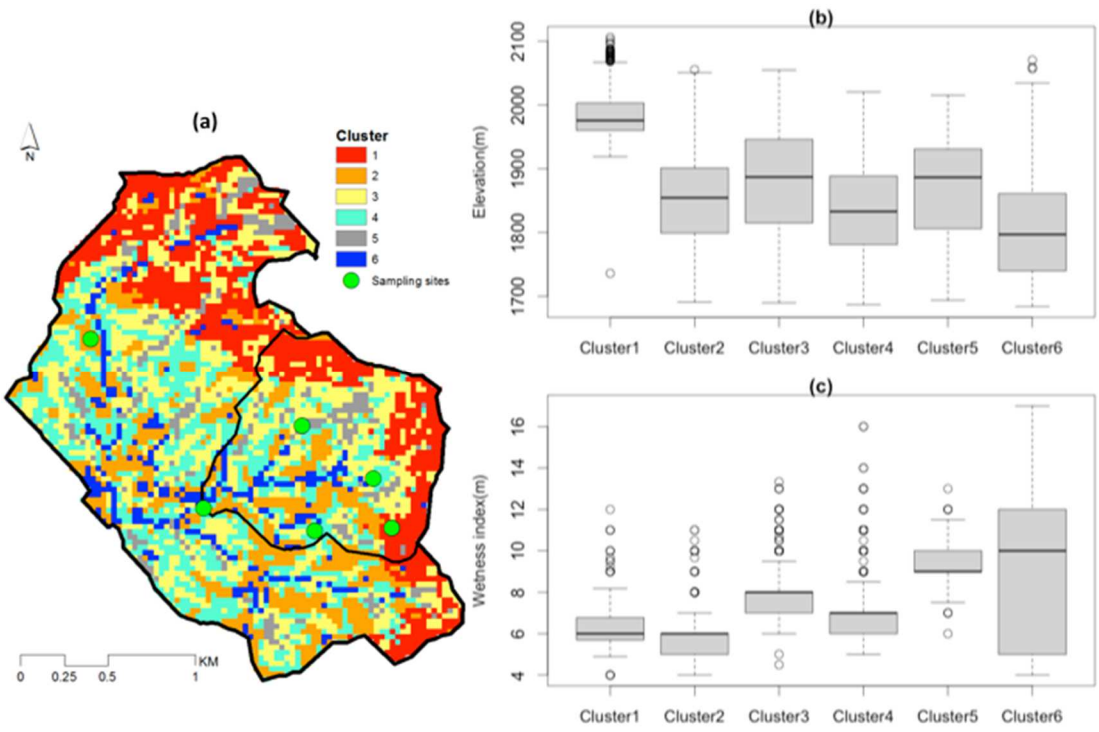

Figure 4.5. Clustering map and location of the selected sampling sites, and topographic parameter distribution at six clusters: (a) clustering map, (b) elevation distribution at the six clusters, and (c) wetness index distribution at the six clusters.

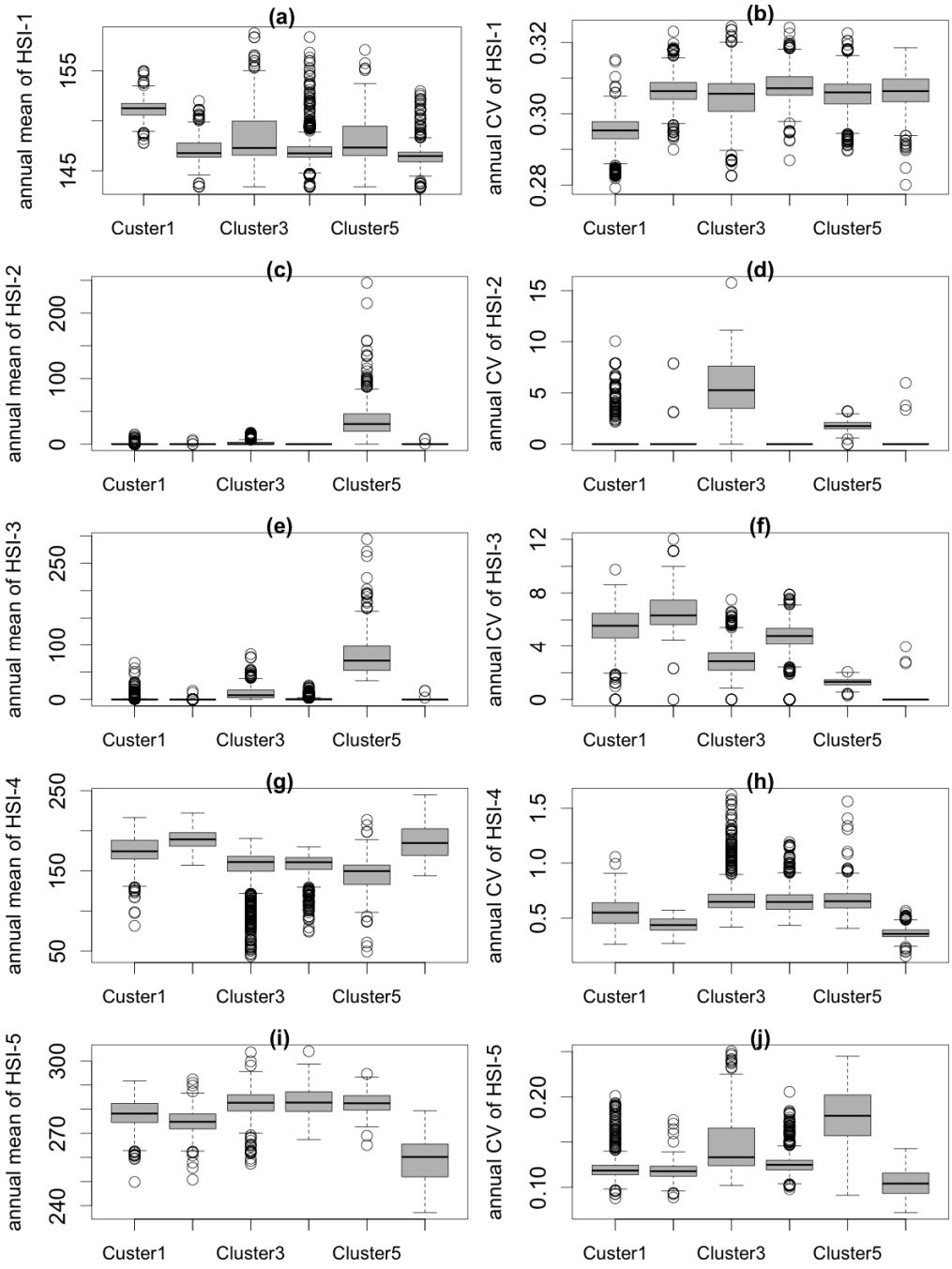

Figure 4.6. Clustering analysis results of three hydrologic similarity indices: (a) annual mean of HSI -1, (b) annual variance (COV) of HSI-1, (c) annual mean of HSI -2, (d) annual variance (COV) of HSI -2, (e) annual mean of HSI-3, (f) annual variance (COV) of HSI -3, (g) annual mean of HSI -4, (h) annual variance (COV) of HSI -4, (i) annual mean of HSI-5, and (j) annual variance (COV) of HSI-5.

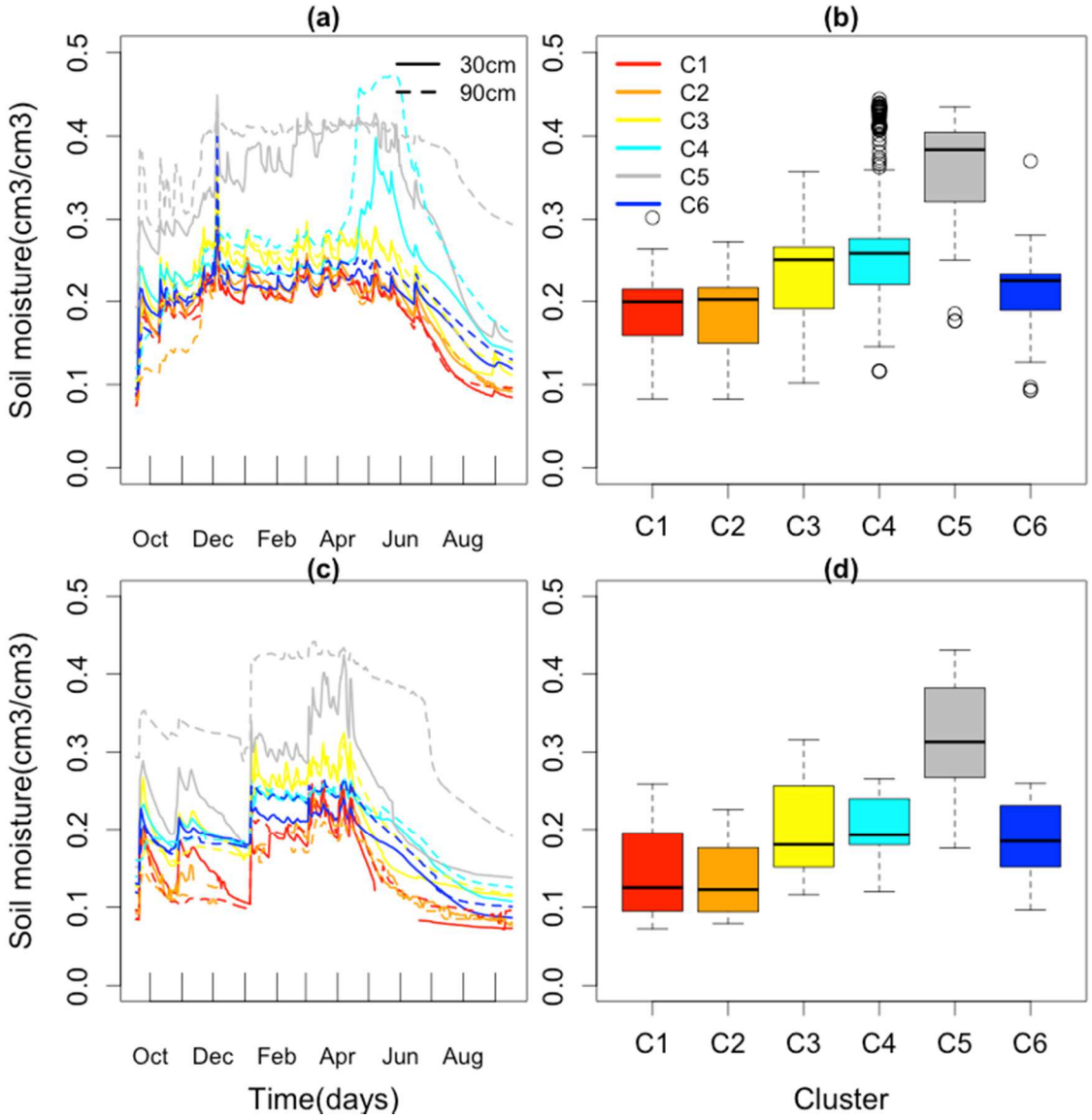

Figure 4.7. Spatial and temporal variation of daily soil moisture at 30cm and 90cm in selected sampling locations: (a) the time series of daily soil moisture at the depth of 30cm and 90cm in year 2011, (b) the distribution of average daily soil moisture within 90cm soil column in year 2011, (c) the time series of daily soil moisture at the depth of 30cm and 90cm in year 2012, and (d) the distribution of average daily soil moisture within 90cm soil column in year 2012. Solid line is the measured volume water content at 30cm, and dotted line is the volume water content at 90cm

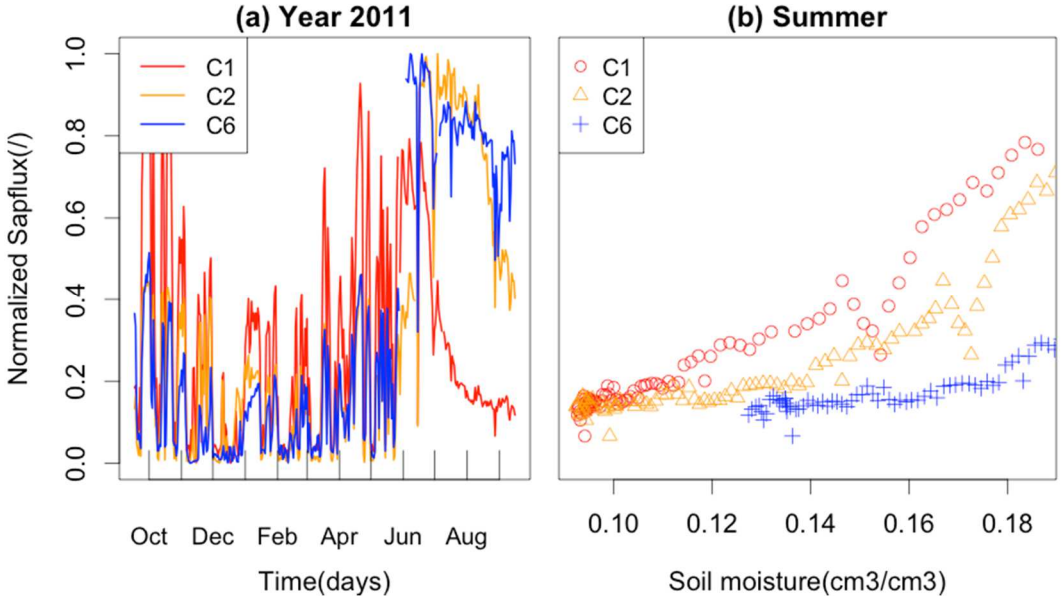

Figure 4.8. Spatial and temporal variability of sapflux at the sampling sites: (a) year 2011, and (b) the relationship between soil moisture and sapflux in summer (07/1/2011 to 09/30/2011).

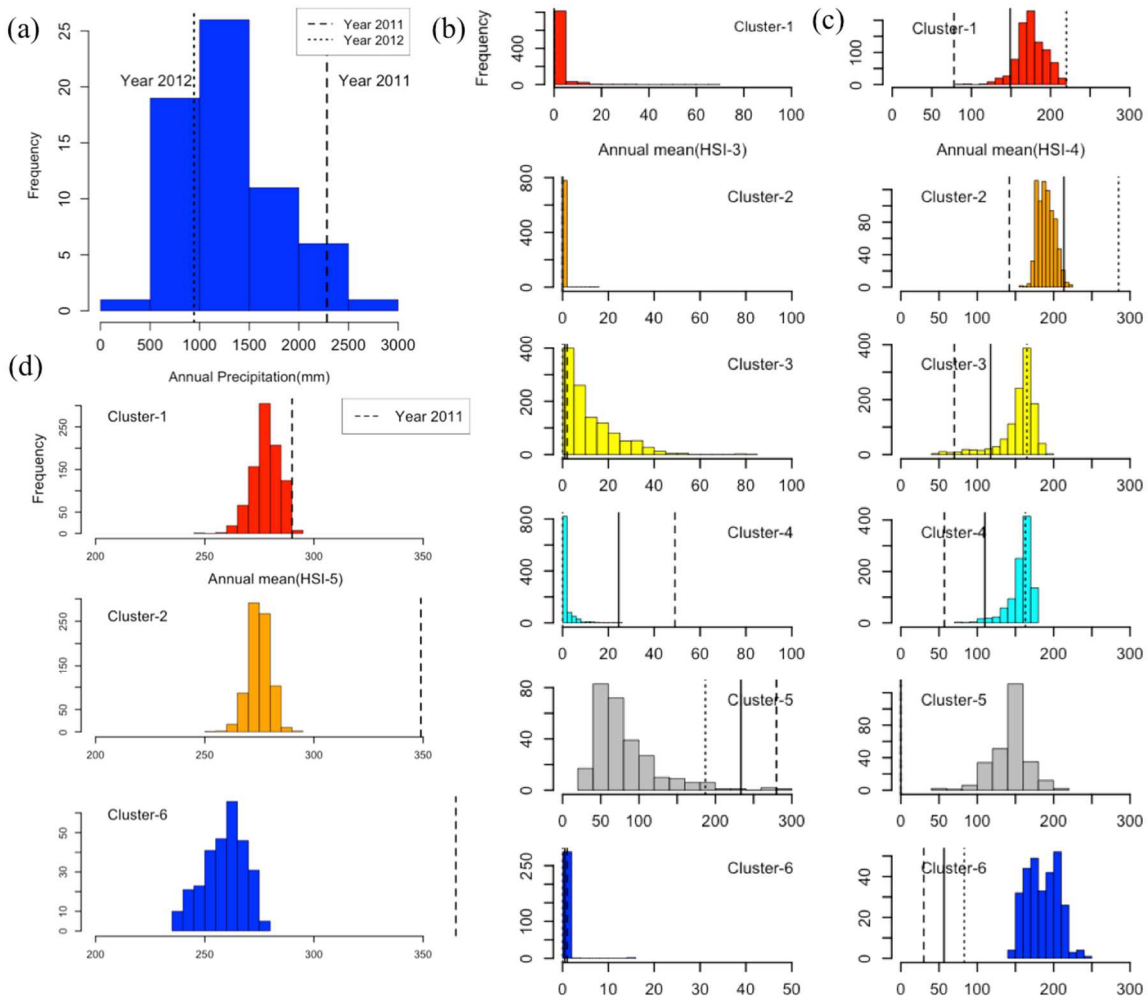

Figure 4.9. Comparison of modeled annual mean HIS values and measured HSI values for year 2011 and 2012: (a) the distribution of annual precipitation over 63 years, (b) comparison of modeled HSI-3 values and measured HSI-3 valeus for year 2011 and 2012, (c) comparison of modeled HSI-4 values and measured HSI-4 values for year 2011 and 2012, and (d) comparison of modeled HSI-5 values and measured HSI-5 values for year 2011. Solid line is the average value for year 2011 and 2012. Dotted line is the values for year 2011, and dashed line is values for year 2012.

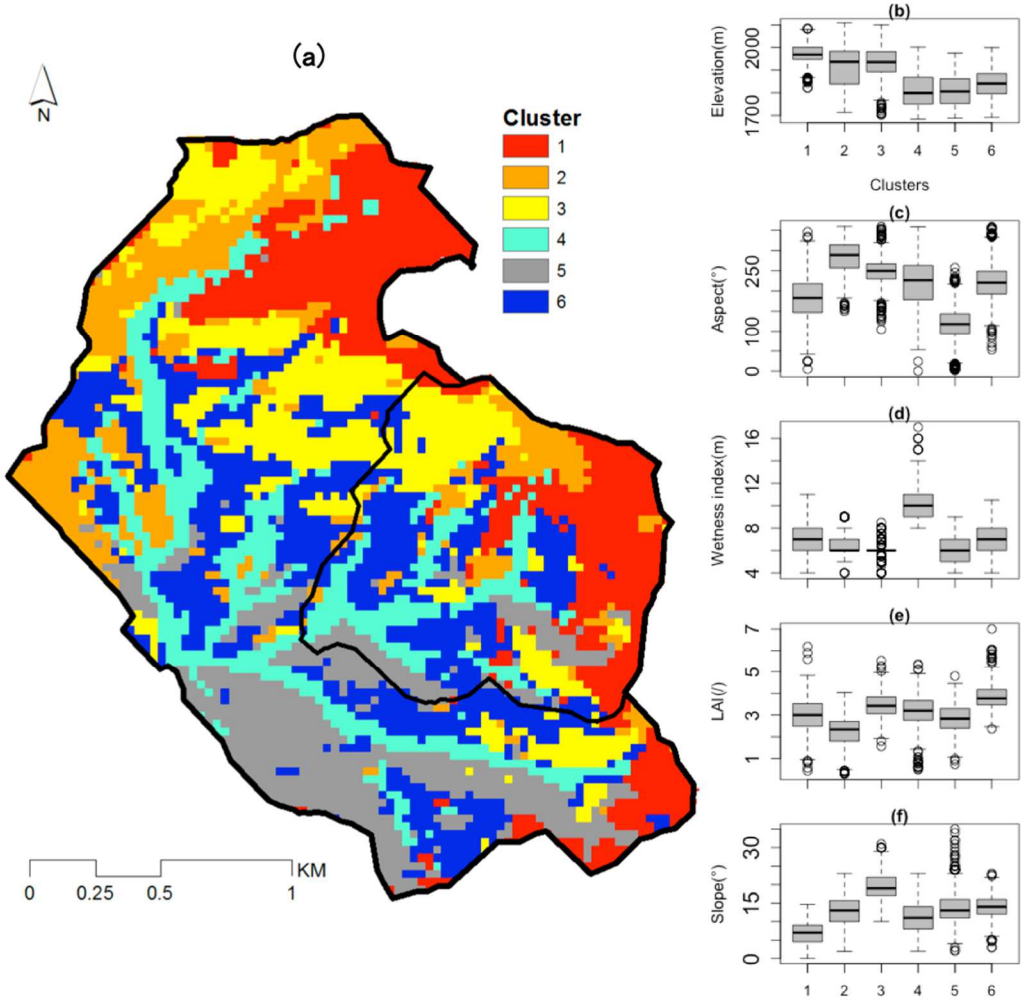

Figure 4.10. The result of clustering analysis using environmental layers: (a) clustering map, (b) elevation distribution per each cluster, (c) aspect distribution per each cluster, (d) wetness index distribution per each cluster, (e) LAI distribution per each cluster, and (f) slope distribution per each cluster.

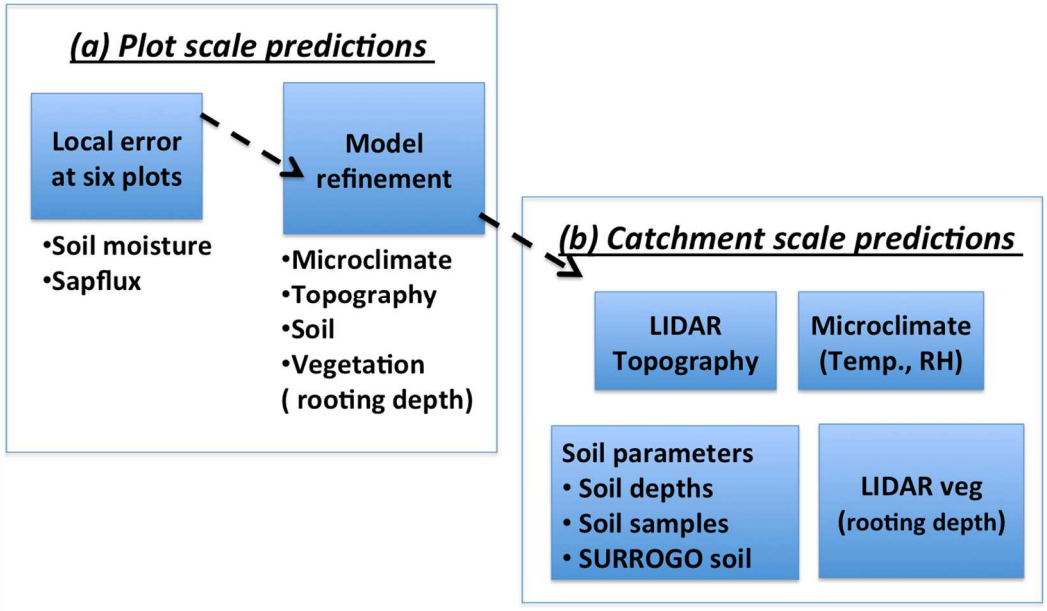

Figure 4.**Error! Use the Home tab to apply 0 to the text that you want to appear here.**-11. The framework for improving an ecohydrologic model using observed soil moisture and sapflux data.

Tables

Table 4.1. Initial model implementation and used assumptions.

Parameters	Used assumptions
Precipitation	• Precipitation is spatially uniform
Air temperature	• Spatial air temperature is estimated with a simple lapse rate.
	• Dew point is assumed to be equal to minimum daily temperature.
Topography	• 30m Digital Elevation map
Vegetation	• 30m Leaf area index (estimated using Landsat image)
	• Rooting depth is spatially uniform with 1m
Soil properties	• Soil properties are spatially uniform.

Table 4.2. Calibrated soil-related parameters, parameter ranges.

Soil parameters (Units)	Used parameter ranges (Minimum /maximum)	Behavioral parameter sets for P303
ksat_h[1] (m/day)	6/2000	883/1979(1754.8)[5]
Ksat_v[2](m/day)	6/2000	114/1974(180.9)
m[3](/)	0/6	0.16/0.55(1.72)
Gw1[4](/)	0/0.3	0.04/0.29(0.10)

1: horizontal saturated hydraulic conductivity, 2: vertical saturated hydraulic conductivity 3: Decay coefficient of ksat with depth, 4: Proportion of deep drainage into deep groundwater storage through preferential flow path from net precipitation input. 5: the parenthesis value is the parameter value with the highest streamflow accuracy.

Table 4.3. Suggested hydrologic similarity indicators (HSI): annual mean and inter-annual variation (expressed as coefficients of variation (COV)).

	Variables	Hydrologic Similarity Indicators (HSI)
HSI-1	Snow	Day of water year that snow melt is completed
HSI-2	Soil moisture	The number of days in water year that root zone soil moisture is fully saturated
HSI-3	Soil moisture	The number of days in water year that root zone soil moisture is above 70% of saturation
HSI-4	Soil moisture	The number of days in water year that root zone soil moisture is below midpoint between field capacity and wilting point.
HSI-5	Transpiration	Day of water year that 7 days transpiration declines to 50% of its peak growing season value

Table 4.4. Model streamflow accuracy for P303.

	Accuracy measures (Minimum – maximum, mean)			
	R_{efff} (eq.1)	$R_{logefff}$ (eq.2)	PerErr (eq.3)	Accuracy (eq.4)
P303	0.59-0.82 (0.70) [1]	0.63-0.90(0.71)	-22.2-26.9 (0.5)	0.40-0.53(0.45)

1: the parenthesis value shows the mean accuracy value.

Table 4.5. Topography, soil and vegetation properties of selected six sites.

	Elevation (m)	Aspect[1] (°)	Slope (°)	Upslope area (m^2)	LAI (/)	Dominant species	Soil texture
C1	1953	135	8	900	2.2	White fir	Sand (5%[2])
C2	1876	297	13	900	1.9	White fir	Loamy sand (5%)
C3	1903	185	15	4500	3.2	White fir	Loamy sand (7%)
C4	1849	182	10	900	3.9	White fir	Sandy loam (7%)
C5	1869	230	8	119700	3.0	Incense cedar	Sandy loam (15%)
C6	1722	134	14	1800	3.9	White fir	Loamy sand (6%)

1:Aspect is calculated with Grass GIS program (r.slope.aspect): 90° is North, 180° is West, 270° is South, and 360° is East. The aspect having zero is used to indicate undefined aspect in flat areas with slope having zero. 2: the parenthesis value shows clay content (%)

References

Ambroise, B., K. Beven, and J. Freer (1996), Toward a Generalization of the TOPMODEL Concepts: Topographic Indices of Hydrological Similarity, *Water Resour. Res.*, *32*(7), 2135–2145, doi:10.1029/95WR03716.

Bales, R. C., N. P. Molotch, T. H. Painter, M. D. Dettinger, R. Rice, and J. Dozier (2006), Mountain hydrology of the western United States, *Water Resour. Res.*, *42*(8), n/a–n/a, doi:10.1029/2005WR004387.

Bales, R. C., J. W. Hopmans, A. T. O'Geen, M. Meadows, P. C. Hartsough, P. Kirchner, C. T. Hunsaker, and D. Beaudette (2011), Soil Moisture Response to Snowmelt and Rainfall in a Sierra Nevada Mixed-Conifer Forest, *Vadose Zo. J.*, *10*(3), 786, doi:10.2136/vzj2011.0001.

Becker, P., and W. Edwards (1999), Corrected heat capacity of wood for sap flow calculations, *Tree Physiol.*, 767–768.

Beven, K., and J. Freer (2001), Equifinality, data assimilation, and uncertainty estimation in mechanistic modelling of complex environmental systems using the GLUE methodology, *J. Hydrol.*, *249*, 11–29.

BEVEN, K. J., and M. J. KIRKBY (1979), A physically based, variable contributing area model of basin hydrology / Un modèle à base physique de zone d'appel variable de l'hydrologie du bassin versant, *Hydrol. Sci. Bull.*, *24*(1), 43–69, doi:10.1080/02626667909491834.

Blois, J. L., J. W. Williams, M. C. Fitzpatrick, S. T. Jackson, and S. Ferrier (2013), Space can substitute for time in predicting climate-change effects on biodiversity, , doi:10.5061/dryad.d5f1r.1.

Case, M. J., and D. L. Peterson (2005), Fine-scale variability in growth-climate relationships of Douglas-fir, North Cascade Range, Washington, *Can. J. For. Res.*, *35*, 2743–2755, doi:10.1139/x05-191.

Cayan, D. R., E. P. Maurer, M. D. Dettinger, M. Tyree, and K. Hayhoe (2008), Climate change scenarios for the California region, *Clim. Change*, *87*(S1), 21–42, doi:10.1007/s10584-007-9377-6.

Chaubey, I., a. S. Cotter, T. a. Costello, and T. S. Soerens (2005), Effect of DEM data resolution on SWAT output uncertainty, *Hydrol. Process.*, *19*(3), 621–628, doi:10.1002/hyp.5607.

Christensen, L., C. Tague, and J. Baron (2008), Spatial patterns of simulated transpiration response to climate variability in a snow dominated mountain ecosystem, *Hydrol. Process.*, *3588*(January), 3576–3588, doi:10.1002/hyp.

Clapp, R., and G. Hornberger (1978), empirical equations for some soil hydraulic properties, *Water Resour. Res.*, *14*(4).

Cleveland, W. S., and E. Grosse (1991), Computational methods for local regression, *Stat. Comput.*, *1*, 47–62, doi:10.1007/BF01890836.

Cline, D., K. Elder, and R. Bales (1998), Scale effects in a distributed snow water equivalence and snowmelt model for mountain basins, *Hydrol. Process.*, *1536*(March), 1527–1536.

Coughlan, J. C., and S. W. Running (1997), Regional ecosystem simulation: A general model for simulating snow accumulation and melt in mountainous terrain, *Landsc. Ecol.*, (Running 1984), 119–136.

Croley, T. (1989), Verifiable evaporation modeling on the Laurentian Great Lakes, *Water Resour. Res.*, *25*(5), 781–792.

Dahlgren, R., J. L. Boettinger, G. L. Huntington, and R. G. Amundson (1997), Soil development along an elevational transect in the western Sierra Nevada, California, *Geoderma*, *78*(3-4), 207–236, doi:10.1016/S0016-7061(97)00034-7.

Dickinson, R., and M. Shaikh (1998), Interactive canopies for a climate model, *J. Clim.*, 2823–2836.

Dunn, S. M. (1999), Imposing constraints on parameter values of a conceptual hydrological model using baseflow response, *Hydrol. Earth Syst. Sci.*, *3*, 271–284, doi:10.5194/hess-3-271-1999.

Emanuel, R. E., H. E. Epstein, B. L. McGlynn, D. L. Welsch, D. J. Muth, and P. D'Odorico (2010), Spatial and temporal controls on watershed ecohydrology in the northern Rocky Mountains, *Water Resour. Res.*, *46*(11), n/a–n/a, doi:10.1029/2009WR008890.

Farquhar, G., S. Von Caemmerer, and J. Berry (1980), A biochemical model of photosynthetic CO2 assimilation in leaves of C3 species, *Planta*, *90*, 78–90.

Freer, J., K. Beven, and B. Ambroise (1996), Bayesian Estimation of Uncertainty in Runoff Prediction and the Value of Data: An Application of the GLUE Approach, *Water Resour. Res.*, *32*(7), 2161–2173, doi:10.1029/95WR03723.

Freer, J., J. J. McDonnell, K. J. Beven, N. E. Peters, D. a. Burns, R. P. Hooper, B. Aulenbach, and C. Kendall (2002), The role of bedrock topography on subsurface storm flow, *Water Resour. Res.*, *38*(12), 5–16, doi:10.1029/2001WR000872.

Glassy, J., and S. Running (1994), Validating Diurnal Climatology Logic of the MT-CLIM Model Across a Climatic Gradient in Oregon, *Ecol. Appl.*, *4*(2), 248–257.

Goulden, M. L., and R. C. Bales (2014), Mountain runoff vulnerability to increased evapotranspiration with vegetation expansion, *Proc. Natl. Acad. Sci.*, *111*(39), doi:10.1073/pnas.1319316111.

Goulden, M. L., R. G. Anderson, R. C. Bales, a. E. Kelly, M. Meadows, and G. C. Winston (2012), Evapotranspiration along an elevation gradient in California's Sierra Nevada, *J. Geophys. Res.*, *117*(G3), G03028, doi:10.1029/2012JG002027.

Grant, L., M. Seyfried, and J. McNamara (2004), Spatial variation and temporal stability of soil water in a snow-dominated, mountain catchment, *Hydrol. Process.*, *18*(18), 3493–3511, doi:10.1002/hyp.5798.

Green, S., B. Clothier, and B. Jardine (2003), Theory and Practical Application of Heat Pulse to Measure Sap Flow, *Agron. J.*, *95*(6), 1371, doi:10.2134/agronj2003.1371.

Holmgren, P. (1994), Multiple flow direction algorithms for runoff modelling in grid based elevation models: An empirical evaluation, *Hydrol. Process.*, *8*, 327–334, doi:10.1002/hyp.3360080405.

Howat, I. M., and S. Tulaczyk (2005), Climate sensitivity of spring snowpack in the Sierra Nevada, *J. Geophys. Res.*, *110*(F4), F04021, doi:10.1029/2005JF000356.

Hunsaker, C., and D. Neary (2012), Sediment loads and erosion in forest headwater streams of the Sierra Nevada, California, *in: Revisiting Experimental Catchment Studies in Forest Hydrology, Proceeeding of a Workshop held during the XXV IUGG General Assembly in Melbourne, June-July 2011, IAHS Publ.353, 2012*.

Hunsaker, C. T., T. W. Whitaker, and R. C. Bales (2012), Snowmelt Runoff and Water Yield Along Elevation and Temperature Gradients in California's Southern Sierra Nevada, *JAWRA J. Am. Water Resour. Assoc.*, *48*(4), 667–678, doi:10.1111/j.1752-1688.2012.00641.x.

Hwang, T., L. Band, and T. C. Hales (2009), Ecosystem processes at the watershed scale: Extending optimality theory from plot to catchment, *Water Resour. Res.*, *45*(11), n/a–n/a, doi:10.1029/2009WR007775.

Istanbulluoglu, E., O. Yetemen, E. R. Vivoni, H. a. Gutiérrez-Jurado, and R. L. Bras (2008), Eco-geomorphic implications of hillslope aspect: Inferences from analysis of landscape morphology in central New Mexico, *Geophys. Res. Lett.*, *35*(14), L14403, doi:10.1029/2008GL034477.

Jasper, K., P. Calanca, and J. Fuhrer (2006), Changes in summertime soil water patterns in complex terrain due to climatic change, *J. Hydrol.*, *327*(3-4), 550–563, doi:10.1016/j.jhydrol.2005.11.061.

Jefferson, A., and A. Nolin (2008), Hydrogeologic controls on streamflow sensitivity to climate variation, *Hydrol. Process.*, *4385*(June), 4371–4385, doi:10.1002/hyp.

Jefferson, A. J. (2011), Seasonal versus transient snow and the elevation dependence of climate sensitivity in maritime mountainous regions, *Geophys. Res. Lett.*, *38*(16), a, doi:10.1029/2011GL048346.

Johnson, J., and G. Schaefer (2002), The influence of thermal, hydrologic, and snow deformation mechanisms on snow water equivalent pressure sensor accuracy, *Hydrol. Process.*, *3542*(August), 3529–3542, doi:10.1002/hyp.1236.

Jost, G., M. Weiler, D. R. Gluns, and Y. Alila (2007), The influence of forest and topography on snow accumulation and melt at the watershed-scale, *J. Hydrol.*, *347*(1-2), 101–115, doi:10.1016/j.jhydrol.2007.09.006.

Jothityangkoon, C., M. Sivapalan, and D. . Farmer (2001), Process controls of water balance variability in a large semi-arid catchment: downward approach to hydrological model development, *J. Hydrol.*, *254*(1-4), 174–198, doi:10.1016/S0022-1694(01)00496-6.

Jung, I.-W., H. Moradkhani, and H. Chang (2012), Uncertainty assessment of climate change impacts for hydrologically distinct river basins, *J. Hydrol.*, *466-467*, 73–87, doi:10.1016/j.jhydrol.2012.08.002.

Kay, A. L., H. N. Davies, V. A. Bell, and R. G. Jones (2010), Comparison of uncertainty sources for climate change impacts: flood frequency in England, *Clim. Change*, *92*, 41–63.

Kenward, T., D. P. Lettenmaier, E. F. Wood, and E. Fielding (2000), Effects of Digital Elevation Model Accuracy on Hydrologic Predictions, *Rem. Sens. Environ.*, 74, 432–444.

Kerkez, B., S. D. Glaser, R. C. Bales, and M. W. Meadows (2012), Design and performance of a wireless sensor network for catchment-scale snow and soil moisture measurements, *Water Resour. Res.*, *48*(9), n/a–n/a, doi:10.1029/2011WR011214.

Kim, E., S. Kang, and B. Lee (2007), Parameterization and Application of Regional Hydro-Ecologic Simulation System (RHESSys) for Integrating the Eco-hydrological Processes in the Gwangneung Headwater Catchment, *Korean Journal of Agricultural and Forest Meteorology, 9*(2), 121–131.

Knowles, N., and D. R. Cayan (2002), Potential effects of global warming on the Sacramento/San Joaquin watershed and the San Francisco estuary, *Geophys Res Lett*, *29*, 1891.

Krueger, T., J. Freer, J. N. Quinton, C. J. a. Macleod, G. S. Bilotta, R. E. Brazier, P. Butler, and P. M. Haygarth (2010), Ensemble evaluation of hydrological model hypotheses, *Water Resour. Res.*, *46*(7), n/a–n/a, doi:10.1029/2009WR007845.

Kuo, W., T. S. Steenhuis, C. E. Mcculloch, C. L. Mohler, D. A. Weinstein, Degloria, and D. P. Swaney (1999), Effect of grid size on runoff and soil moisture for a variable-source-area hydrology model, *Water Resour. Res.*, *35*, 3419–3428, doi:10.1029/1999WR900183.

Landsberg, J. J., and R. H. Waring (1997), A generalised model of forest productivity using simplified concepts of radiation-use efficiency, carbon balance and partitioning, *For. Ecol. Manage.*, *95*(3), 209–228, doi:10.1016/S0378-1127(97)00026-1.

Lassueur, T., S. Joost, and C. F. Randin (2006), Very high resolution digital elevation models: Do they improve models of plant species distribution?, *Ecol. Modell.*, *198*, 139–153, doi:10.1016/j.ecolmodel.2006.04.004.

Liu, F., C. Hunsaker, and R. C. Bales (2012), Controls of streamflow generation in small catchments across the snow-rain transition in the Southern Sierra Nevada, California, *Hydrol. Process.*, n/a–n/a, doi:10.1002/hyp.9304.

Loosvelt, L., V. R. N. Pauwels, W. M. Cornelis, G. J. M. De Lannoy, and N. E. C. Verhoest (2011), Impact of soil hydraulic parameter uncertainty on soil moisture modeling, *Water Resour. Res.*, *47*(3), 1–16, doi:10.1029/2010WR009204.

Lundquist, J. D., and S. P. Loheide (2011), How evaporative water losses vary between wet and dry water years as a function of elevation in the Sierra Nevada, California, and critical factors for modeling, *Water Resour. Res.*, *47*, 1–13, doi:10.1029/2010WR010050.

Maechler, M., P. Rousseeuw, A. Struyf, M. Hubert, and K. Hornik (2013), Cluster Analysis Basics and Extensions. R package version 1.14.4., *CRAN*.

Mahmood, T. H., and E. R. Vivoni (2011), Breakdown of hydrologic patterns upon model coarsening at hillslope scales and implications for experimental design, *J. Hydrol.*, *411*(3-4), 309–321, doi:10.1016/j.jhydrol.2011.10.011.

Marks, D., A. Winstral, M. Reba, J. Pomeroy, and M. Kumar (2013), An evaluation of methods for determining during-storm precipitation phase and the rain/snow transition elevation at the surface in a mountain basin, *Adv. Water Resour.*, *55*, 98–110, doi:10.1016/j.advwatres.2012.11.012.

Maurer, E. and, and P. P. B. Duffy (2005), Uncertainty in projections of streamflow changes due to climate change in California, *Geophys. Res. Lett.*, *32*(3), L03704, doi:10.1029/2004GL021462.

McDonnell, J. J. et al. (2007), Moving beyond heterogeneity and process complexity: A new vision for watershed hydrology, *Water Resour. Res.*, *43*(7), n/a–n/a, doi:10.1029/2006WR005467.

Merz, B., and E. Plate (1997), An analysis of the effects of spatial variability of soil and soil moisture on runoff, *Water Resour. Res.*, *33*(12), 2909–2922.

Miller, N. L., K. E. Bashford, and E. Strem (2003), POTENTIAL IMPACTS OF CLIMATE CHANGE ON CALIFORNIA HYDROLOGY, *J. Am. Water Resour. Assoc.*, *39*(4), 771–784, doi:10.1111/j.1752-1688.2003.tb04404.x.

MO, X., S. LIU, D. CHEN, Z. LIN, R. GUO, and K. WANG (2009), Grid-size effects on estimation of evapotranspiration and gross primary production over a large Loess Plateau basin, China, *Hydrol. Sci. J.*, *54*(1), 160–173, doi:10.1623/hysj.54.1.160.

Monteith, J. L. (1965), Evaporation and environment., *Symp. Soc. Exp. Biol.*, *19*, 205–234.

Mote, P. W., A. F. Hamlet, M. P. Clark, and D. P. Lettenmaier (2005), Declining Mountain Snowpack in Western North America*, *Bull. Am. Meteorol. Soc.*, *86*(1), 39–49, doi:10.1175/BAMS-86-1-39.

Musselman, K. N., N. P. Molotch, and P. D. Brooks (2008), Effects of vegetation on snow accumulation and ablation in a mid-latitude sub-alpine forest, *Hydrol. Process.*, *22*(15), 2767–2776, doi:10.1002/hyp.7050.

Nash, J. E., and J. V. Sutcliffe (1970), River flow forecasting through conceptual models part I — A discussion of principles, *J. Hydrol.*, *10*(3), 282–290, doi:10.1016/0022-1694(70)90255-6.

Nolin, A. W., and C. Daly (2006), Mapping "At Risk" Snow in the Pacific Northwest, *J. Hydrometeorol.*, *7*(5), 1164–1171, doi:10.1175/JHM543.1.

Null, S. E., J. H. Viers, and J. F. Mount (2010), Hydrologic response and watershed sensitivity to climate warming in California's Sierra Nevada., *PLoS One*, *5*(4), e9932, doi:10.1371/journal.pone.0009932.

Oyler, J. W., S. Z. Dobrowski, A. P. Ballantyne, A. E. Klene, and S. W. Running (2015), Artificial amplification of warming trends across the mountains of the western United States, *Geophys. Res. Lett.*, *42*(1), 153–161, doi:10.1002/2014GL062803.

Parton, W. J., M. Hartman, D. Ojima, and D. Schimel (1998), DAYCENT and its land surface submodel: description and testing, *Glob. Planet. Change*, *19*(1-4), 35–48, doi:10.1016/S0921-8181(98)00040-X.

Peel, M. C., and G. Bloschl (2011), Hydrological modelling in a changing world, *Prog. Phys. Geogr.*, *35*(2), 249–261, doi:10.1177/0309133311402550.

Penna, D., M. Borga, D. Norbiato, and G. Dalla Fontana (2009), Hillslope scale soil moisture variability in a steep alpine terrain, *J. Hydrol.*, *364*(3-4), 311–327, doi:10.1016/j.jhydrol.2008.11.009.

Philip, J. (1957), The theory of infiltration: 4. Sorptivity and algebraic infiltration equations, *Soil Sci.*, 257–263, doi:10.1097/00010694-195709000-00010.

Regonda, S. K., B. Rajagopalan, M. Clark, and J. Pitlick (2005), Seasonal Cycle Shifts in Hydroclimatology over the Western United States, *J. Clim.*, *18*(2), 372–384, doi:10.1175/JCLI-3272.1.

Richardson, J. J., L. M. Moskal, and S.-H. Kim (2009), Modeling approaches to estimate effective leaf area index from aerial discrete-return LIDAR, *Agric. For. Meteorol.*, *149*, 1152–1160, doi:10.1016/j.agrformet.2009.02.007.

Rodriguez-Iturbe, I. (2000), Ecohydrology□: A hydrologic perspective of climate-soil-vegetation dynamics, *Water Resour. Res.*, *36*, 3–9, doi:10.1029/1999WR900210.

Running, S. W., R. R. Nemani, and R. D. Hungerford (1987), Extrapolation of synoptic meteorological data in mountainous terrain and its use for simulating forest evapotranspiration and photosynthesis, *Can. J. For. Res.*, *17*, 472–483, doi:10.1139/x87-081.

Ryan, M. G. (1991), Effects of Climate Change on Plant Respiration, *Ecol. Appl.*, *1*(2), 157, doi:10.2307/1941808.

Safeeq, M., and G. Grant (2012), Coupling snowpack and groundwater dynamics to interpret historical streamflow trends in the western United States, *Hydrol. Process.*, doi:10.1002/hyp.9628.

Samaniego, L., R. Kumar, and S. Attinger (2010), Multiscale parameter regionalization of a grid-based hydrologic model at the mesoscale, *Water Resour. Res.*, *46*(5), n/a–n/a, doi:10.1029/2008WR007327.

Hungerford R.D., Nemani, R.R. Running S.W. and Coughlan, K.C (1989), MTCLIM: A Mountain Microclimate Simulation Model, USDA Forest Service Research Paper INT-414. Ogden, Utah.

Seyfried, M. S., L. E. Grant, D. Marks, A. Winstral, and J. McNamara (2009), Simulated soil water storage effects on streamflow generation in a mountainous snowmelt environment, Idaho, USA, *Hydrol. Process.*, *23*(6), 858–873, doi:10.1002/hyp.7211.

Shields, C. a., and C. L. Tague (2012), Assessing the Role of Parameter and Input Uncertainty in Ecohydrologic Modeling: Implications for a Semi-arid and Urbanizing Coastal California Catchment, *Ecosystems*, (July 2011), doi:10.1007/s10021-012-9545-z.

Singh, R., T. Wagener, K. van Werkhoven, M. E. Mann, and R. Crane (2011), A trading-space-for-time approach to probabilistic continuous streamflow predictions in a changing climate –accounting for changing watershed behavior, *Hydrol. Earth Syst. . Sci.*, *15*(11), 3591–3603, doi:10.5194/hess-15-3591-2011.

Son, K and C.L. Tague (2012), Strategic sampling of microclimate, soil moisture and sapflux for improving ecohydrological model estimates in the California Sierra, Fall meeting, American Geophysical Union, December 2012. Abstract H31G-1208.

Son, K and C.L. Tague (2014), Effect of soil parameter uncertainty in assessing climate change projection in two small Sierra Nevada watersheds, CUAHSI 2014 Biennial Colloquium.

Steinschneider, S., A. Polebitski, C. Brown, and B. H. Letcher (2012), Toward a statistical framework to quantify the uncertainties of hydrologic response under climate change, *Water Resour. Res.*, *48*(11), W11525, doi:10.1029/2011WR011318.

Stewart, I., D. Cayan, and M. Dettinger (2005), Changes toward earlier streamflow timing across western North America, *J. Clim.*, 1136–1155.

Stewart, I. T., D. R. Cayan, and M. D. Dettinger (2004), Changes in Snowmelt Runoff Timing in Western North America under a `Business as Usual' Climate Change Scenario, *Clim. Change*, *62*, 217–232, doi:10.1023/B:CLIM.0000013702.22656.e8.

Tague, C., and A. Dugger (2010), Ecohydrology and climate change in the mountains of the Western USA–A review of research and opportunities, *Geogr. Compass*, *11*, 1648–1663.

Tague, C., and G. E. Grant (2009), Groundwater dynamics mediate low-flow response to global warming in snow-dominated alpine regions, *Water Resour. Res.*, *45*(7), W07421, doi:10.1029/2008WR007179.

Tague, C., and H. Peng (2013), The sensitivity of forest water use to the timing of precipitation and snowmelt recharge in the California Sierra: Implications for a warming climate, *J. Geophys. Res. Biogeosciences*, *118*(2), 875–887, doi:10.1002/jgrg.20073.

Tague, C., K. Heyn, and L. Christensen (2009), Topographic controls on spatial patterns of conifer transpiration and net primary productivity under climate warming in mountain ecosystems, *Ecohydrology*, *2*(4), 541–554, doi:10.1002/eco.88.

Tague, C. L., and L. E. Band (2004), RHESSys: Regional Hydro-Ecologic Simulation System—An Object-Oriented Approach to Spatially Distributed Modeling of Carbon, Water, and Nutrient Cycling, *Earth Interact.*, *8*(19), 1–42, doi:10.1175/1087-3562(2004)8<1:RRHSSO>2.0.CO;2.

Thornton, P. E., S. W. Running, and M. a. White (1997), Generating surfaces of daily meteorological variables over large regions of complex terrain, *J. Hydrol.*, *190*(3-4), 214–251, doi:10.1016/S0022-1694(96)03128-9.

Trompvanmeerveld, H., and J. Mcdonnell (2006), On the interrelations between topography, soil depth, soil moisture, transpiration rates and species distribution at the hillslope scale, *Adv. Water Resour.*, *29*, 293–310, doi:10.1016/j.advwatres.2005.02.016.

Van Mantgem, P. J., and N. L. Stephenson (2007), Apparent climatically induced increase of tree mortality rates in a temperate forest., *Ecol. Lett.*, *10*(10), 909–16, doi:10.1111/j.1461-0248.2007.01080.x.

Van Mantgem, P. J. et al. (2009), Widespread increase of tree mortality rates in the western United States., *Science*, *323*(5913), 521–4, doi:10.1126/science.1165000.

Wagener, T., N. McIntyre, M. J. Lees, H. S. Wheater, and H. V Gupta (2003), Towards reduced uncertainty in conceptual rainfall-runoff modelling: dynamic identifiability analysis, *Hydrol. Process.*, *17*, 455–476, doi:10.1002/hyp.1135.

Westerling, A. L., H. G. Hidalgo, D. R. Cayan, and T. W. Swetnam (2006), Warming and earlier spring increase western U.S. forest wildfire activity., *Science*, *313*(5789), 940–3, doi:10.1126/science.1128834.

Western, A. W., and G. Blöschl (1999), On the spatial scaling of soil moisture, *J. Hydrol.*, *217*(3-4), 203–224, doi:10.1016/S0022-1694(98)00232-7.

White, J. D., S. W. Running, R. Nemani, R. E. Keane, and K. C. Ryan (1997), Measurement and remote sensing of LAI in Rocky Mountain montane ecosystems, *Can. J. For. Res.*, *27*(11), 1714–1727, doi:10.1139/x97-142.

White, M. a., P. E. Thornton, S. W. Running, and R. R. Nemani (2000), Parameterization and Sensitivity Analysis of the BIOME–BGC Terrestrial Ecosystem Model: Net Primary Production Controls, *Earth Interact.*, *4*(3), 1–85, doi:10.1175/1087-3562(2000)004<0003:PASAOT>2.0.CO;2.

Wigmosta, M. S., L. W. Vail, and D. P. Lettenmaier (1994), A distributed hydrology-vegetation model for complex terrain, *Water Resour. Res.*, *30*(6), 1665–1679, doi:10.1029/94WR00436.

Wilby, R., and I. Harris (2006), A framework for assessing uncertainties in climate change impacts: low flow scenarios for the River Thames., *Water Resour. Res.*, *42*, 1–10, doi:10.1029/2005WR004065.

Wilby, R. L. (2005), Uncertainty in water resource model parameters used for climate change impact assessment, *Hydrol. Process.*, *19*(16), 3201–3219, doi:10.1002/hyp.5819.

Wood, A. W., E. P. Maurer, A. Kumar, and D. P. Lettenmaier (2002), Long range experimental hydrologic forecasting for the eastern US, *J. Geophys. Res.*, *107*, 4429.

Zhu, A. X., and D. Scott Mackay (2001), Effects of spatial detail of soil information on watershed modeling, *J. Hydrol.*, *248*(1-4), 54–77, doi:10.1016/S0022-1694(01)00390-0.

Zierl, B., H. Bugmann, and C. L. Tague (2007), Water and carbon fluxes of European ecosystems: an evaluation of the ecohydrological model RHESSys, *Hydrol. Process.*, *21*(24), 3328–3339, doi:10.1002/hyp.6540.